CLIMATE CHANGE ATTRIBUTION OF EXTREME WEATHER EVENTS USING SPECTRALLY NUDGED EVENT STORYLINES

Dissertation

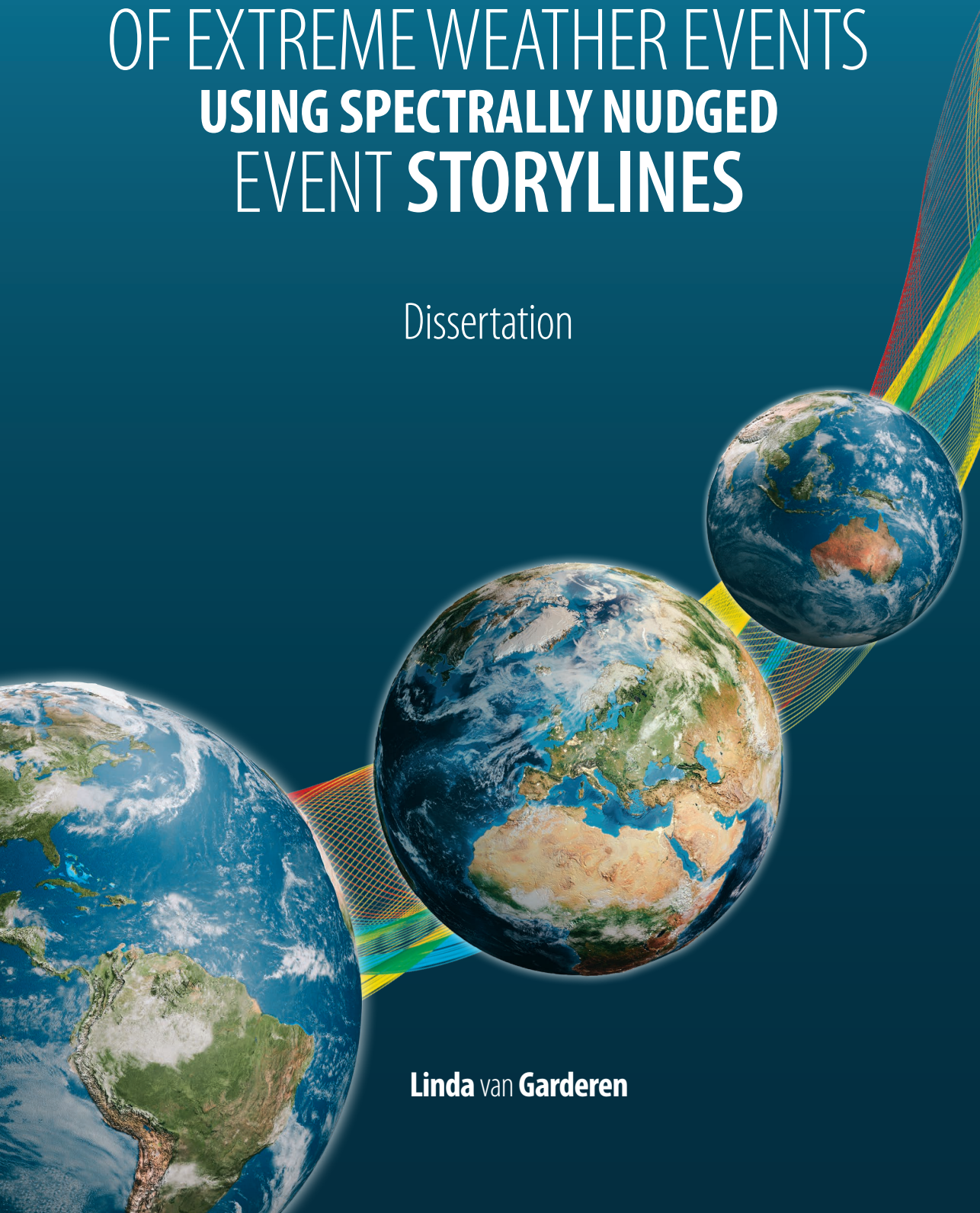

Linda van **Garderen**

Climate Change Attribution of Extreme Weather Events Using Spectrally Nudged Event Storylines

Dissertation
with the aim of achieving a doctoral degree
at the Faculty of Mathematics, Informatics and
Natural Sciences
Department of Earth Sciences
at Universität Hamburg

submitted by
Linda van Garderen

Hamburg, 2022

Department of Earth Sciences

Date of Oral Defense:	11 July 2022
Reviewers:	Dr. Frauke Feser Prof. Dr. Nedjeljka Žagar
Members of the examination commission:	Prof. Dr. Nedjeljka Žagar Dr. Frauke Feser Prof. Dr. Theodore G. Shepherd Prof. Dr. Beate Ratter Prof. Dr. Gerhard Schmiedl
Chair of the Subject Doctoral Committee Earth System Sciences:	Prof. Dr. Hermann Held
Dean of Faculty MIN:	Prof. Dr. Heinrich Graener
ISBN 13	978-94-6458-670-1

The research presented in this thesis
was conducted at

Helmholtz-Zentrum Hereon
Institute of Coastal Systems - Analysis and Modeling
Department of Climate Extremes and Impacts
Coordination of Storm Themes

Director of Institute: Prof. Dr. Corinna Schrum
Head of Department: Dr. Birgit Hünicke
Supervisor: Dr. Frauke Feser

To all those who were given an unfair starting point
and still managed to win the race.

Abstract

Heatwaves, droughts, floods, storms and other types of extreme weather events cause significant human suffering as well as material and economic damages. Discerning how climate change is influencing different extremes is a prerequisite to understand what we may expect in the future and how we can reduce loss of life and damage. A generally accepted method for attributing extreme weather events to climate change is the probabilistic approach, which is a statistical analysis of the unusual dynamical conditions that steer the extreme. It computes the probability of such an event in a world with and without climate change. However, the signal-to-noise ratio of the dynamical aspects of climate change appears to be small, which means that the results of the unconditional probabilistic approach are generally quite uncertain. The thermodynamic aspects of climate change, on the other hand, are readily apparent from observations and are far more certain since they are anchored in agreed-upon physical understanding. A novel conditional attribution approach, which is not based on probabilities, is the 'storyline' approach which quantitatively estimates the magnitude of thermodynamic aspects of climate change, taking the dynamical conditions as a given. Each storyline places a particular extreme event in different circumstances, e.g. a world without or with increased global warming, and quantifies the effect climate change has on the thermodynamic aspects of the event. The main goal of the work presented here is thus to obtain high-quality conditional climate change attribution of singular extreme weather events by developing a conditional storyline method.

The spectrally nudged event storylines presented here have globally enforced dynamical conditions by spectrally nudging the large-scale vorticity and divergence in the free atmosphere towards reanalysis data, leaving the lower atmosphere free to respond. Historical extreme weather events are then simulated in three storylines: 1) the factual storyline, which is the world as we know it with a changing climate, 2) the pre-industrial counterfactual storyline which is defined as an imagined modern world without climate change and 3) the plus 2 °C counterfactual storyline which is a world that might be, a world with 2 °C global warming compared to pre-industrial.

The results show a consistent increase in both global average temperature and precipitation due to climate change, which is in line with well established results using unconditional methods and indicates that nothing is lost when applying a conditional setup. Regional seasonal precipitation characteristics are changing, for example the Mexican monsoons of 2012 and 2014 became dryer and the Indian monsoons of 2011 and 2014 became wetter. Temperature extremes show robust results on small spatial and temporal scales. The 2003 European heatwave was on average 0.6 °C warmer due to climate change and the 2010 Russian heatwave was on average 2 °C warmer which is an amplified climate-change signal. The southeastern South American drought of 2011/2012 was at risk of intensification due to climate change, but was counter balanced by the general background wetting trend also due to climate change.

Spectrally nudged event storylines provide both a continuous and specific event attribution by enabling a robust separation of climate change from natural variability on small temporal and spatial scales. The drought example proves the method is capable of distinguishing between opposing climate signals on different time scales. The method is widely applicable as it is not limited to the technical setup presented here, which means a convection permitting model can be included to enable accurate attribution of local precipitation extremes. Moreover, the ensemble size required for robust results is small, reducing computational costs. The methodology has the great potential to be used for realistic stress testing of resilience strategies for climate impacts when coupled to an impact model. Furthermore, the spectrally nudged event storylines can be used for operationalising extreme event attribution, which until now has been difficult. In conclusion, the nudged global storyline method is an important step towards a holistic approach within the attribution of individual extreme events, which can quantify the role of both dynamical variability and known thermodynamic aspects of climate change, and the interplay between them.

Contents

Part I

Rationale

The first chapter shows why detection and attribution of extreme weather events is of great societal importance and how generally used attribution methods struggle with uncertainties and communication challenges. This is followed by an in-depth explanation of what storylines are and the difference between the standard frequentist and the newer storyline approach. Specifically the theory behind event storylines is elaborated on. The final chapter clarifies the motivation and research questions of this study.

1

Extreme weather event attribution

The societal impact of extreme weather events is great in relation to human suffering as well as material and economical damages. The destruction due to floods, storms, heatwaves and droughts costs millions and endangers the safety of many homes. In July 2021, destructive rain-fed floods swept through Germany, Belgium, Luxemburg and the Netherlands. Two days of severe rainfall from an almost stationary storm, on top of already wet soil conditions, caused the rivers to overflow and instigated flash floods and landslides in the more mountainous regions. Germany and Belgium suffered more than 200 fatalities; the economic damages rose above €6 billion (Kreienkamp et al., 2021). Large international rescue operations, volunteer initiatives and donation funds were set up to combat the disaster.

A few months later, December 10th 2021, eight states in the USA were shaken by one of the most severe tornado outbreaks in recorded history. The National Oceanic and Atmospheric Administration (NOAA) confirmed 61 tornadoes in one night, with strengths on the Enhanced Fujita Scale (EF) between EF-1 (weak) and EF-4 (violent). In some regions, the violent tornadoes left close to no structures standing. More than 80 fatalities were counted, and the economic damages are expected to be in the order of millions of dollars. (Pirtle, 2021)

A more investigated example is the 2019 European twin heatwaves that broke temperature records throughout Belgium, France, Germany, Luxembourg, the Netherlands

and the United Kingdom. Extremes above 40°C were measured in the Netherlands, Belgium and Germany. The first heatwave in June, which was caused by hot North African air being transported northwards through a ridge across Western Europe, depleted the soil moisture, and so intensified the second heatwave in July via drought (Sousa et al., 2020). The lasting heat caused tremendous loss of life, estimated at 2500 casualties throughout the region, which was a 50% excess mortality. Additional damages to the ecosystem through wildfires, to infrastructure through damaged train lines and to food production through crop losses were astounding (Bastos et al., 2021; Vautard et al., 2020).

The global climate is warming, primarily due to increasing greenhouse gas (GHG) concentrations in the atmosphere (IPCC, 2021). This has significant implications for extreme events similar to the examples described above. Several studies are estimating the 'extremeness' of extremes in the context of climate change. First reports on the climate attribution of the European flood estimated a significant intensification due to climate change, and an increased likelihood of such events to happen in the future (Kreienkamp et al., 2021). In-depth studies on the attribution of the tornado outbreak are not yet available. However, NOAA has published a statement that they expect climate change can intensify these type of events (Pirtle, 2021). Without human-induced climate change, the 2019 heatwaves would have been very unlikely as the return time of this event is estimated at 1 in 400 years in the present climate, but 1 in 1000 years in the pre-industrial climate (Vautard et al., 2020).

The extreme events mentioned above are very different in characteristics and meteorological circumstances. However, the damages are significant in all of them. Understanding how climate change is influencing different extremes is a prerequisite to understand what we may expect in the future and how we can reduce loss of life and damages.

1.1 Defining extreme events

When weather observations are tracked, for instance on a daily basis for thirty years or more, in order to tally variables such as maximum daily temperature or total daily precipitation, the result is a statistical distribution called 'climatology'. For example, the daily maximum temperature distribution as in Figure 1.1, shows that 20 °C is the most common temperature on the black curve, and 10 °C or 30 °C days are uncommon with a low number of appearances. Note that while a simplified normal distribution is used for explanatory purposes, in reality most meteorological variables show skewness in

their distribution (Tamarin-Brodsky et al., 2019). What society perceives as normal, is what appears around the middle of the distribution with the highest number of occurrences, roughly marked with a green band. The definition of extreme events, as adopted in climatology, is the so-called 'tail of the distribution', marked with a grey shading under the black curve, with events below the 5 % (cold event) or above the 95 % (hot event) threshold. The further into that tail of the distribution, the more rare the event. Weather extremes are part of every climate and therefore not something that are necessarily a result of climate change.

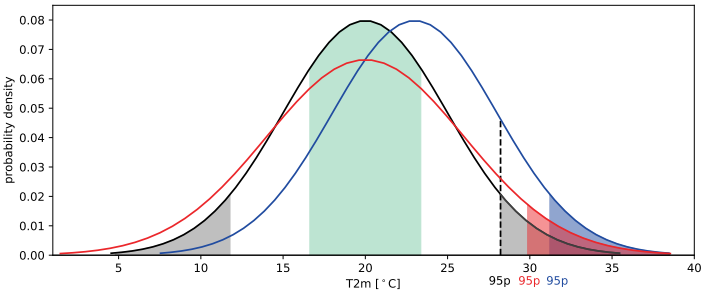

Figure 1.1: Normal distribution of example theoretical maximum daily temperature, in black the theoretical present-climate curve with a mean at 20°C, 25-75th percentile shaded in green and extremes shaded in grey for below the 5th percentile and above the 95th percentile, the blue curve is a shift of the mean to 23°C, the red curve is a flattened curve with an unaltered mean but larger tail. The curves are shaded in their respective colours above the 95th percentile, showing that a climate change induced shift or flattening of the curve can cause a different temperature to be the 95th percentile and thus changing the understanding of what is an extreme temperature.

However, climate change influences extremes by increasing their frequency, or by intensifying them (warmer heatwaves, stronger rainfall, longer droughts, etc.). This means that climate change can influence the shape of the distribution in several possible ways. Either the curve is flatter (red curve) and the tails reach further, introducing both warmer and colder temperatures, or the whole distribution shifts in its totality (blue curve) representing a stable warming with less cold days and an increased number of warmer days (Otto, 2017). For both types of changes, a maximum daily temperature of 28°C (vertical black dashed line), which would correspond to the 95th percentile and be quite uncommon in the present climate, now corresponds to a lower percentile of both the red and blue curves, and thus becomes far more common. In what way climate change will alter the curve depends on the region and the variable under investigation.

Whenever an extreme event occurs, the event is compared to the climatological distribution and a return time estimation is computed based on where, in the distribution

tail, the event occurs. This widely used and accepted statistical method is called probabilistic attribution, as it calculates the probability, or return time, that an extreme event would have had with or without climate change. To make sure the attribution has statistical meaning, the estimations have to be made using a large number of climate model simulations (further explanation in section 1.2).

It is important to note that an extreme event is not just defined by its meteorological characteristics, but is often categorised based on impact. Impact is influenced by much more than the weather, it relates to geographical characteristics and human action such as land use and mitigation options available in the region where the event is taking place. This is essential as extreme impacts are not always associated with extreme meteorology or the rarity of an event (van der Wiel et al., 2020). The work presented here focuses on meteorological attribution of high-impact events.

1.2 Challenges when attributing extremes

The probabilistic attribution of extreme events is an important and necessary method for understanding the influence of climate change. However, attributing extreme events in this way has some limitations and uncertainties connected to it, especially when applying the widely used statistical methods for events that are rare by definition.

To perform a statistical analysis on only one event is impossible, therefore the most commonly used attribution approach is to generalize the event into an event class. An event class is a group of similar events of the same type (comparable heatwaves, comparable storms, etc.), and the probabilities of these event types are usually computed from simulation experiments with or without climate change. How a class of events is defined depends on the expert judgement of the scientist, which makes it an arbitrary choice and introduces personal values and uncertainties to the analysis (Olsson et al., 2022; Pulkkinen et al., 2022; van Oldenborgh et al., 2021b). For the 2019 heatwaves and 2021 flood examples mentioned in the introduction, the attributions were calculated with such event classes resulting in a rough estimation of return times. In general, the probabilistic attribution uses model ensembles. An ensemble is a large number of model simulations with the same conditions, only slightly altered initial states. The difference between the 'factual' ensemble, corresponding to observed forcings (e.g. sea surface temperature (SST) and greenhouse gases (GHG) concentrations), and a 'counter-factual' ensemble, corresponding to an alternative world without climate change is then computed. The latter is usually constructed by removing an estimate of the changes in SSTs, and imposing pre-industrial GHG concentrations. An

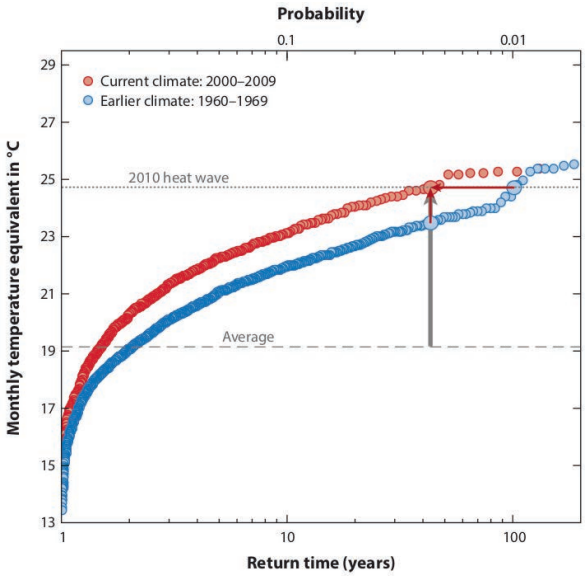

Figure 1.2: Probabilistic attribution study for heatwaves in western Russia, triggered by the 2010 extreme heatwave event. The monthly average temperature in this region for the present climate is given in red and in blue for the earlier climate. Vertical grey arrows show the distance between the event and the monthly average temperature, the horizontal red line shows the difference in frequency between present and earlier climate. The vertical red line shows the difference caused by climate change. Figure 1 from Otto (2017).

example is given in Figure 1.2 from Otto (2017) showing the probabilistic attribution of the Russian heatwave 2010. The event class is a group of comparable heatwaves for roughly the same Russian region, in red the monthly mean temperatures in the present climate and in blue for the earlier climate. On the x-axis the return times, which corresponds to the top axis with probabilities, are shown. On the y-axis, the monthly averaged temperature is given in °C. The difference between the blue and red, denoted by the red horizontal arrow, shows the changes in frequency between an event of the same monthly average temperature in current and earlier climates. A conclusion made from this example is that a similar heatwave in a comparable region of Russia has an increased return time from 1 in 100 years for preindustrial climate, to 1 in 40 years due to climate change. In short, if an extreme event triggers the need for attribution, the research is done with an event class and is computed by simulating large ensembles, usually with an atmosphere-only climate model (Watanabe et al., 2013). Since every extreme event is unique, the construction of a general event class blurs the connection to the actual event and makes it difficult to link the event attribution to climate impacts.

There is surprisingly little knowledge on the extreme dynamical conditions associated

with extreme events. In particular, there is no agreement on how those dynamical conditions might respond to climate change (Hoskins and Woollings, 2015; Shepherd, 2014). This represents an uncertainty in the probabilistic estimates that is difficult to quantify. On the other hand, thermodynamic aspects of climate change such as warming and increased specific humidity are robust in sign, anchored in agreed-upon physical understanding, and clearly emerging in observations (IPCC, 2018). Moreover, in many cases it is hard to distinguish where the noise of natural variability inherent to the system stops, and the signal of climate change starts, since the signal-to-noise ratio of the forced dynamical changes is small (Deser et al., 2016; Schneider et al., 2012).

In addition to knowledge related to how present day extremes are influenced by climate change, there is a need in society to know what extreme events can be expected in the future. A scientific approach, with a reproducible result, comes with scenario building. The idea is to formulate several, equally plausible, future projections of the climate. Trying to project the future comes with large uncertainties. In addition to the uncertainties connected to either knowledge deficiencies and technical limitations within climate science (epistemic uncertainty), or uncertainties that are part of the climate system itself like natural variability (aleatoric uncertainty), arguably the largest uncertainty comes from the dependency on human decisions and actions that will shape the future (Shepherd, 2019).

Finally, it is important to look at communication difficulties that uncertainties and probabilities form for decision makers and society. Public misinterpretation of climate science is a reality of everyday life. Besides that, the question asked in the public often concerns the effect of climate change on a specific event, not a type of event. The crucial work, done in attribution of extreme events, is not yet at a level it can satisfyingly answer the questions asked in society in a generally understandable manner.

2
Storylines

A novel attribution approach, which is not based on probabilities, is the 'storyline' approach and is formulated as *"physical self-consistent unfoldings of past events, or of plausible future events or pathways"* (Shepherd et al., 2018). The idea behind this approach is strongly related to how we regularly think in terms of 'what if...' and 'if only...'. It is the human way of estimating hypothetical results for each of the possible choices we can make. We think in future scenarios, trying to determine what choice will lead to which consequence, which is a causal interpretation of possibilities. In the storyline method, this exact mind-set is applied. What if there was no climate change, would this specific heatwave have been the same? What if the world was 2 °C warmer, what would this drought be like then? Instead of trying to predict if or when 2 °C warming might happen, storylines show the results of an intervention such as the effect a 2 °C level of global warming has on extreme events. This moves the approach away from prediction space (scenarios) where the likelihood of a possible intervention is estimated, towards decision space (storylines) where the impact of an intervention is evaluated (Shepherd, 2019).

The large uncertainties and gaps in knowledge concerning dynamical circumstances, as mentioned in the previous chapter, make it difficult to attribute extreme dynamical circumstances leading to an extreme event. The dynamics could, therefore, be regarded as given, i.e. arising by chance. The question that can be asked instead, is how the event was modified by the known thermodynamic aspects of climate change (Tren-

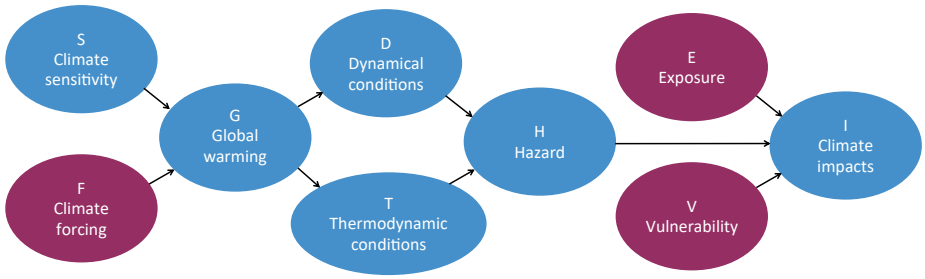

Figure 2.1: Causal network for discussing storylines. The direction of causal influence is indicated with arrows. Purple coloured balloons indicate the element is human influenced, blue coloured balloons are not directly human influenced. Adapted from Figure 4 in Shepherd (2019).

berth et al., 2015). The storyline thus depends on the question asked, and assumes the event is a given to provide a conditional attribution (Lloyd and Shepherd, 2020). In the real climate system the separation between dynamic and thermodynamic is not absolute, as they are interwoven, but it is useful to study the uncertainties in their forced response to climate change as being separable, at least to a first approximation. The idea of attributing thermodynamics separate from the dynamics was preceded by the dynamical adjustment approach to extreme seasonal climate anomalies (Cattiaux et al., 2010; Terray, 2021), which is an empirical method to construct circulation analogues and estimate the dynamical component while the thermodynamic component is obtained as residual (Deser et al., 2016). Thermodynamic attribution is also the mindset behind 'Pseudo global warming' (Schär et al., 1996), which simulates a surrogate scenario using a regional model, and adding 2 K (or any other value) to the atmospheric, land-surface and sea-surface fields for both the initial state and lateral boundary input.

Although it is not probabilistic, the storyline approach enables a quantitative estimate of climate change with a clear causal interpretation (Pearl and Mackenzie, 2018). The effect of climate change on extreme weather events links to climate risk, which can be thought of via a causal network (Shepherd, 2019), as shown in Figure 2.1. In a causal network the relationship between elements, and the direction of that relationship, are indicated with arrows. The flow of causality (from left to right) includes the uncertainties that come along with each element. If the uncertainty of dynamical conditions (D) is large, the following elements (hazard (H) and climate impacts (I)) will have a large uncertainty as well. However, each of the relationships (arrows) can be treated as a separate storyline, locking the uncertainty with the element it belongs to. In this study, the storylines represent the relationship between global warming (G)

and thermodynamic conditions (T). Studying causal links, as done with storylines, is also favoured over the probabilistic attribution approach because it reduces the sense of false objectivity that probabilistic approaches can bring (Olsson et al., 2022).

By focusing on the known effect of climate change, storylines try to avoid 'Type 2' errors (missed warnings), in contrast to the probabilistic approach which, by needing to reject the null hypothesis of no climate change whatsoever, tries to avoid 'Type 1' errors (false alarms) (Lloyd and Oreskes, 2018). Notwithstanding the need to look at the problem from both sides, as they provide different kinds of information (Lloyd and Shepherd, 2021), one could arguably say that preventing a false alarm is less beneficial for safety and damage reduction than avoiding a missed warning.

There is increasing interest in understanding and quantifying the impact of climate change on specific extreme weather and climate events, looking at singular historical events instead of recurrence likelihoods. Moreover, extreme events are regional, and their impact is regional. Therefore, an approach that can quantify the influence of climate change on a specific extreme event, without blurring over regional details and differences, is more likely to answer the questions asked by society and decision makers. The storylines approach studies the effect of particular events, focusing on their regional impact (Shepherd, 2016).

2.1 Dynamic and event storylines

Storylines are much broader than extreme event attribution. Examples of storyline application are found in a large range of fields, from fundamental meteorology and extreme event impact (Chan et al., 2021) all the way to estimations of agricultural risk related to climate change (Sillmann et al., 2021) and decision-making for food security (Young et al., 2021). There are roughly two types of meteorological storylines, dynamical (Mindlin et al., 2020; Zappa and Shepherd, 2017) and event based as presented in this study. While dynamical storylines explore the causal relationship between global warming and dynamical conditions (Figure 2.1, G and D), event storylines (as applied in this study) focus on the causal relationship between global warming and thermodynamic conditions (Figure 2.1, G and T).

The method applied in this study concerns event storylines. However, it is practical to understand the application of dynamical storylines as this formed the foundation of the storyline method in meteorology. Each dynamical storyline is a plausible response of remote drivers to climate change. Since the response of dynamical variables

to climate change is so uncertain, these storylines show the effect of climate change on a range of possibilities. For example, climate change is expected to strengthen the stratospheric polar vortex in the Southern Hemisphere, which will influence precipitation patterns over South-Africa, South-America and Australia. However, there is a large range of uncertainty linked to the amount of strengthening climate change might cause. Mindlin et al. (2020) created plausible storylines with the level of strengthening of the polar vortex in the low and high end of the uncertainty range, and studied the effect of both ends on precipitation and wind speed. The researchers applied this method for both the polar vortex strengthening and the tropical amplification (stronger than average warming in the tropical upper-troposphere) of global warming to create strong storylines (strong polar vortex, strong tropical amplification), weak storylines (weak stratospheric strengthening and weak tropical amplification) and intermediate storylines (strong polar vortex, weak tropical amplification and *vice versa*) as is shown in Figure 2.2. Here, the effect of the remote drivers and global warming is represented in zonal wind speed anomalies per Kelvin of global warming ($ms^{-1}K^{-1}$). A strong storyline (panel b) has an increased wind speed up to 0.8 $ms^{-1}K^{-1}$, a weak storyline reaches an increase up to 0.4 $ms^{-1}K^{-1}$. The asymmetric circulation response under different storylines and their deviation from the multimodel ensemble mean shows the relevance of considering a range of physically plausible changes. Dynamical storylines were formed for the precipitation anomalies in the Mediterranean by Zappa and Shepherd (2017) as shown in Figure 2.3. The y-axis shows the storyline index (strength of the storyline), the x-axis the level of global warming in Kelvin, and in colour the precipitation anomalies in mm/day. When considering a high-impact storyline, under a 3 K global warming scenario, the effect on precipitation would be a reduction just short of 0.3 $mm \cdot day^{-1}$. This type of research is critical for decision makers as it helps understand which changes in weather to prepare for under which circumstances.

Event storylines, as applied in this study, prescribe the dynamical conditions and study the thermodynamic response of a particular event to global warming. Instead of offering a range of possible dynamical responses, the dynamics are forced identically in all experiments. Since the prescribed dynamics is reproducing the dynamical state as observed, it enables the study of specific events and nullifies the need for an event class. While dynamical storylines can give a range of possible circumstances for future weather, event storylines place a particular extreme weather event in different circumstances, e.g. a world without or with increased global warming (van Garderen et al., 2021), and studies how these circumstance have influenced the event itself. Wehrli et al. (2019) applied such event storylines to study the key drivers on a range of heatwaves. In each storyline an added variable is changed which shows the influence of

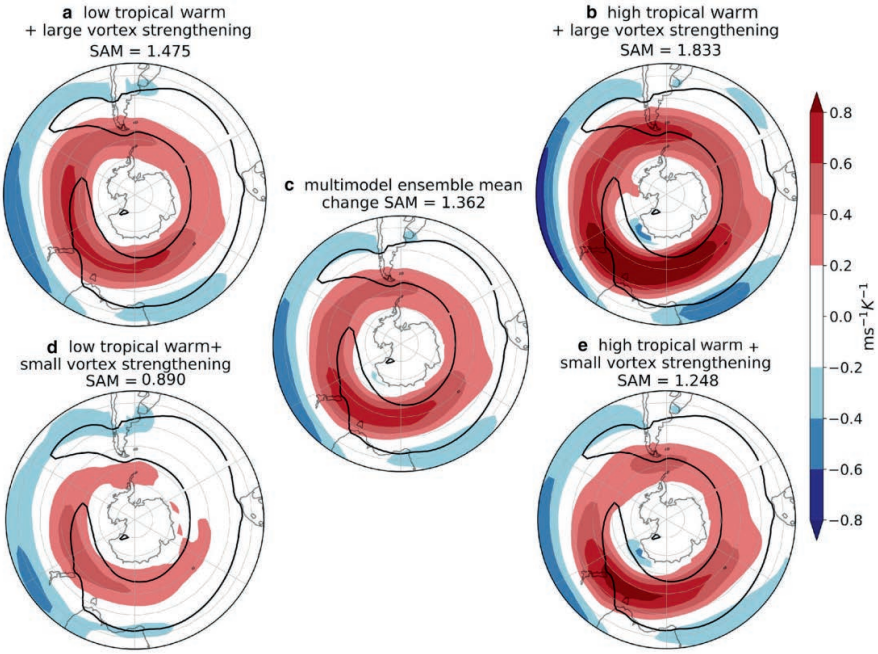

Figure 2.2: Dynamical storylines showing the effect of either a strong or weak polar vortex, and/or a strong or weak tropical amplification per degree of global warming on the zonal wind speed in the Southern Hemisphere. Subplot **d** shows a weak storyline, where a low tropical amplification and a small level of vortex strengthening causes limited zonal wind speed anomalies. Subplot **b** shows a strong storyline with a larger influence on the zonal wind speed. SAM is Southern Annular Mode. Figure 14 from Mindlin et al. (2020) .

one specific driver. In Figure 2.4 the behaviour of maximum temperature and soil moisture during the 2010 Russian heatwave are shown, when influenced by different drivers. Without getting into the experimental details, what is clearly visible in the graph is that the temperature event (marked grey) is well captured by the storylines with a prescribed dynamical condition in the atmosphere (lines marked with aF_smF and aF_smC in Figure 2.4), and the effect of soil moisture depletion is needed to reach the maximum temperature comparable to the reference. This example shows that event storylines can reproduce the details of historical events and study the causal link between aspects such as soil moisture or GHG and the characteristics of an extreme weather event.

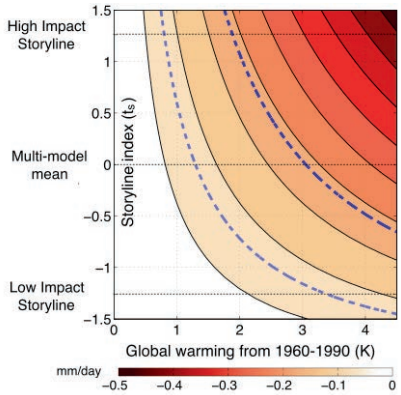

Figure 2.3: Dynamical storylines based on either a strong or weak polar vortex, and a strong or weak tropical amplification as well as different levels of global warming and its effect on Mediterranean precipitation. The y-axis shows the storyline index representing the strength of the storyline, the x-axis the level of global warming in Kelvin, and colours the precipitation anomalies in mm/day. The light dashed line is the change in precipitation related to the time at which the climate change response starts to emerge, and the dark dashed line is one standard deviation in year-to-year variability. Figure 9a from Zappa and Shepherd (2017) ©American Meteorological Society. Used with permission.

2.2 Prescribing the dynamics through spectral nudging

Creating event storylines requires a method to prescribe the atmospheric state of a model in agreement with observations. One of those methods is called spectral nudging. The term nudging means to force the atmospheric circulation of an atmospheric model towards the dynamical conditions from an external data set. Nudging can be used to recreate past weather events that are captured in the source data (e.g. reanalysis data) but with the more refined resolution of the atmospheric model. The climate model thus adds value and regional detail to the coarser-resolution forcing data set (von Storch et al., 2018; Waldron et al., 1996). Moreover, nudging a model gives room for experimentation, for instance a set of different boundary conditions to study their effect on past weather events. The spectral nudging technique is well established within the context of regional climate modelling (Feser et al., 2011; Miguez-Macho et al., 2004; Scinocca et al., 2016) and in boundary-layer sensitivity studies (van Niekerk et al., 2016). More recently, the method has been dynamically downscaled for global modelling applications (Schubert-Frisius et al., 2017)

Often, when the term nudging is used, the method referred to is grid nudging. In this case, a set of variables are corrected towards reanalysis data at a number of grid points in the domain, throughout the complete vertical column. This type of nudging is strict, as it leaves little freedom for the model to resolve anything on its own, reducing

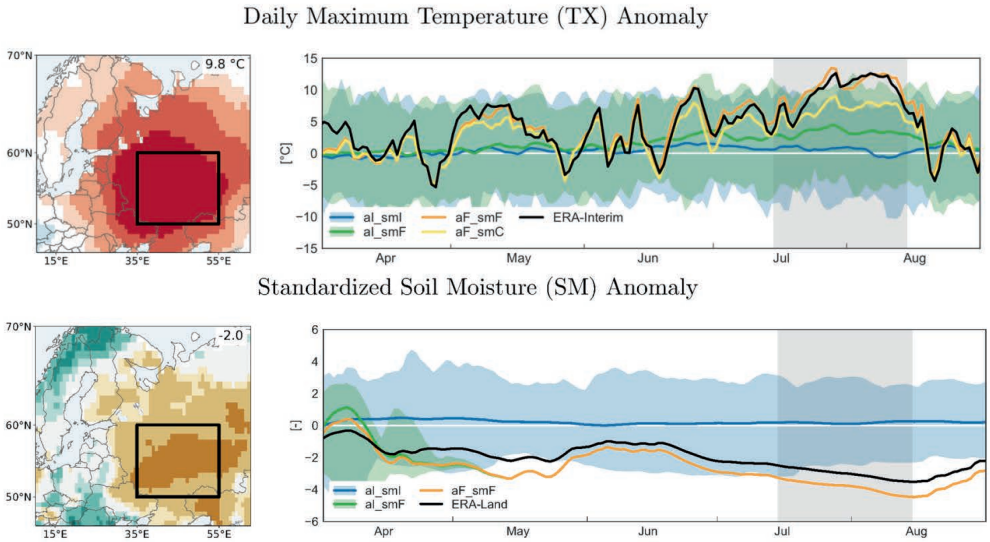

Figure 2.4: Russian heatwave 2010 daily maximum temperature anomaly in °C in the top panel, and standardized soil moisture anomaly in the upper 1 m in the bottom panel. Maps on the left show the monthly anomaly in T2m for ERA-Interim and soil moisture for ERA-land respectively; the region under study is marked with a black box. al_sml = influence of SST, al_smF = influence of soil moisture, aF_smF = influence of a nudged atmosphere and aF_smC is the influence of soil moisture while using a nudged atmosphere. ERA-Interim and ERA-land form comparison. Shading (green, blue) represents the range of anomalies in non-nudged simulations. Note that in the bottom panel, the green line becomes identical to the yellow line and therefore is no longer visible. Adapted from Figure 3 and 4 in Wehrli et al. (2019).

the benefit of fine scale computations that the model would resolve better than the reanalysis. This can cause unwanted smoothing of variables near the surface, and thus a loss of accuracy (Vincent and Hahmann, 2015). The spherical harmonics in a spectral global model provides a significant benefit when applying nudging. A spectral global model computes its variables as a combination of different simple wave functions instead of a specific computation bound to a grid point (Nese et al., 2018). Since spectral nudging is based on wave numbers instead of grid points (Kim and Hong, 2012; Schubert-Frisius et al., 2017; Yoshimura and Kanamitsu, 2008), it can be used more flexible such as scale selection, meaning that large-scale waves (lower wave numbers) are forced, and smaller waves (with higher wave numbers), including those relevant to extreme events, are free to be simulated by the high-resolution model (von Storch et al., 2018, 2000; Waldron et al., 1996). Another merit of the approach is the potential to reduce inhomogeneities in the data set by nudging only a limited number of reanalysis variables. In grid nudging there are commonly up to four variables forced

(pressure, temperature, vorticity and divergence), in spectral nudging generally up to two (divergence and vorticity) though experimental setup of nudged variables can differ. Moreover, applying spectral nudging globally brings the benefit of not having to deal with lateral boundaries common to regional models, since the waves are unhindered in their path around the globe.

2.3 State of the art in event storyline attribution

In the IPCC AR6 report (§10.6.4.8), storylines are briefly explained and the IPCC recognises the need for understanding the thermodynamic processes and their changes due to climate change (Doblas-Reyes et al., 2021). Moreover, the application of storylines is starting to find its place in regional climate scenarios such as the Dutch 2014 climate scenarios where the dynamic and thermodynamic aspect of global warming were studied separately, as well as combined (KNMI, 2014). These climate scenarios are the basis for Dutch climate policy. Application of event storylines in the UK National Flood Resilience Review (NFRR, 2016) shows that policymakers require the combination of probabilistic and storylines attribution. The policy requires probabilistic terminology such as return-times, but impact assessment requires a conditional approach to link the meteorological aspects (defined in storylines) to impact modelling (Sillmann et al., 2021).

The storyline concept using constrained or conditioned atmospheric states has been applied in a version of analogues (Goulart et al., 2021; van der Wiel et al., 2021) and more recently in the updated dynamical adjustment approach (Terray, 2021) which uses observations and reanalysis instead of model simulations. The general idea of analogues is to find a close to identical present and past dynamic situation, for instance a storm that caused a flood, to study the difference that climate change must have caused in the impact of the present event compared to the past event. Another way of conditional attribution is by dynamically constraining through boundary conditions applied to a regional model (Meredith et al., 2015) or by controlling the initial conditions in a weather forecast model (Patricola and Wehner, 2018). A new development along that line is the application of storylines in a weather forecast model by Leach et al. (2021), which is beneficial for high-resolution but short timescale event attribution, as it depends on short lead times to create the atmospheric conditioning.

Event storylines with a conditioned atmospheric state using the new global spectral nudging setup had not been implemented prior to the initiation of this work. The method allows for attribution of extreme events independent of their location on

the globe due to the global setup. Moreover, the spectral nudging model has more freedom for small-scale variables than other methods of atmospheric conditioning, which might give far more insight on the effect of climate change on processes connected to extreme weather events. As this study was being undertaken, some new work with comparable methods to the one presented here were published, which will be explained and compared in the Discussion (chapter 9).

3
Motivation and Research Questions

It is pivotal to learn how climate change is influencing specific extreme weather events, in order to understand what may be expected in the future and how to reduce loss of life and damages. To find meaningful answers to questions concerning the climate change influence on singular extreme weather events, requires a method that provides answers with more certainty and detail than the existing approaches. Combining the methods of constraining the atmosphere through spectral nudging with storylines will enable such single extreme weather event attribution. This tool may assist in progressing our scientific understanding of processes that bridge climate change and extreme events. The main goal of the work presented here is thus to obtain high-quality conditional climate change attribution of singular extreme weather events by developing a conditional storyline method. The thought of doing so has been gaining traction, yet there is no insight in the effectiveness of such a method in following and attributing individual extreme events, nor is it known how much there is gained in matters such as reduced uncertainty.

Based on the motivation stated above, this study will endeavour to answer the following research questions:

1. How well can spectrally nudged storylines follow extreme events?
   Motivation: To attribute individual extreme events, it is paramount to test if the method is capable of resolving individual extremes properly.

2. How clearly can spectrally nudged storylines distinguish signal from noise?
   Motivation: Results found by applying spectrally nudged storylines are only meaningful if the climate signal is beyond the noise of either natural variability or the method itself.

3. What is the relative role of climate change vs. natural variability in extreme events?
   Motivation: Attributing the thermodynamic element of individual extreme weather events to climate change is the next step in understanding how global warming is influencing recently experienced extreme events.

   (a) for heatwaves?

   (b) for droughts?

   (c) for precipitation extremes?

Part II

Methodology

The technical set-up of the storyline attribution experiment revolves around the high resolution version of the global atmospheric general circulation model ECHAM6. In Chapter 4, a short overview of the ECHAM6 model is given, and the application of spectral nudging is elaborated on. Chapter 5 explains how different storylines are created.

4

ECHAM6 Spectrally Nudged

4.1 ECHAM6

The sixth European Centre/Hamburg Model (ECHAM6) is a spectral general circulation model (GCM) based on an early version of the European Centre for Medium-Range Weather Forecasts (ECMWF) model, though it has been altered significantly since then. It is the atmospheric part of the Max Planck Institute - Earth System Model (MPI-ESM) coupled model (Stevens et al., 2013) used in the recent climate model intercomparison project (CMIP).

For this study, the high-resolution T255L95 version of ECHAM version 6.1.00 is used, translating to 0.54 °or roughly 60 km grid space at the equator. The model contains a dry spectral transform dynamical core and a transport model for the different water species and chemical tracers. Prognostic variables are: vorticity (ξ), divergence (D), temperature (T), cloud ice content (q_i), the natural logarithm of surface pressure ($ln(p_s)$) in the horizontal as well as zonal and meridional winds (u, v), specific humidity (q_v), cloud liquid water content (q_l) and cloud ice water content (q_i) in the vertical. The land-atmosphere interaction is calculated through the Jena Scheme for Biosphere-Atmosphere Coupling in Hamburg (JSBACH) sub-model (Reick et al., 2013), convection is parameterized using the Tiedtke-Nordeng scheme. The sea surface temperature (SST) and sea ice concentration (SIC) are prescribed from the first National Centers for Environmental Prediction (NCEP-R1) reanalysis data (Kalnay

et al., 1996).

A spectral global model, such as ECHAM6, differs from a gridded model by computing its variables as a combination of different simple wave functions instead of a specific computation bound to a grid point (Nese et al., 2018). A resolution of T255 means that the highest wave number (and thus the smallest waves) has a frequency of 255 in its circle around the earth. High wave numbers therefore resolve small-scale processes, whereas low wave numbers resolve large-scale processes. Working with spherical harmonics like that is beneficial in a global model as so-called dynamical variables, such as surface pressure and geopotential height, behave like waves over the globe. Moreover, there is a computational benefit when computing in spectral space. However, variables such as cloud water or specific humidity, which are irregular, or variables that need to be parameterized are not suited for computation in spherical harmonics. For these type of variables, the model uses a quadratic transform grid.

ECHAM6 is a state-of-the-art model, with high-level performances throughout many published works. The version used in this study benefits from a high global resolution, in both the horizontal and the vertical, and simulates challenging phenomena such as extratropical circulation, tropical intra seasonal variability and vertical temperature representation in the upper troposphere adequately (Hertwig et al., 2015; Stevens et al., 2013). ECHAM6 is not exempt from challenges generally known to global models, such as accurate resolving of weather close to the equator (Žagar et al., 2016). That said, it performs in the mid-range when compared with other global models (Flato et al., 2013).

4.2 Spectral nudging towards NCEP-R1

In the experiments presented here, spectral nudging is only applied in the free atmosphere, at altitudes above 750 hPa. It constrains the model's large-scale weather patterns, that is the lower wave numbers of divergence and vorticity (horizontal flow), to stay close to reanalysis data in order to derive a global high-resolution weather reconstruction. The nudging of variable X in spectral space over time is done as in Equation 4.1 (adapted from Jeuken et al. (1996)):

$$\frac{\partial X}{\partial t} = \begin{cases} F_x + G(X_{NCEPR1} - X) & for\, n \leq 20, p < 750hPa \\ F_x & otherwise \end{cases} \tag{4.1}$$

where X is the variable to be nudged (either vorticity or divergence), F_x is the model tendency for variable X, and X_{NCEPR1} is the state of that variable in NCEP-R1. G is the relaxation coefficient in units of 10^{-5} s^{-1} determining the nudging strength.

Most settings are applied according to the Schubert-Frisius et al. (2017) methodology, including the usage of spectral nudging in both meridional and zonal directions, as well as a plateau nudging-strength height profile (see Figure 4.1a). This profile starts at 750hPa, then quickly increases to its maximum nudging strength, remains constant for higher tropospheric and the lower and medium stratospheric levels until it again quickly tapers back to zero at a height corresponding to 5 hPa. Reduced nudging above 5 hPa is necessary as there is no NCEP-R1 reanalysis data available at that altitude.

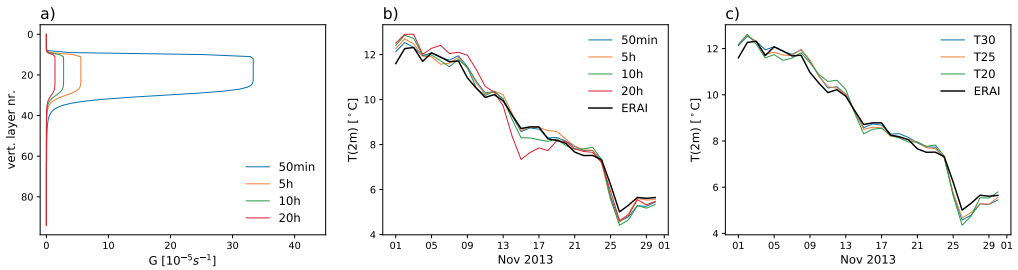

Figure 4.1: a) Nudging strength G [10^{-5} s^{-1}] as a function of model level, for different choices of minimum e-folding time as indicated. b) the impact of the tested e-folding time settings on the temporal evolution of the T2m average over Europe (10 °W - 35 °E/35 - 60 °N) in comparison to ERA-Interim for November 2013. c) Daily mean temperatures as in panel b, but with a 50-minute nudging timescale at different truncations in comparison, again in comparison to ERA-Interim.

The strength of nudging is determined by the relaxation coefficient (G, in $10^{-5}s^{-1}$), see Equation 4.1. The relaxation coefficient is often described using the e-folding time (G^{-1}, in 10^5s) which represents the simulated time necessary for nudging to dampen out a model-introduced disturbance. For example, if the model is computing a storm, but this storm is not present in the reanalysis, this is a disturbance. If the e-folding time is 10 hours, then the nudged model will dampen out that disturbance (with an assumed amplitude of 1) to a value of $\frac{1}{e}$ and thus greatly reduce it within 10 hours. A larger relaxation coefficient implies a stronger nudging and translates into a shorter e-folding time or dampening time (von Storch et al., 2000). The settings of Schubert-Frisius et al. (2017) for nudging strength and truncation are fine-tuned for the application in this study.

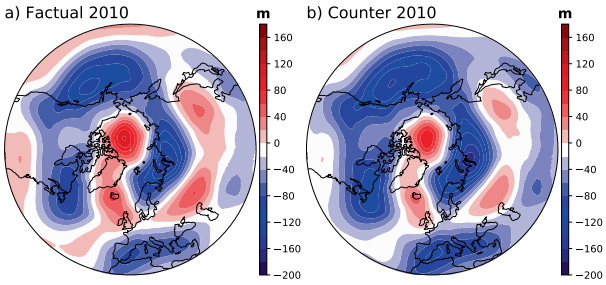

Figure 4.2: Geopotential height (z500) June-July-August (JJA) anomalies [m] for the Northern Hemisphere showing the 2010 summer atmospheric blocking situation. The spectrally nudged dynamic situation are averaged over a) factual members and b) counterfactual members. Anomalies were calculated relative to the ECHAM_SN 1980-2014 JJA climatology.

In fine-tuning the Schubert-Frisius et al. (2017) setup, the first aim is to test any relaxation possibilities of the e-folding settings while still reproducing the correct large-scale weather conditions. In Figure 4.1b the impact of the tested e-folding time settings is shown for November 2013 on the temporal evolution of the two-meter temperature (T2m) averaged over Europe (10 °W - 30 °E, 35 - 60 °N) in comparison to ERA Interim. There is little difference visible between the 50-minute and 5-hour e-folding times. The 10-hour results start to show small deviations, whilst the 20-hour results deviate even more noticeably. Based on this sensitivity study, the e-folding time is safely relaxed from 50 minutes to 5 hours without losing the accuracy of the results. The second aim is to limit the range of spatial scales being nudged as much as possible. In Figure 4.1c we show the T2m results for the different nudging wavelengths in comparison to ERA-Interim. The original T30 settings used by Schubert-Frisius et al. (2017), which translate to a minimum wavelength of approximately 1300 km ($\frac{360°}{30} \cdot$ 111 km), show comparable results to the T25 and T20 resolutions. The nudging is therefore relaxed to the T20 resolution, which translates to a minimum wavelength of approximately 2000 km ($\frac{360°}{20} \cdot$ 111 km). This should be sufficient to resolve the large-scale circulation while allowing smaller scale processes to develop freely.

To test if the fine-tuned setup is indeed capable of capturing complex dynamical states, the geopotential height anomalies for summer 2010 in the factual and counterfactual simulations are compared and have a strong resemblance (see Figure 4.2). Even though the background conditions of the two simulations are different (which is explained further in chapter 5), the blocking pattern formed over Russia in 2010 is clearly present in both simulations, demonstrating the capability of our nudging method with relaxed settings to reproduce the complex dynamical situation.

Throughout this study, the Schubert-Frisius ECHAM_SN data set is used to calculate climatologies for comparison. ECHAM_SN is a spectrally nudged global historical simulation from 1948-2015 (Schubert-Frisius et al., 2017). It nudged vorticity and divergence towards NCEP-R1 in a vertical plateau shaped profile, at spatial scales corresponding to T30 or larger, with an e-folding time of 50 minutes.

5
Creating Storylines

Three storylines are simulated, which can be interpreted as three different worlds:

1. The factual storyline, which is the world as we know it with a changing climate
2. The pre-industrial counterfactual (counter) is defined as an imagined modern world without climate change
3. The plus 2 degrees counterfactual storyline (plus2) is a world that might be, a world with 2 degrees global warming compared to pre-industrial.

The counter storyline has, besides simulations of equal length to the factual and plus2 storylines, also a long simulation covering the years 1948-2015 called ECHAM_SNC. ECHAM_SNC was created with the aim to provide a publicly available dataset comparable to the ECHAM_SN 1948-2015 factual simulation. The technicalities of ECHAM_SNC are explained in detail, as it has some unique characteristics compared to the counter storyline.

Before further elaborating the differences between each storyline, it is important to understand the similarities. Each storyline has three members and is run for five years (2010-2014). The land-use and volcanic activity, as well as aerosol forcing and SIC, are unchanged between the storylines except for SIC in ECHAM_SNC. Each world is spectrally nudged in the same way, as is explained in Section 4.2.

The differences between the three worlds are created by altering two important boundary conditions: a) sea surface temperature (SST) and b) greenhouse gases (GHG). This means that, strictly speaking, the attribution is the combined effects of anthropogenic climate change recorded in the SSTs (and thus including some indirect aerosol forcing), as well as the direct radiative effects of GHG forcing. The changes, which are explained in detail in the following sections, resulted in an average global T2m of 13.60 °C in the counter storyline; 14.28 °C in the factual storyline; and 15.15 °C in the plus2 storyline.

5.1 Factual

The factual storyline is the world as we know it, with a changing climate and a warming ocean surface. ECHAM6 has these settings available, including the GHGs, which change according to observed values (Meinshausen et al., 2011). The SSTs and SICs are prescribed using NCEP-R1 reanalysis data, as is done by Schubert-Frisius et al. (2017). The simulation is nudged as explained in section 4.2. The three factual members were initiated one month apart from each other (in November and December 2009, and January 2010), with the corresponding atmospheric state from the ECHAM_SN data set as start-up situation.

5.2 Pre-industrial counterfactual

As there are two different counterfactual simulations, the 2010-2014 counter and the ECHAM_SNC, with distinct differences in their setup, each of these simulations are explained separately.

5.2.1 2010-2014 simulations

SST patterns such as the Atlantic Multidecadal Oscillation (AMO) or El Niño–Southern Oscillation (ENSO) greatly influence weather extremes. It is therefore considered imperative to reduce the climate signal in the SST without losing such natural variability. The same SST variability is thus imposed on each of the different storylines, based on the observed SST pattern in the NCEP-R1 reanalysis. Note that SST variability may be less critical in the storylines presented here due to the forced atmosphere. The counterfactual SST conditions are created by subtracting a climatological warming pattern from the observed pattern, which is a standard procedure in probabilistic event attribution studies (Otto et al., 2012; Stott et al., 2016; Vautard et al., 2016). The warming pattern is computed using the 1850-2013 CMIP6 MPI-ESM1.2-HR pre-industrial control (PiCon) and historical simulations at an atmospheric horizontal resolution of

T127 (Müller et al., 2018). The procedure is shown in Equation 5.1:

$$SST_{t,c} = SST_t^{NCEPR1} - (SST_b^{CMIP6} - SST_{pi}^{CMIP6}) \tag{5.1}$$

where $SST_{t,c}$ is the counterfactual SST at time t, SST_t^{NCEPR1} is the NCEP-R1 original SST at time t, SST_b^{CMIP6} is the 2000-2009 average CMIP6 historical SST and SST_{pi}^{CMIP6} is the average CMIP6 PiCon SST. In Figure 5.1 the CMIP6 SST warming pattern closely resembles the observed Hadley Centre SST data set (HadSST3) (Kennedy et al., 2011a,b) warming pattern. The HadSST3 pattern is obtained by subtracting the 1880-1890 average from the 1980-1990 average SST values. The general warming and cooling patches in the Pacific Ocean and Atlantic Ocean south of Greenland agree well. Also, the warming north of Scandinavia is clearly visible in both warming patterns. Despite the observational data devoid region east of Greenland and north of Iceland, there is a close resemblance of the modelled warming pattern with observations. Note that early SST observations were dependent upon ship records, which in the polar region were very few (Rayner et al., 2006), causing this part of the observational data set to be incomplete.

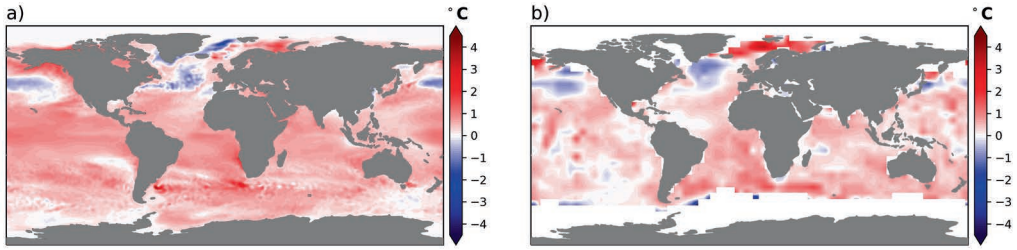

Figure 5.1: The sea surface temperature (SST) warming pattern [°C] a) calculated from MPI-ESM CMIP6 modelled data, and b) from HadSST3 observed data.

Given that the atmospheric circulation is nudged, changes in SIC are not expected to be relevant. The temperature gradient between pole and equator is influenced by SIC and thus SIC influences the formation of storms and the position and strength of the jet stream. In the nudging setup these atmospheric variables are forced towards reanalysis and therefore have limited influence from SIC. In order to check if the SST and SIC remain self-consistent, meaning that SST patches that are below -2 °C must have SIC formation, the pre-industrial counterfactual SSTs for July 2003 and July 2010 are shown together with the SIC in Figure 5.2. This shows that under counterfactual conditions, the SST remains almost completely physically self-consistent with

the SIC according to the constraints of Hurrell et al. (2008). There are only a very limited isolated regions where the SST falls below -2 °C. The counterfactual storyline has stationary pre-industrial GHG values, comparable to that of 1890, as listed in Table 5.1.

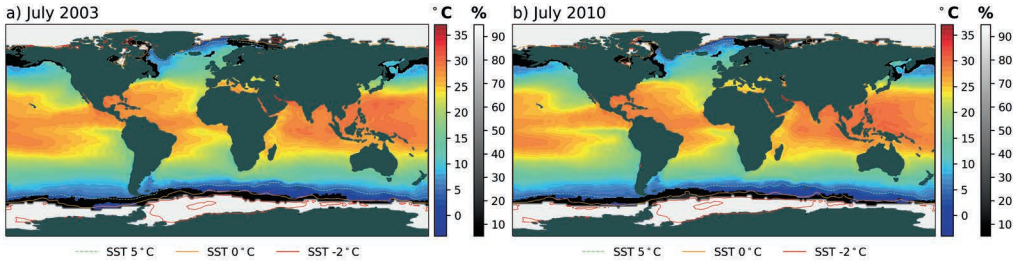

Figure 5.2: Counterfactual SST [°C] in shaded colours and factual SIC [%] in greyscales for (a) July 2003 and (b) July 2010. The SST 5 °C (dashed green), 0 °C (orange) and -2 °C (red) are marked for reference.

Table 5.1: greenhouse gases (GHG) for the ECHAM6 pre-industrial counterfactual simulations.

Greenhouse Gas	Concentration
Carbon dioxide (CO2)	285 ppmv
Methane (CH4)	790 ppbv
Nitrous oxide (N2O)	275 ppbv
Chlorofluorocarbons (CFC's)	0

The default initial conditions of ECHAM6 is a random atmospheric state in equilibrium with boundary conditions that are comparable to those in the mid-1990s. Changing that initial state to a counterfactual state requires a spin-up time, as the atmosphere and land surface need sufficient time to reach a new equilibrium with the altered SST and GHG boundary conditions. To accomplish this, a non-nudged counterfactual spin-up ensemble was run for three model years with three members. Each member was initiated at a different starting date (January, February, March 1995). The results of these spin-ups are three random atmospheric counterfactual states, which are used as initial conditions for the counterfactual experiments. For the model to correct the free atmospheric state to the nudged state requires approximately two model weeks, this is different from the spin-up time required to balance the new climatological background mentioned previously. The three counterfactual members are initiated on the 1st of January 2010.

5.2.2 European 2003 heatwave case study

For the European 2003 heatwave case study experiment, a smaller, separate simulation is run in both factual and counterfactual settings. The setup is identical to the one described in Section 5.1 and Section 5.2. However the members run for six months only, from the 1st of March 2003. Each member is initialized with a different member of the counterfactual spin-up (year three, March).

5.2.3 1948-2014 simulation

The 1948-2014 spectrally nudged counterfactual (ECHAM_SNC) data set is created to provide a pre-industrial counterfactual simulation, comparable to the 1948-2014 ECHAM spectrally nudged (ECHAM_SN) factual simulation by Schubert-Frisius et al. (2017). Note that ECHAM_SNC is not used for the case studies in this thesis, but is meant as a data set available to peers. Even so, ECHAM_SNC has distinct technical differences compared to the counterfactual storyline described in section 5.2 and therefore the method is explained in full.

The ECHAM_SNC simulation requires a more sophisticated approach in calculating SST and SIC values due to the length of the simulation. This is captured in the flow chart in Figure 5.3. The general idea of using a warming pattern is comparable to the 2010-2014 simulations (Equation 5.1). The big difference, however, is that ECHAM_SNC has twelve warming patterns, one for each month of the year, where the 2010-2014 counterfactual simulation has only one. Monthly warming patterns are beneficial over a general warming pattern, as they prevent the blurring of seasonal differences. Moreover, the monthly SST warming patterns have to be weighted over time, as a 2000-2009 monthly average would cause an overestimation of the climate signal if applied in earlier years. The weighting is facilitated using yearly globally averaged weighting factors.

The process of creating the monthly SST warming patterns is shown in Equation 5.2:

$$SST_{y,m,c} = SST_{y,m}^{NCEPR1} - w_y(SST_{h,m}^{CMIP6} - SST_{pi,m}^{CMIP6}) \tag{5.2}$$

where $SST_{y,m,c}$ is the counterfactual weighted SST for year y and month m, using $SST_{y,m}^{NCEPR1}$ as the SST observed for year y and month m, w_y is the weighting factor for year y, $SST_{h,m}^{CMIP6}$ is the 2000-2009 average CMIP6 historical SST for month m and $SST_{pi,m}^{CMIP6}$ is the average CMIP6 PiCon pre-industrial SST for month m.

The yearly weighting factors were calculated using the CMIP6 MIP-ESM historical and PiCon pre-industrial T2m, to make sure the weights are related to an atmospheric warming of 2 °C, as shown in the upper right part of Figure 5.3 and in more detail concerning the progression over each year in Figure 5.4. The historical T2m values were normalised to the 163 year averaged PiCon T2m, see Equation 5.3. This normalisation requires a bias correction, as the PiCon simulation has a slightly lower temperature average than the historical pre-industrial years (1850-1900), by 0.036 °C (α in Equation 5.3). After normalisation, any negative values are set to zero, to prevent negative weighting factors. The temperature progression is smoothed using a rolling mean (window=30 and periods=5, which means an average of 30 values, minimum of 5 values have to be present to calculate a usable result), as shown in Figure 5.4b. Smoothing a positive trend causes the smoothed average to be below the non-smoothed values, as is the case with the 2000-2009 smoothed average. The rolling mean is thus bias corrected by multiplying it with 1.05 to make the smoothed curve fit the not smoothed values. The process of creating the rolling mean weights is shown in Equation 5.4.

$$T^n = \frac{1}{5}\sum_{i=1}^{5}(T_{b,i} - T_{pi}) + \alpha \tag{5.3}$$

$$w_y = \frac{\frac{1}{5}\sum_{k=-2}^{2}(T^n_{(y-k)})\beta}{T^n_{2000-2009}} \tag{5.4}$$

where T^n is the normalized 1850-2013 yearly historical CMIP6 T2m, $T_{b,i}$ is the historical 1850-2013 CMIP6 two-meter temperature (5 members), T_{pi} is the 1850-2013 CMIP6 PiCon T2m (one member only), and α is the bias correction constant of 0.036. To compute the warming pattern w_y, the rolling mean of T^n (window=30, periods=5) is multiplied by the bias correction constant β (1.05) and divided by the normalised 2000-2009 historical T2m average ($T^n_{2000-2009}$), which is the set of years selected to compute the SST warming pattern and thus is equal to a weighting of 1.

The SIC values are computed based on the weighted counterfactual SST values as described by Hurrell et al. (2008), see the bottom part of the flow chart in Figure 5.3. The relationship between ice fraction and SST, is tested for several upper temperature limits. In Figure 5.5 the effect of 4.9 °C, 3 °C and 1 °C upper temperature limits is shown in comparison with Modern-Era Retrospective Analysis version 2 (MERRA-2) SIC reanalysis data (Gelaro et al., 2017). The upper limit temperature is a threshold above which no sea ice is permitted to form. The exact threshold will influence the SIC avail-

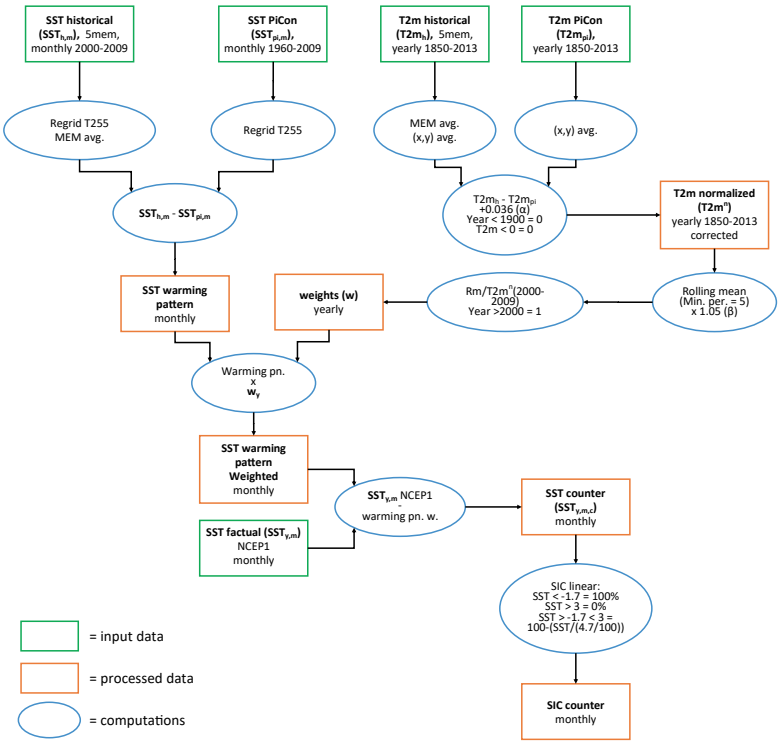

Figure 5.3: Flowchart for creating ECHAM_SNC counterfactual SST and SIC.

able in the simulations. Although none of the temperature limits agrees completely with the MERRA-2 reanalysis, the 3 °C SIC concentrations give the best results for the Boreal summer. Since the Northern Hemisphere land mass is much closer to its pole than the land mass of the Southern Hemisphere, deviations of Arctic ice may cause the largest influences on the simulations of over land weather. Therefore, the 3 °C upper temperature limit is selected. Note that the influence of SIC is limited in the storyline experiment, due to the nudging of the atmosphere overwriting the pole to equator temperature gradient influence on the formation of storms and the position and strength of the jet stream.

The nudging conditions and GHG values are equal to those in the 2010-2014 counterfactual simulations (see Table 5.1). In addition, the initialisation is performed the same way, using the counterfactual spin up result.

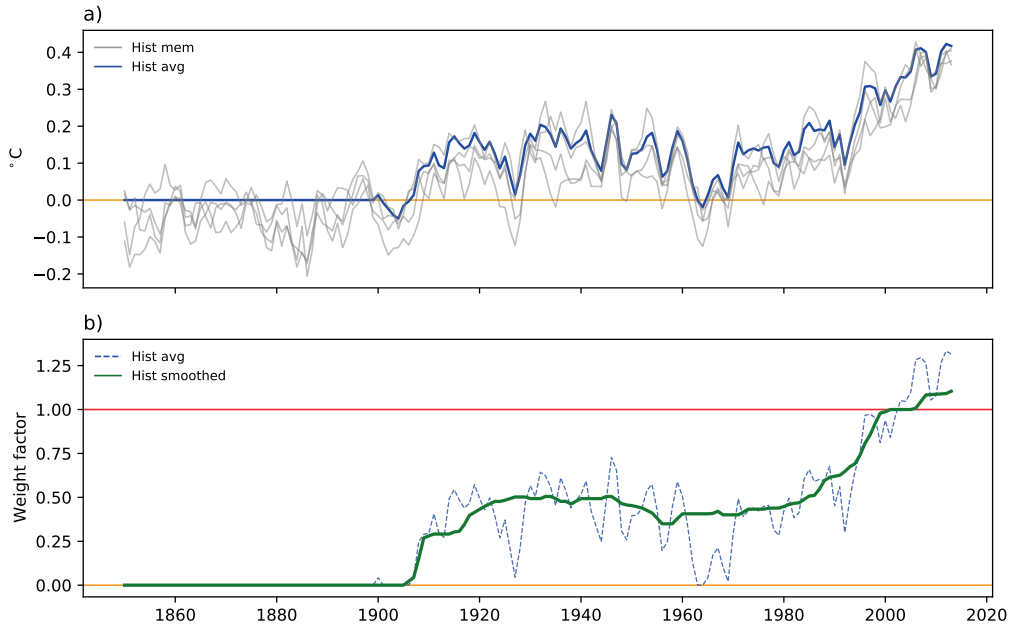

Figure 5.4: Process of computing counterfactual weighting factors. a) time series of CMIP6 MPI-ESM historical T2m, individual members (grey lines), member average (blue line), normalised using the CMIP6 MPI-ESM PiCon pre-industrial average, orange line on zero for reference. b) time series of weighting factors, non-smoothed weighting factors (blue dashed line), the smoothed weighting factors (green line), pre-industrial zero lower limit (orange line) and the warming pattern 2000-2009 upper limit (red line).

Analysis of the ECHAM_SNC simulation shows that the procedure does not adequately account for the averaged global T2m. Figure 5.6a shows the global average T2m for the ECHAM_SN, ECHAM_SNC and an offset ECHAM_SNC. The averaged global temperature of ECHAM_SNC is systematically too cold. The offset temperatures are bias corrected for 1.008 °C to check for the expected fit with ECHAM_SN, meaning that the pre-industrial years of both ECHAM_SN and the offset ECHAM_SNC are overlapping, the recent years show an increase in temperature for the ECHAM_SN dataset due to the climate signal where ECHAM_SNC remains stable at pre-industrial levels. This means that the ECHAM_SNC global average T2m is 1 °C too cold. In panel b, the difference in temperature between ECHAM_SN and ECHAM_SNC in °C is shown, and in panel c, the average T2m versus degree latitude. These two panels depict where the temperature underestimation originates. There is a clear temperature problem at the poles, where the ECHAM_SNC is locally up to 10 °C too cold. The zonal averages show that this is unique to the ECHAM_SNC simulation, as the difference between factual and counterfactual is

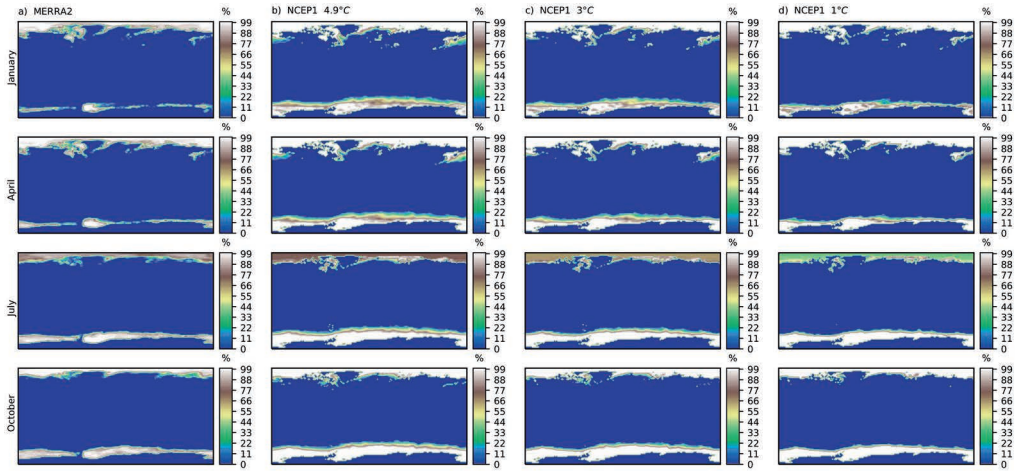

Figure 5.5: Comparison of a) MERRA-2 SIC and the SIC based on the NCEP SST values for different upper temperature limit above which no sea ice is permitted to form b) 4.9 °C, c) 3 °C and d) 1 °C.

much more subtle than ECHAM_SNC portrays. The problem lies in the SIC alterations made for the long simulation, meaning that the counterfactual SIC is overestimated and causes a temperature drop in the atmosphere directly above the ice.

However, the spectral nudging limits the influence of the underestimated polar temperature. For example, the number and strength of storms is nudged towards NCEP-R1 and therefore not influenced by an altered pole-equator temperature gradient, the same holds for the location and duration of an atmospheric blocking. Despite the polar region temperature underestimation, the data remains usable for attribution research between 50 °S and 65 °N, noted with dashed grey lines in Figure 5.6 panel b and c. The truncated dataset will be made available for peers, be it with a user warning.

5.3 Plus 2 degrees counterfactual

The technical aspects of the plus2 storyline is based on the same principle as the 2010-2014 counterfactual, including unaltered SIC, but with different SST and GHG levels. The boundary conditions are estimated using the CMIP6 MPI-ESM ssp585 scenario, a scenario based on a combination of the representative concentration pathways (RCP) 8.5 global forcing, with the shared socioeconomic pathway (ssp) number five. Both these RCP and SSP scenarios simulate a high-end possible future (O'Neill et al., 2014) and shows a close to linear increase in temperature until after the 2 °C global warming mark, where other scenarios tend to stabilize before that point. Despite the low chances of the RCP8.5 scenario actually materialising in the future (Stammer et

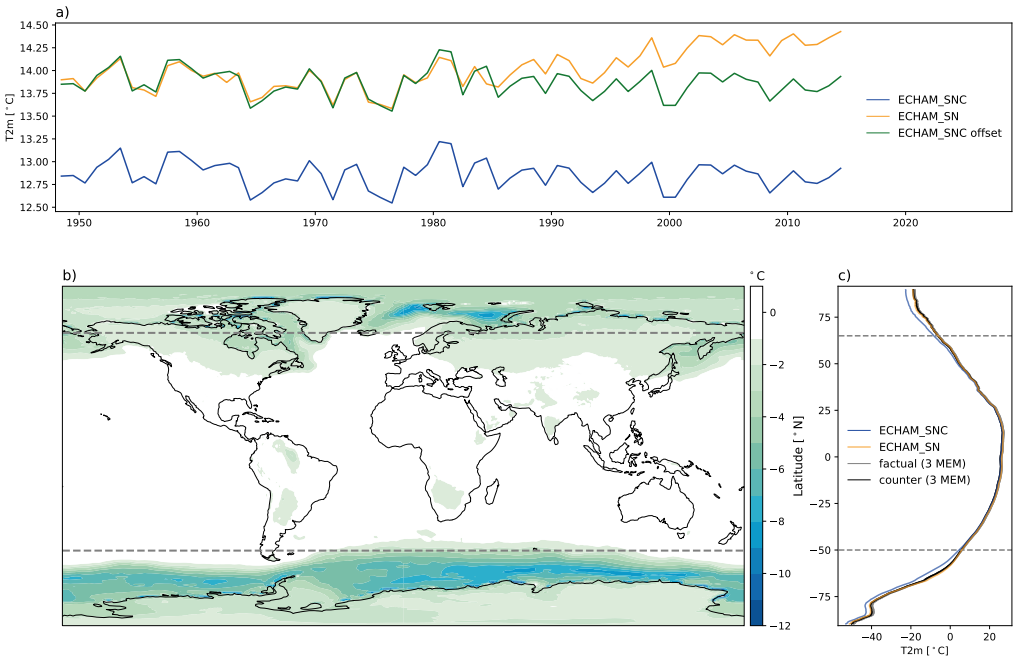

Figure 5.6: 1948-2015 2 meter temperature for a) ECHAM_SNC, ECHAM_SN and an offset of ECHAM_SNC by adding 1.008 °C to the ECHAM_SNC global average values b) difference between ECHAM_SNC and ECHAM_SN time average, and c) 2 meter temperature averages per latitude for ECHAM_SNC in blue, ECHAM_SN in orange, the three factual and counterfactual members (2010-2014 simulations) in grey and black respectively. Grey dashed line is the set limit of reliable data based on T2m underestimation, which is at 65 °N and 50 °S.

al., 2021), the plus2 storylines can be accurately built with it as only the GHG and SST values are used as a reference for a two degrees warmer world. The T2m exceeds two degrees global warming, with respect to the pre-industrial temperature, between the years 2044 to 2053. That time period is then used to create an SST warming pattern and calculate the GHG concentrations, which form the new boundary conditions. The latter are the 2044-2053 average GHG concentrations, as listed in Table 5.2.

To create SSTs for the plus2 storyline, a weighted warming pattern is added to the NCEP-R1 observed SST as shown in Equation 5.5. As with the 2010-2014 counterfactual simulation (Equation 5.1), one general warming pattern is computed. This warming pattern translates to a 2 °C global warming in comparison to pre-industrial circumstances. The NCEP-R1 SST values include a climate-change signal, and thus the warming pattern needs to be weighted to account for the inherent transient climate-change signal in the time series. As an example, the NCEP-R1 SST file of January 2012 will already have a climate signal in it that corresponds to the level of climate change

Table 5.2: The greenhouse gases (GHG) concentrations for the ECHAM6 plus 2 degree counterfactual simulations.

Greenhouse Gas	Concentration
Carbon dioxide (CO2)	553 ppmv
Methane (CH4)	2411 ppbv
Nitrous oxide (N2O)	357 ppbv
Trichlorofluoromethane (CFC11)	142 pptv
Dichlorodifluoromethane (CFC12)	370 pptv

in 2012. If a warming pattern with the difference between a plus2 and pre-industrial world would be added, the result would overshoot. The warming pattern has to be weighted in such a way that it adds only the climate signal between 2012 and the plus2 degree world, so that it totals to the correct climate signal. The process of calculating the plus2 SST is therefore as in Equation 5.5.

$$SST_{y,m,p2} = SST_{y,m}^{NCEPR1} + w_y(SST_s^{CMIP6} - SST_{pi}^{CMIP6}) \tag{5.5}$$

where $SST_{y,m,p2}$ is the plus2 weighted SST at year y and month m, using $SST_{y,m}^{NCEPR1}$ as the SST observed at year y and month m, w_y is the weighting factor at year y, SST_s^{CMIP6} is the 2044-2053 average of the CMIP6 ssp585 scenario SST and SST_{pi}^{CMIP6} is the CMIP6 historical 1850-1920 average.

The weighting factors are computed based on the normalised atmospheric near-surface temperature member values shown in the Figure 5.7a, which runs from 1850-2100. These years of data are a combination of the historical simulation (1850-2014) and the ssp585 scenario (2015-2100) T2m, and exhibits a smooth transition from one dataset to the other. The normalised T2m is computed as shown in Equation 5.6, where T_{p2}^n is the normalized CMIP6 historical and ssp585 yearly T2m, $T_{b,i}$ is the CMIP6 historical and ssp585 scenario T2m (1850-2100, 10 members) and T_{pi} is the 1850-1920 T2m reference, computed from the CMIP6 historical MPI-ESM simulation (10 members). As normalisation was performed with the years 1850-1920, their values are set to zero to prevent negative weighting factors. To compute the warming pattern (w_y) as in Equation 5.7, the rolling mean (windows=30, periods=5) is calculated for the complement of T^n divided by T_{max} with T_{max} being the 2 °C of global warming considered. The weighting factors have to be computed from the complement to ensure both the smaller climate signals in earlier years and the large climate signal in the more recent years all increased to a maximum of 2 °C warming. In Figure 5.7b the results show

a good fit of the smoothed weighting factors (green) with the member average (blue dashed).

$$T_{p2}^{n} = \frac{1}{10}\sum_{i=1}^{10}(T_{h,i} - T_{pi,i}) \tag{5.6}$$

$$w_y = \frac{1}{5}\sum_{k=-2}^{2}\left(\left(1 - \frac{T_{p2}^{n}}{T_{max}}\right)_{(y-k)}\right) \tag{5.7}$$

Figure 5.7 shows the computation for weights based on T2m. In panel a, the T2m for the 10 members of the CMIP6 MPI-ESM ssp585 scenario, an average of the members and a rolling mean of that average are visualized. The values are normalized for the pre-industrial average (orange line). The red horizontal line represents the two degrees of increased global temperature. In panel b these temperatures are then transferred to weights with a value of one for the years that have no inherit climate-change signal, zero for the years used for the warming pattern average, and a negative number (which would cause a strengthening of the warming pattern) for the years after which the warming pattern is made. Since the plus2 simulation spans the years 2010-2014, there is no need for negative weights in this application.

Note that the boundary conditions used to create the storyline were taken from a two degree warmer world, the resulting difference is only 1.55 °C between plus2 (global average mean temperature 15.15 °C) and counterfactual (global average mean temperature 13.60 °C). The storyline is labelled plus2 based on the underlying boundary conditions, but resulted in a conservative estimation of the actual climate-change signal.

5.4 Reference data-sets

Throughout this study there are several observation and reanalysis datasets used for comparison with the findings. They are shortly listed here:

1. Reanalysis
    (a) ECMWF Reanalysis v5 (ERA5) (Hersbach et al., 2020)

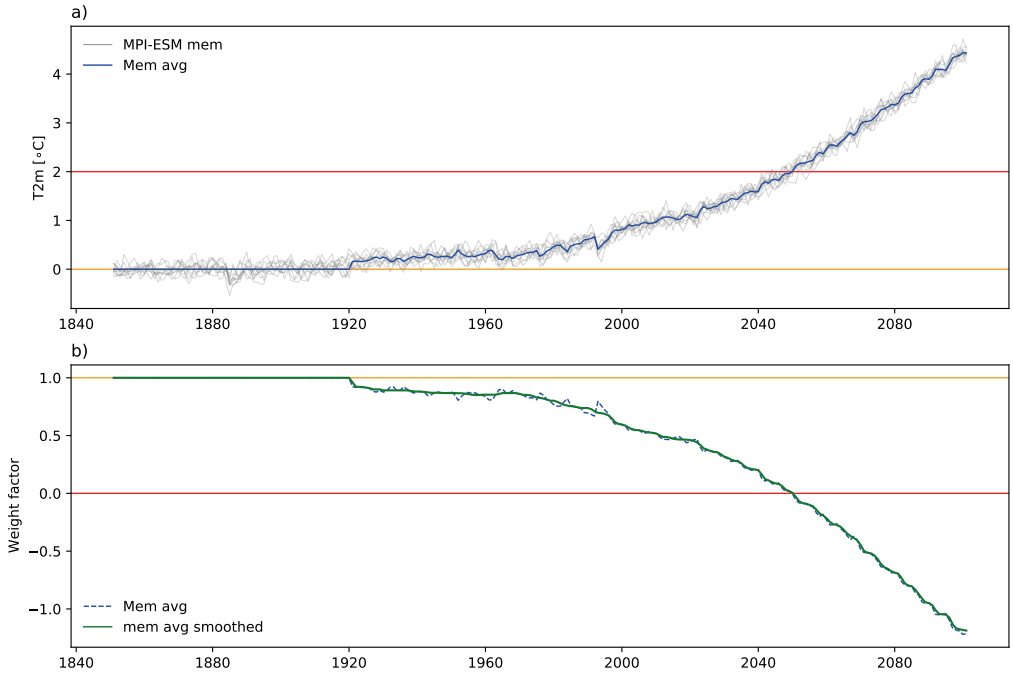

Figure 5.7: Process of computing plus2 weighting factors where a) is the two-meter temperature of the CMIP6 MPI-M historical and ssp585 scenario simulations, 10 members (grey lines). The member average is shown in blue. b) weighting factors of inverse member average in blue and rolling mean in green.

(b) ECMWF Reanalysis vInterim (ERA-Interim) (Dee et al., 2011)

2. Observations

(a) Global Precipitation Climatology Centre (GPCC) (Schneider et al., 2015)

(b) Global Precipitation Climatology Project (GPCP) (Huffman et al., 2009)

(c) Met Office Hadley Centre United Kingdom gridded climate observations (HadUK-Grid) (Hollis et al., 2019)

Results with temperature fields are generally compared to those in ERA-Interim and later in ERA5. Since the change from the older ERA-Interim to the new ERA5 happened during the time of this study, there are results still compared to the first and others to the second. NCEP-R1 is the nudging data and therefore at times it is used for reference to show if the extreme event under study is well resolved in the nudging dataset. Precipitation results are compared to either GPCC or GPCP depending on the need for over sea data (GPCP, lower resolution) or over land only (GPCC, higher resolution). As for precipitation in the United Kingdom, the HadUK-Grid dataset

provides a high resolution observational dataset to compare results with. Generally, the choice for observational references when studying precipitation is based on the known struggles of reanalysis data to resolve precipitation correctly (Bosilovich et al., 2008).

Part III

Results

The conditional attribution of global and regional temperature and hydrological changes are first shown. This will offer insight into the performance of the storyline method, and the large scale climate change induced alterations. Secondly, the case study results for both temperature and hydrological extremes are analysed in detail. The case studies involve the European heatwave of 2003 and the Russian heatwave of 2010. The hydrological extreme case studies are the southeastern South-American drought of 2011/2012 and the South-England flooding of 2014.

6 Global Trends

6.1 Temperature

The world has observed the effect of climate change on global average air temperatures, approximately 0.7 - 0.8 °C between pre-industrial times and 2010 (IPCC, 2018). Well simulated average global temperatures will therefore be a good indication that the experiments are performed reliably. The average global T2m could be reproduced by combinations of different forcings. Therefore, it is important to also look into the spatially resolved pattern of climate change during historical times to validate the robustness of the climate model and associated simulations. In Figure 6.1a, the 2010-2014 two-meter temperature (T2m) global averaged temperatures of the three storylines are compared, with ERA5 as a reference. ERA5 and the factual storyline members follow the same values closely. The storylines are clearly split from each other, and the three members per storyline show little differences between them. The dashed horizontal lines show the average of each storyline respectively, which are 13.60 °C in the counter storyline; 14.28 °C in the factual storyline; and 15.16 °C in the plus2 storyline. The difference between pre-industrial and present day is therefore 0.68 °C, and a good approximation of global warming. The plus 2 degree storyline is actually 1.6 °C warmer than the counterfactual storylines, which makes the experiment conservative as it underestimates the global warming by 0.4 °C. In Figure 6.1b the factual member average two-meter temperature shows a realistic temperature gradient over the globe, in panel c and d the different storylines are compared to each other with stippling to indicate

robustness (where the members of each storylines are separated by at least 0.1 °C from the members of the other storyline).

The SST warming pattern is clearly visible in the over sea air temperatures (see also Figure 5.1). When comparing the factual and counterfactual (panel c), the warming is uniformly robust over the globe and is especially evident over land, with a maximum regional warming up to 2.0°C. For the warming in the plus2 degree world, the signal becomes even clearer. The signal stays equally robust but has now reached a maximum regional temperature increase up to 2.3°C. Despite the signal being globally robust, the actual value of warming is not the same over each area of landmass, nor is it the same between past (panels c) and future (panels d). A remarkable difference is found for the warming of Scandinavia, where in the past a strong warming has been counter balanced by a cooling SST patch near the coast, and in the future that cooling patch has strongly diminished, causing Scandinavia to warm up as strongly as central Russia. The cooling SST pattern mostly occurs in the central Atlantic, affecting not only Scandinavia but also large portions of the North East Atlantic and Nordic seas. It is generally related to the so-called North Atlantic Warming hole. There is no consensus on the cause of the warming hole, a possible cause is a decrease in the North Atlantic Meridional Overturning Circulation (NAMOC). This effect might, however, be compensated in the future by a steady increase in temperatures (Keil et al., 2020). Overall, there is a strong and robust climate signal in the global two-meter temperatures.

The climate signal in temperature varies between seasons as much as it varies per location. In Figure 6.2 the factual and the differences between factual and counterfactual, as well as plus2 and factual, are shown per season (December-January-February (DJF), March-April-May (MAM), June-July-August (JJA), September-October-November (SON)). The strongest temperature increases over land are visible for JJA with a maximum regional temperature increase between factual and counter of 2.8 °C and between plus2 and factual of 3.7 °C, see also Table 6.1. The overall largest regional temperature differences between factual and counter can be found in the Middle East in JJA and SON, when this region is going through their summer. Despite a difference in the absolute temperatures per season, the robustness of the climate signal stays equally strong over the seasons.

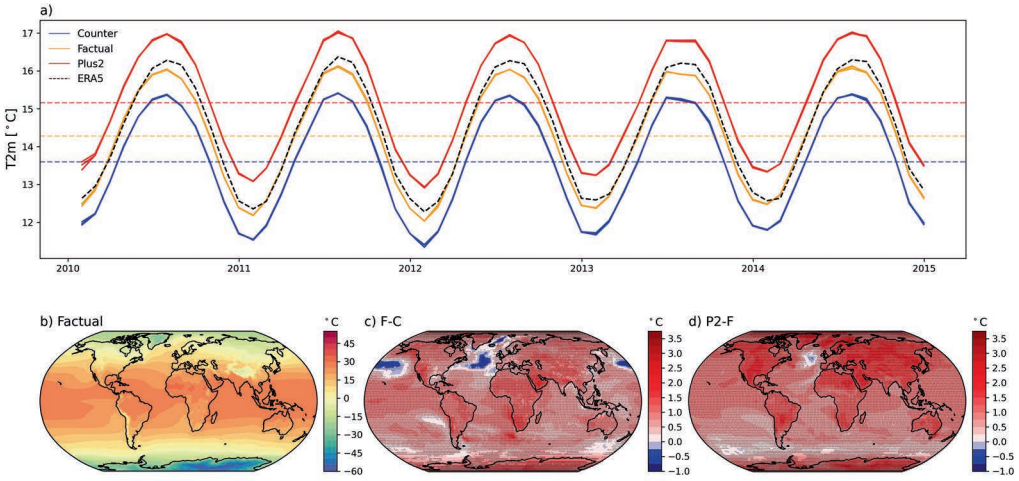

Figure 6.1: Global 2010-2014 two-meter temperature for a) monthly global average for the three storylines and ERA5 for reference, the average temperature per storyline in dashed coloured lines respectively. b) factual member average, c) difference between factual and counterfactual member average storylines, d) difference between the plus2 and the factual member average storylines. Stippling indicates robustness, where all the members of each storyline are well separated from those of the other storyline by at least 0.1 °C.

Table 6.1: Average and maximum global seasonal temperature differences

Season	F-C max	F-C mean	P-F max	P-F mean
DJF	2.34	0.69	2.68	0.95
MAM	2.06	0.70	2.46	0.89
JJA	2.76	0.69	3.67	0.89
SON	2.70	0.73	3.41	0.94

6.2 Precipitation

Precipitation response to climate change is not as uniform over the globe as is temperature. Figure 6.3 shows the average precipitation anomaly over 2010-2014 for a) Factual anomaly calculated based on ECHAM_SN climatology, b) Global Precipitation Climatology Project (GPCP) observations, c) ERA5 reanalysis, d) difference between factual member average and the GPCP observations, e) difference between the factual member average and ERA5 reanalysis, f) difference between GPCP observations and ERA5 reanalysis, g) difference between factual and counterfactual member averages, h) difference between plus2 and factual member averages, i) difference between plus2 and counterfactual, j) overview of domains used in the global precipitation study: A is Mexico, B is Scandinavia, C is Australia and D is India. The global regions are NH

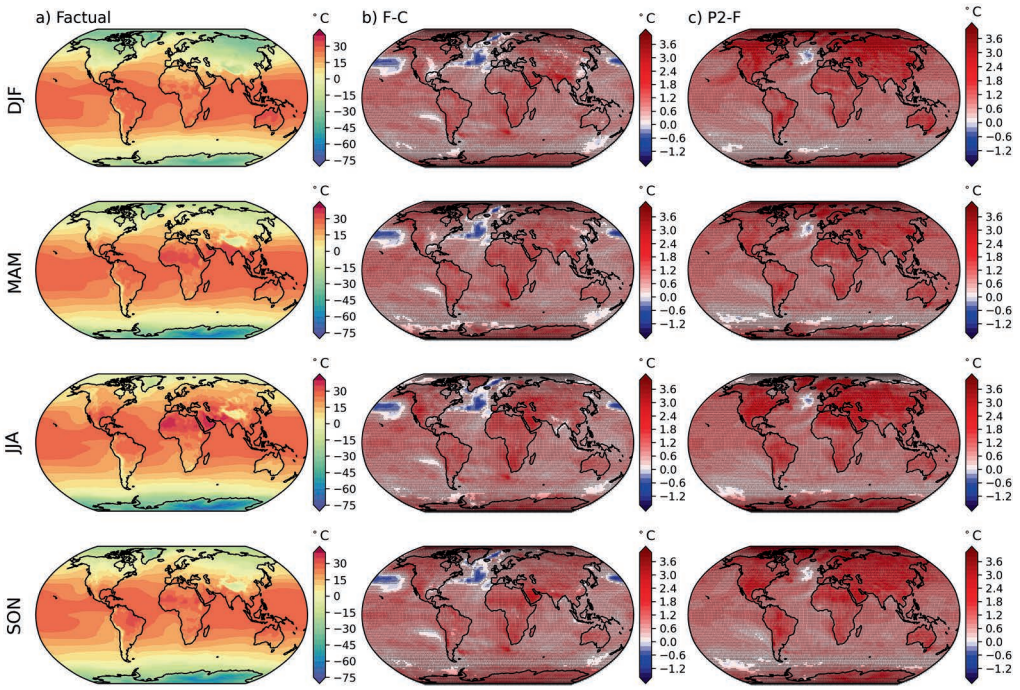

Figure 6.2: Seasonal 2010-2014 averaged two-meter temperature for a) factual member average, b) difference between factual and counterfactual member average, and c) the difference between plus2 and factual member average.

for Northern Hemisphere, TR for tropical region and SH for Southern Hemisphere. Precipitation anomalies are shown for a clearer view on the differences between the worlds, where for temperature in the previous section the climatology maps were sufficient. Over the Pacific, the Americas, the North Atlantic, Europe and Russia the factual simulation matches well with the observations and reanalysis. However, over the Indian Ocean, northern Africa and the Middle East ECHAM6 overestimates the precipitation. This is clear from panel d and e where the difference between the factual member average and the observations and reanalysis are shown. Note that the reanalysis also has over and underestimation issues, as shown in panel f, as precipitation is a complex variable to resolve. The difference between the storylines for global precipitation show a clear pattern of drying over Europe, north-west Africa, Central America and west United States, and a pronounced wetting over Canada, most of South America and equatorial Africa. The difference in the past (panel g) and the future (panel h) are not linear, presumably due to the differences in SST warming patterns for the past and future, and so affecting the alterations in precipitation patterns.

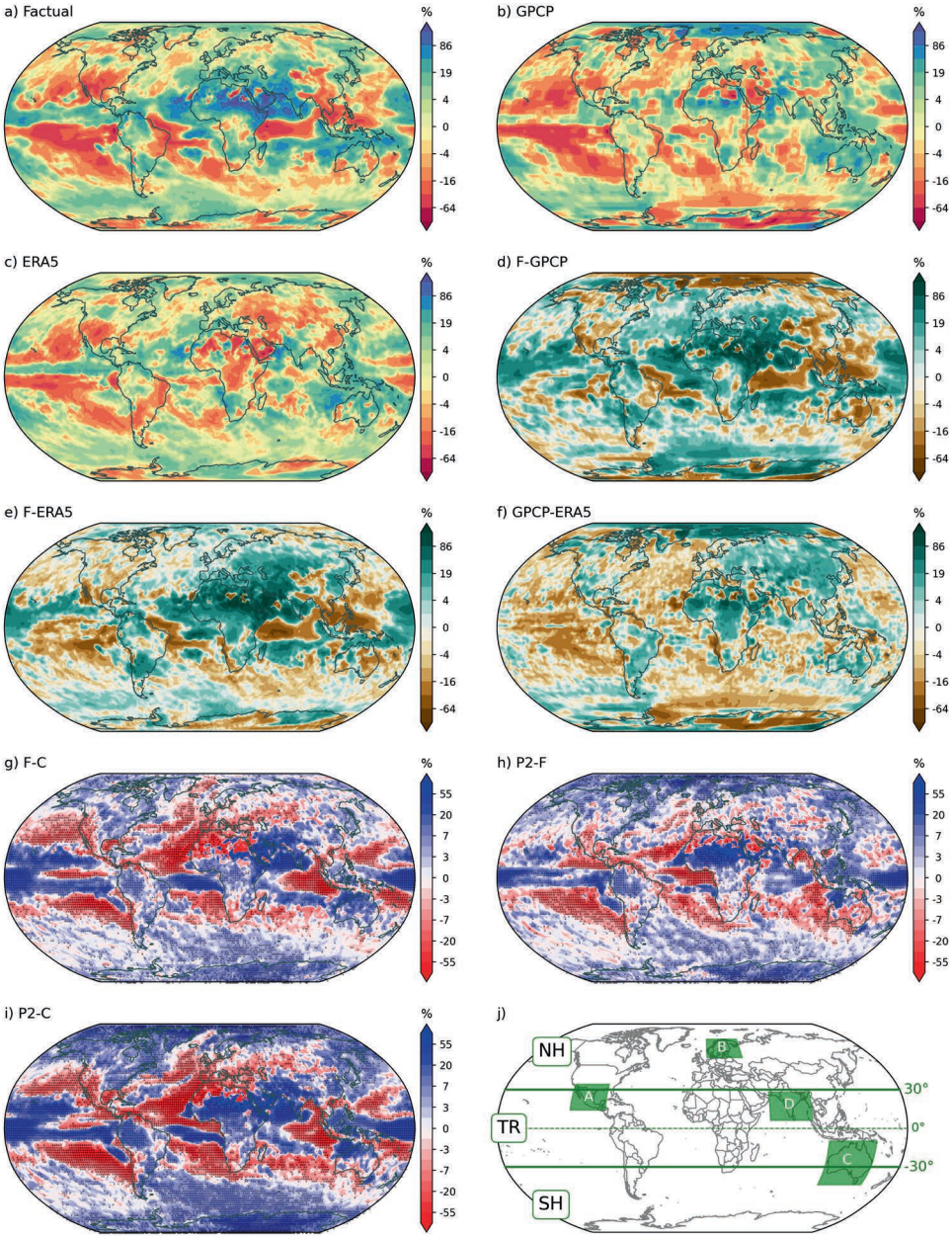

Figure 6.3: Global 2010-2014 precipitation anomalies in % based on 1981-2010 climatology for a) Factual anomaly calculated based on ECHAM_SN climatology, b) Global Precipitation Climatology Project (GPCP) observations, c) ERA5 reanalysis, d) difference between factual member average and the GPCP observations, e) difference between the factual member average and ERA5 reanalysis, f) difference between GPCP observations and ERA5 reanalysis, g) difference between factual and counterfactual member averages, h) difference between plus2 and factual member averages, i) difference between plus2 and counterfactual, j) overview of domains used in the global precipitation study: A is Mexico, B is Scandinavia, C is Australia and D is India. The global regions are NH for Northern Hemisphere, TR for tropical region and SH for Southern Hemisphere.

The areas that show a consistent sign generally are the regions for which there is a robust signal (denoted with stippling where all members of each storylines are well separated from those of the other storyline). This leaves uncertainties for regions such as Asia and Australia. Precipitation attribution is more complex than temperature attribution due to the complexity in the generation of precipitation of either convective or stratiform precipitation processes, which are depending on localised hydroclimate variability.

In Figure 6.4 the average precipitation in $mm \cdot day^{-1}$ for a) the globe, b) the Northern Hemisphere, c) the Tropical region and d) the Southern Hemisphere are shown (see also Figure 6.3j for the definition of each of these subregions), in comparison to MPI-M coupled model climatology and both ERA5 reanalysis and GPCP observations for reference. As precipitation is strongly influenced by SSTs, especially in the vicinity of coastal areas and the tropics, the outcome of our atmosphere-only simulations are compared to the MPI-M coupled simulations. The nudged storylines nicely capture the year to year variability in precipitation. The total precipitation in the model is overestimated compared to observations, which can be traced back to the precipitation simulations of the tropical region in panel c. Each storyline shows a clear separation from the others, meaning that the precipitation amounts in the storylines are altered due to climate change. A good example of climate change induced alterations to the thermodynamics of precipitation is the winter of 2013/2014 for the Northern Hemisphere, where the plus2 storyline completely separates from the factual and counterfactual. The climate signal is variable over time, and shows differences in each season. In the tropics, the largest difference between storylines is found in the summers. In the Southern Hemisphere the signal is far less strong, though still clearly visible for austral winter, where the precipitation peaks. The global precipitation increases systematically in line with increased global warming, according to the Clausius-Clapeyron relationship.

Some regions have been found to become dryer with climate change, while others become wetter (IPCC, 2018). However, the year-to-year seasonal climate-change signal variability within a region is unknown. Due to the strong regional differences, the precipitation response to climate change is further analysed using 4 regional domains (denoted with A to D in Figure 6.3j): Mexico, Scandinavia, Australia and India. The selection is based on the Intergovermental Panel on Climate Change (IPCC) reported effects of climate change on the precipitation of each of these regions. In the following sections, the results are further explained per region. Since each section will follow the same structure, the analysis applied is first briefly explained before going into the separate sections.

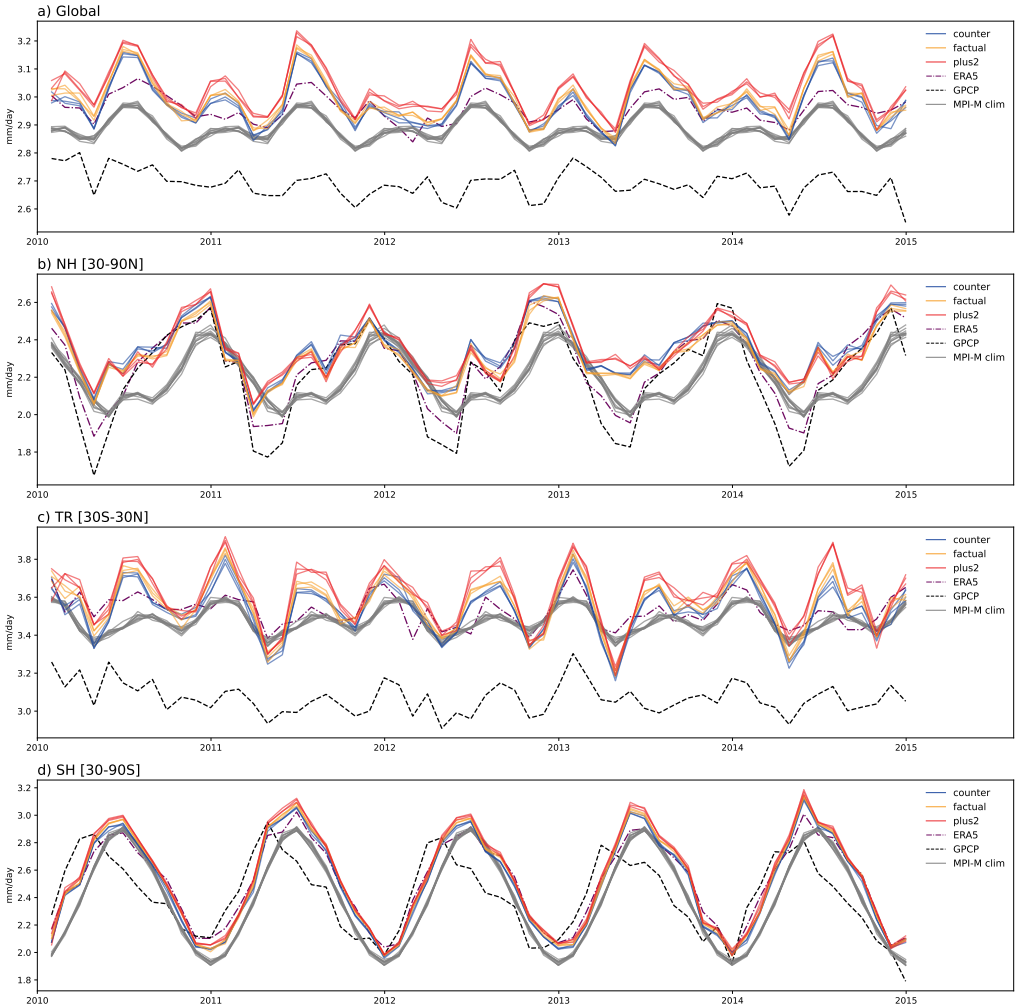

Figure 6.4: Monthly total precipitation over time for a) global, b) Northern Hemisphere (30 °N-90 °N), c) Tropics (30 °S-30 °N) and d) Southern Hemisphere (30 °S-90 °S). In blue the counterfactual, yellow the factual and red the plus2 simulation, black dashed line is GPCP observations, purple dashed-dotted line is ERA5 reanalysis and grey the MPI-M mean climatology (1981-2010) for 10 members.

The 2010-2014 precipitation analysis per region is followed by an analysis of two seasons per region. The events are marked with a black box in Figure 6.5 and further detailed in Table 6.2. The Scandinavian events exemplify the effect of climate change in two different seasons, Australia showcases two events in the same season but with different anomalies. India and Mexico both showcase monsoon seasons, though very different in characteristics from each other. In Figure 6.5 the monthly average precip-

itation over each region is shown. The storylines are compared to GPCP observations for reference. Since El Niño–Southern Oscillation (ENSO) and Circumglobal Teleconnection Index (CGTI) have a large influence on precipitation and monsoon patterns (further explained in section 6.2.4), their index is added in panel e. In Figure 6.6 the maps for factual precipitation is found in panel a, the past (difference between factual and counter) in panel b, the future (difference between plus2 and factual) in panel c, and the overall climate signal (difference between plus2 and counter) in panel d. The stippling in the maps shows robustness, where all the members of one storyline are well separated from the members of the other storyline by at least 1 %. The precipitation differences found between the factual, counterfactual and plus2 simulations are meaningful if they are outside of the internal variability within each ensemble. A different way of saying this, is that the differences are meaningful if the two ensembles are distinguishable from each other. To assess this in a statistical manner, temperature differences between pairs of factual members (FF), counterfactual members (CC), plus2 member (PP), factual-counterfactual pairs (FC), plus2-factual pairs (PF) and plus-counterfactual pairs (PC) are plotted for each extreme in Figure 6.7. The FF, CC and PP pairs have a median close to zero and represent the noise level and consist each of three pairs (F1-F2, F2-F3, F3-F1 / C1-C2, C2-C3, C3-C1 / P1-P2, P2-P3, P3-P1). The FC, PF and PC pairs contain the signal, each consisting of nine pairs (FC example: F1-C1, F2-C2, F3-C3, F2-C1, F3-C2, F1-C3, F3-C1, F1-C2, F2-C3). Each box plot represents the distribution of precipitation differences across the pairs and across all grid points. The grey horizontal band is the noise level of the median based on the CC, FF and PP medians. The grey dotted line is for reference only.

6.2.1 Mexico

Mexico has a summer monsoon climate, with precipitation between July and September. Monsoons have a strong dynamical factor in their timing and location, which may explain why attribution studies have struggled with large uncertainties in how the North American Monsoon (NAM) might respond to climate change (Wang et al., 2021). Some studies found a pronounced drying effect (Cook and Seager, 2013; He et al., 2020), others either a weak drying signal, or no effect (Pascale et al., 2019), and again others found an increase in precipitation (Carvalho, 2020). Despite the scarcity of precipitation observations in Mexico, there are observational studies available that found a general decrease in Mexican precipitation between 1970 and 2000 (Cuervo-Robayo et al., 2020). While a lack of observations makes analysis difficult, the large uncertainties in the models can rather be linked to the uncertainties from the dynamical situation (Pascale et al., 2019). That is exactly why the method presented

Table 6.2: Description of case study events per study region.

Region	Event	Months	Seasons	Coordinates	Countries
Mexico	M1	JA	Monsoon	14°-34°N | 117°-86°W	Mexico, Guatamala, Belize, southern United States of America, northern tip of Honduras
	M2	JAS			
Scandinavia	S1	JAS	Summer	55°-71°N | 5°-41°E	Norway, Denmark, Sweden, Finland, Latvia, Estonia, northern Lithuania and Belarus, north-western tip of Russia
	S2	OND	Autumn		
Australia	A1	DJFM	Summer	10°-44°S | 112°-154°E	Australia
	A2	FM			
India	I1	JJA	Monsoon	6°-28°N | 60°-97°E	India, Sri Lanka, Bangladesh, south-eastern tip of Pakistan and Nepal, south Bhutan, west Myanmar
	I2	JJA			

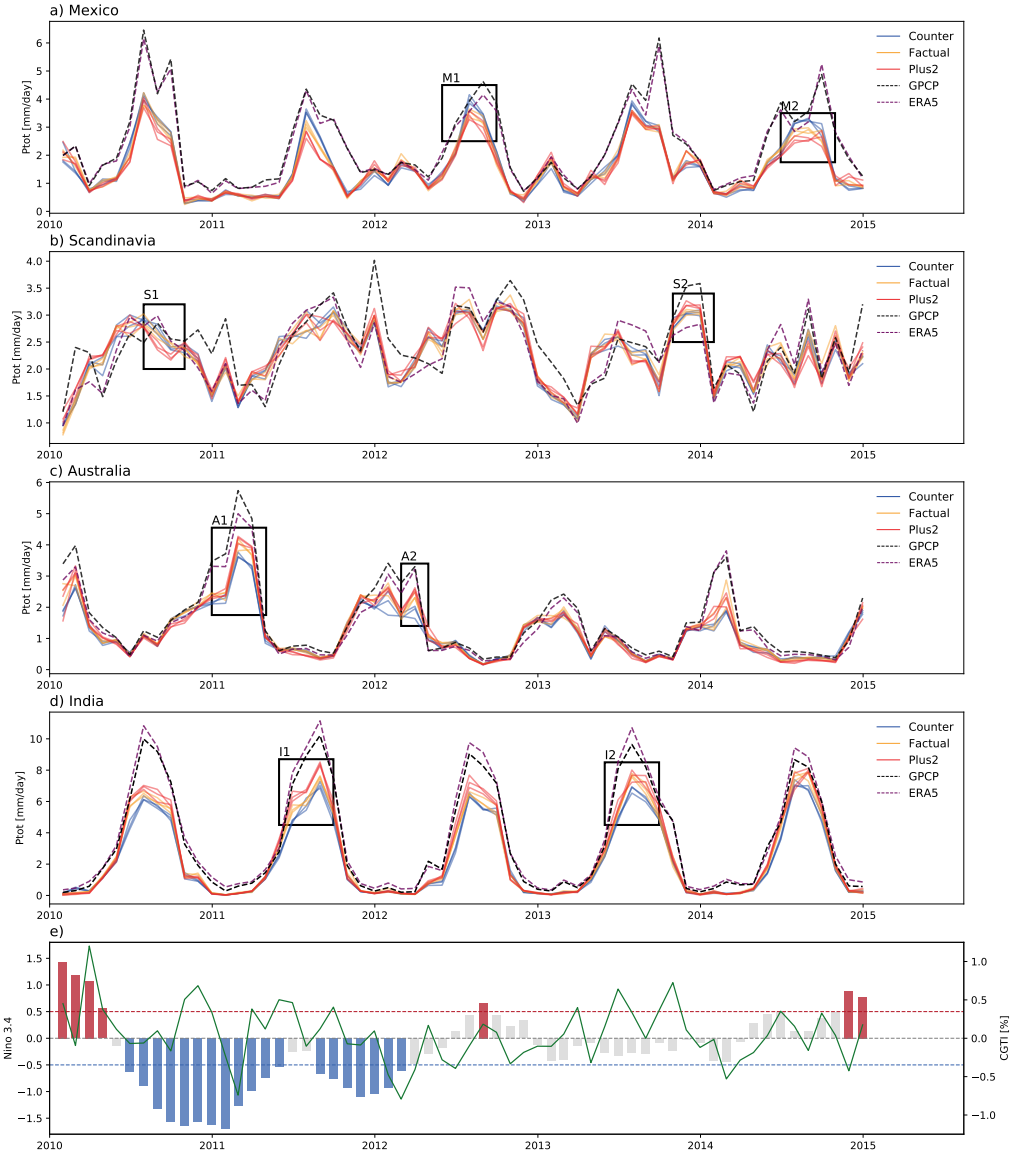

Figure 6.5: Monthly total precipitation [mm/day] and the two case study events marked with a black box for a) Mexico, b) Scandinavia, c) Australia and d) India. For comparison e) is the El Niño Southern Oscillation index (Nino 3.4) in bars, blue for La Niña (values reaching below blue dashed line, axis on the left and red for El Niño (values reaching above red dashed line, axis on the left). The green line is the Circumglobal Teleconnection Index (CGTI) [%], of which positive values indicate increased precipitation in the north-west of India (axis on the right), calculated with NCEP-R1 geopotential height at 200 hPa.

here is an important tool for analysing climate change and monsoonal rains.

In Figure 6.5a, the total domain average precipitation over time shows the distinct inter-annual monsoon variability. During the monsoon precipitation, the counterfactual peaks with the highest amount, which indicates that in a world without climate change there would be more precipitation, and shows a drying of the NAM. Finding an increased climate signal during large precipitation events could indicate a state dependent climate signal.

The two selected case study events (M1 and M2 in Figure 6.5), have comparable anomalies in the factual as shown in Figure 6.6a – M1 and M2, and both have a negative anomaly in the north-west and east coast. There is a positive anomaly visible in a band from north to south at the centre of Mexico. Anomalies are visibly stronger in M2 than M1. The differences between future and past, for both events, show a strong reduction of precipitation on the western half of Mexico, and nearly all of the southern domain. The differences between past (F-C) and future (P2-F) are not equal over space, though they do show the same sign – a drying. In Figure 6.7a the robustness of the drying trend is visualised in the signal-to-noise analysis. Note that despite a clear signal from noise for M1 FC, this is not so clear for the M1 PF. This indicates, as seen in Figure 6.6, that the changes in the past, and those in the future are not the same. There is no linear response of precipitation to the increasing climate signal. That said, the overall climate signal (PC) is robust, moving far out of the region of noise, for a decrease in NAM precipitation during the 2012 and 2014 events.

6.2.2 Scandinavia

Scandinavia's climate goes from mild in the southern regions to alpine tundra climate in the Norwegian and Swedish mountains. Precipitation happens throughout the year, but is generally the most present from mid-summer all the way through to the beginning of winter. Climate change is expected to cause an increase in precipitation (Hanssen-Bauer et al., 2005; Sillmann et al., 2013), but results differ vastly from region to region (Devasthale et al., 2022). Moreover, the characteristics of precipitation is different whereas monsoons are in a tropical climate with a strong seasonal component, northwestern Europe has a year-round precipitation based on stratiform processes. Hegdahl et al. (2020) performed a storylines study on precipitation connected to atmospheric rivers in western Norway. Their conclusion was that climate change will cause more catchments to be affected by extreme precipitation induced flooding. As the air temperatures are expected to increase in the future, atmospheric rivers can make landfall in conditions above freezing point, despite atmospheric rivers being a typical winter phenomenon, which is expected to increase rain instead of snow and

could cause large flooding problems (Whan et al., 2020).

In Figure 6.5b the differences between domain average precipitation (which by default includes all forms such as snow, rain, etc.) of different storylines is not as clear as with Mexico in panel a. Generally, there seems to be little signal. However, when looking into the event boxes, in event S1 the counter peaks above the plus2, possibly indicating a drying from climate change. Then in event S2 the opposite is shown, plus2 peaking above factual and counter, likely indicating a wetting. In the precipitation maps (Figure 6.6 – S1, S2) the factual anomalies for the two events are very different from each other. For S1, which is a summer event, there is a strong negative anomaly over the Russian part of the domain, and a strong positive anomaly over Sweden and Finland. The differences between factual and counter is almost negligible for S1, but show a band of robust increase in precipitation in Norway and Sweden. The aforementioned wetting is not visible in the future (plus2 – factual), though a stronger decrease in precipitation is now visible over Latvia, Estonia and Russia. Overall, there is a clear climate signal in S1, be it for two different signs: an increase in precipitation over the border region between Norway and Sweden, and a decrease in precipitation over Russia, Latvia, Estonia and Lithuania. The autumn event, S2, has positive anomalies overall, with some smaller patches of negative anomalies in south Sweden. A slight future wetting of the northern part of the domain is found. These climate signals are only visible when averaging 3 months or more, and can therefore be considered a seasonal signal.

The robustness of these results are somewhat difficult to determine with Figure 6.7b, as both negative and positive signals are present in the domain, cancelling each other out in an average. Event S1 still shows an almost linear decrease in precipitation, with a clear signal-to-noise ratio in PF and PC. Event S2 has an increase in precipitation, which is not visible in FC, but is clearly visible in PF.

6.2.3 Australia

The Australian climate ranges from desert in the central regions, to tropical with monsoonal precipitation in the north. Climate change projections predict a drying of the southwest and southeast of the Australian continent, though these expectations differ much between seasons (Evans et al., 2021).

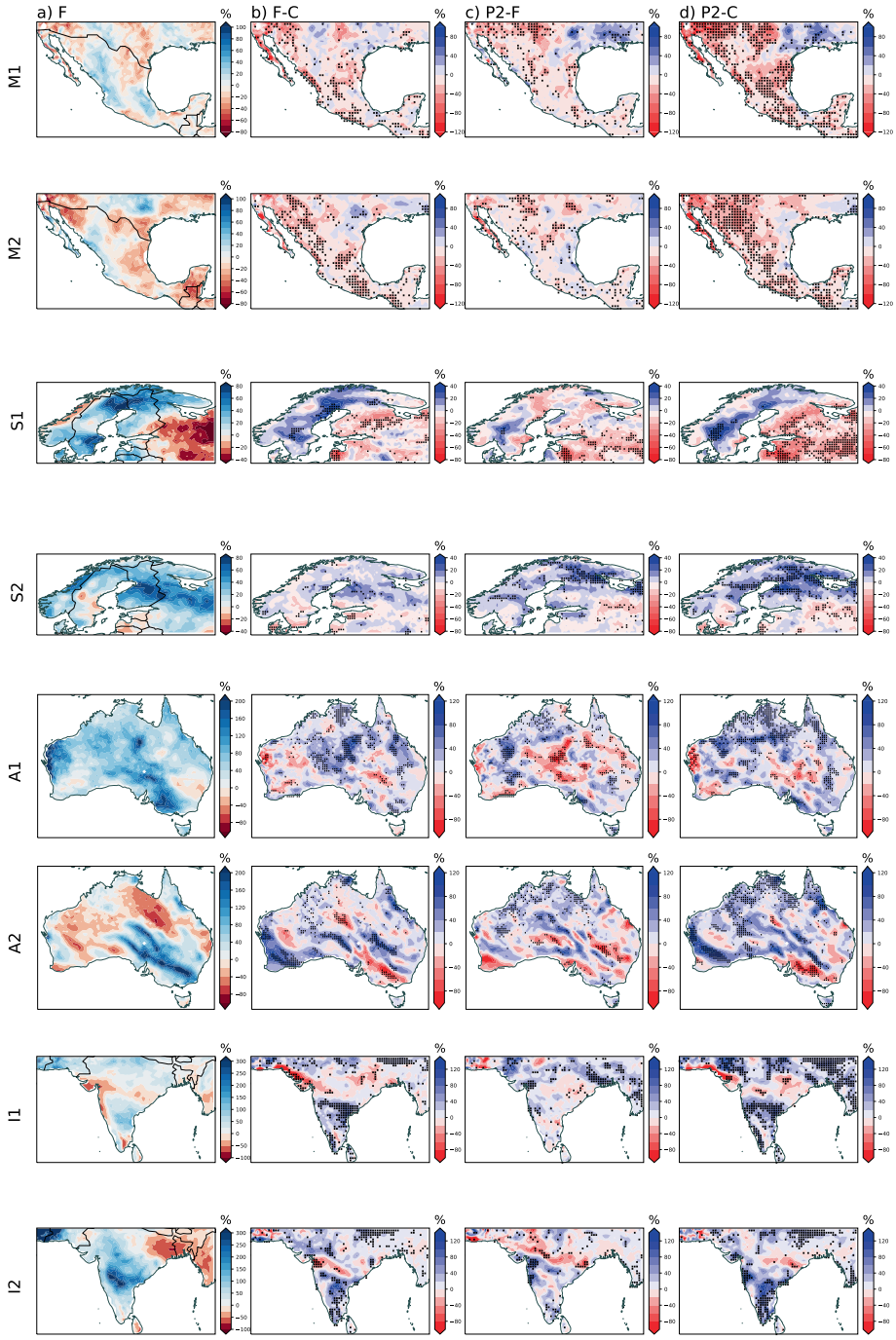

Figure 6.6: Total Precipitation maps for a) Factual anomaly computed with ECHAMS_SN 1980-2010, b) difference between factual and counter, c) difference between plus2 and factual and d) difference between plus2 and counter. M for Mexico, S for Scandinavia, A for Australia, I for India. Each event, two per domain, is marked with 1 or 2 as shown in Figure 6.5.

From observations, the effect of climate change has initiated a positive trend in 'fire weather' in southern Australia, where weather conditions, such as increased temperatures and reduced precipitation, are increasingly favourable for bush fires (Dowdy, 2018). Though the attribution of specific bush fire disasters is complex and plagued with model bias issues, there are studies that found climate change negatively influenced the 2019 fires by enhancing drought, and a general increased bush fire risk (van Oldenborgh et al., 2021a). Mindlin et al. (2020) included precipitation for Australia in a dynamical storylines study of the Southern Hemisphere circulation (see also section 2.1) and found a drying for southern Australia, especially in austral winter, when considering a strengthening of the polar vortex and tropical amplification of global warming. The opposite may happen to the Australian monsoon in the north, which is expected to become stronger with higher amounts of precipitation in the same time frame, which can lead to increased flood risks (Wang et al., 2021).

In Figure 6.5c there is little separation between the storyline members visible, with the strong exception of the 2011 summer precipitation event (A1). The counterfactual is below the factual and plus2 members, indicating a wetting of the precipitation event. The same is visible for summer 2012 (A2) and also for summer 2014, although the differences are smaller and the signal is more noisy. There is no clear climate signal in precipitation during the dryer season. Note that for drought, other variables than precipitation should also be considered, see Chapter 8. In Figure 6.6a - A1 the factual precipitation anomaly shows increased precipitation over most of Australia, while for A2 the picture shows more variability between drying in the west and central north, and wetting in the south and pieces of the north-east coast. Note that central Australia has a desert climate, thus a small difference in precipitation can cause large percentage changes, therefore the results in this region should be treated with care. The A1 event shows a robust wetting in the north when comparing F-C (A1 panel b), which is not visible for the future projection (P2-F, A1 panel c). In total though, the P2-C (A1 panel d) precipitation is clearly robust for wetting in the north, which can be related to the wetting of the Australian monsoon (Wang et al., 2021). This result does not differ significantly for event A2, with wetting in the north, but the robustness is less for the past (A2 panel b). Moreover, there is a band of robust drying visible in the southeastern coastal region starting north from the Spencer Gulf moving south-east towards the coast east from Melbourne, in both past and future (A2 panel b, c and d).

In the signal-to-noise analysis (Figure 6.7c), there is a clear signal for the past attribution, but for the future there is no climate-change signal detectable in either of the events. The overall attribution, however, is clearly showing a wetting climate signal for both events A1 and A2. The signal might be lost or reduced due to the large domain,

with both wetting and drying regions cancelling each other out. Another important point might also be that different sources of influence can have an effect on precipitation for past and potential future scenarios, additionally complicating the detection of robust signals.

6.2.4 India

India is known for its monsoon climate, where the peak precipitation of the South Asian summer monsoon (SASM) is during summer from June to August. Of all the examples given in this chapter, the analysis of climate change impacts on the SASM is arguably the most complex. The complexity lies, among other things, in the SASM dependency on teleconnections such as ENSO, land use that alters the land-atmosphere processes, and strong regional variability in precipitation changes (Di Capua et al., 2020; Ghosh et al., 2018; Singh et al., 2019). This regional component should, however, be true for all subregions under investigation. Observations show a decrease in monsoonal precipitation in India since the 1950s. However, the projections show a strong precipitation increase for future monsoons (Douville et al., 2021).

In the precipitation time series (Figure 6.5d), the plus2 storyline members peak at higher precipitation totals during each monsoon season, compared to both counter and factual storylines, indicating a monsoon wetting in agreement with Douville et al. (2021). As with Mexico, two monsoon events are studied, but like Australia with different precipitation anomalies. In event I1, the plus2 storylines peak visibly higher in amounts than the factual and counter storylines, which seem to peak at roughly the same amount. For event I2, the storylines behave somewhat differently. Here, the plus2 and factual peak roughly at the same lower amount, but the counterfactual storyline is visibly below that. Note that I1 occurs in between two consecutive La Niña events (see Figure 6.5e), whereas I2 is likely under the influence of the Circumglobal Teleconnection Index (CGTI) reaching up to 0.6 % above normal. These two remote drivers, ENSO and the CGT, can cause different precipitation patterns during SASM.

The maps in Figure 6.6a – I1 and I2 show a vastly different factual precipitation anomaly for each event. I1 has negative anomalies on the west coast and somewhat positive anomalies in the south and north of the domain. I2 on the other hand, shows an east-west dipole pattern with strong positive anomalies in the centre and north-west, but negative anomalies in the east. This anomaly pattern is most likely related to the influence of a positive CGTI. When looking at the difference between the factual and counterfactual (F-C) in Figure 6.6b, I1 shows the most robust signal in the south with higher wetting percentages. Simultaneously, the north-west coast is experiencing a

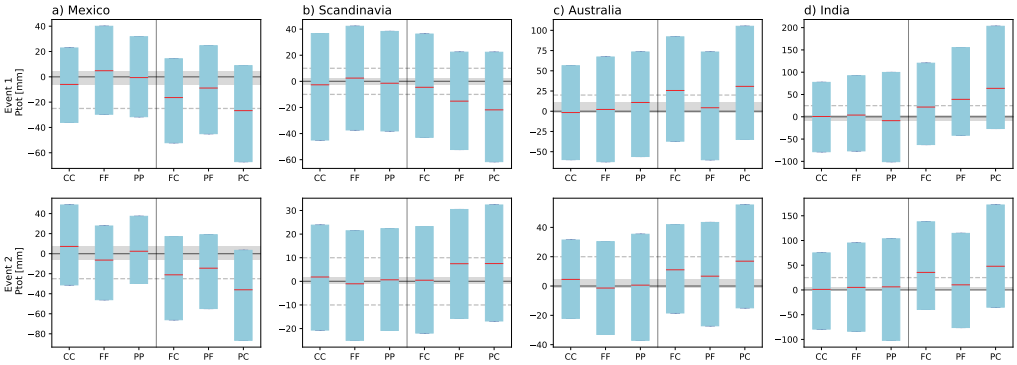

Figure 6.7: Distributions across grid points of differences between ensemble members in precipitation [mm], FF: differences between pairs of factual members; CC: differences between pairs of counterfactual members; PP: differences between pairs of plus2 members; FC: differences between pairs of factual and counterfactual members; PF: differences between pairs of plus2 and factual members and PC: differences between pairs of plus2 and counterfactual members. The boxes represent the 25th-to-75th-percentile range of the distributions, the red lines represent the 50th percentiles (the median), the grey band is the noise level based on the medians in CC, FF and PP for a) Mexico, b) Scandinavia, c) Australia and d) India.

dryer monsoon. The future differences (P2-F) for I1 in Figure 6.6c, shows that the regions of robust signals are in the North, with an increase in precipitation. The effect of climate change on the precipitation pattern is therefore not the same for past and future. Comparing the factual anomaly with the difference between plus2 and counterfactual (P2-C) (Figure 6.6d – I1), the climate signal is making the negative anomalies even dryer and the positive anomalies even wetter, with robust signals over the North and South of India. The differences between factual and counterfactual for I2 are comparable to those of I1, despite the very different factual anomalies, with robustness in roughly the same regions. A clear difference, however, is the band of reduced precipitation from the north-west coast in I1, located centrally and reaching almost entirely from west to east coast. This band has a positive anomaly in the factual, and shows that the climate signal can reduce precipitation over a positive anomaly as well. The difference in I2 precipitation for the future looks very different from that of the past, with a strong increase in precipitation of the central west coast and a strong decrease in precipitation over the central northern band.

The general signal-to-noise ratio, as seen in Figure 6.7d, is strong for I1. In I2, however, the PF difference is too small and within the noise range. That said, the total climate signal in PC is robust. It is clear that the effect of climate change in the past is not the same as it might be in the future, which does not take away that in total (PC) there is a robust and strong climate-change signal in both events for increased precipitation in

SASM.

6.3 Discussion and conclusion

Both the global average T2m and the global spatial T2m patterns simulate well, with highly robust climate signals found between the different storylines. Also, seasonally the differences between worlds are robust, meaning a strong climate change impact on regional and global temperatures. The global increase in temperatures due to climate change is uniform over land areas, though stronger in regions that already experience warm temperatures in summer. These global results show that the model in its current set-up simulates a reliable result and is in agreement with climate-change signals found in the IPCC report on 1.5 °C climate change (Hoegh-Guldberg et al., 2018). In Figure 6.8 the temperature differences analysed with free running CMIP5 models show a recognisable pattern, in agreement with the pattern found in this study. There is an overall robust signal for global temperature increase, stronger over land than over sea. The lack of robustness over the cooling SST patch in the North-Atlantic is visible here as well. The global gradient of less warming in the Antarctic to the strongest warming found in the Arctic, is comparable between the IPCC reference and the storylines. The polar amplification in the Arctic, however, is more pronounced in the IPCC results than the storylines.

Global precipitation is overestimated around arid regions (Sahara, middle-east and south-east Asia) when comparing with observations. Note that small amounts of precipitation can make large anomalies due to the dryness in these type of regions. However, I also show that these biases are the same for ERA5 reanalysis and for the MPI-ESM coupled simulations. Moreover, the observational global datasets also have biases that should be considered (Tapiador et al., 2017). This suggests that the difficulties models have with resolving precipitation, and the related bias, is not made worse by the model setup presented here. When comparing the precipitation difference between the plus2 and counterfactual storylines in Figure 6.3 with the IPCC results in Figure 6.8 bottom centre, the patterns are remarkably similar. There is wetting at the South American west coast, Sahara desert region and towards both the Arctic and Antarctic, and drying over Mexico, Southern Europe, South Africa and parts of Australia. The storylines show larger regions of robustness over land than do the IPCC results. This robustness should be carefully interpreted as here only one model is analysed and with IPCC the results are based on the average of a large number of models that might disagree with each other. The large-scale drying and wetting patterns in the extra-tropics are also comparable to the observations, but the precipitation bias

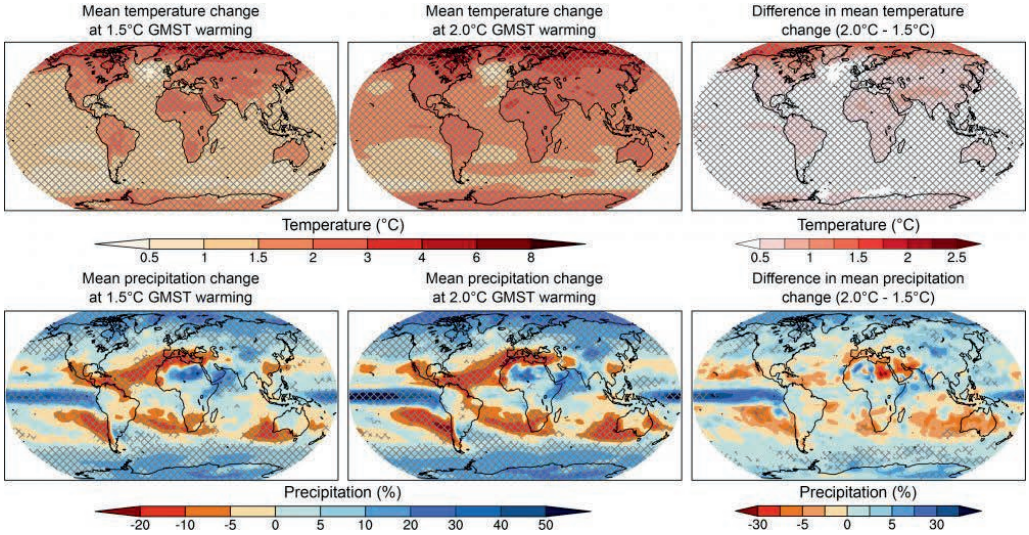

Figure 6.8: Global change in temperature and precipitation according using CMIP5 multi-model ensemble according to IPCC. Top row is temperature difference due to global warming for left) 1.5 °C warming, centre) 2.0 °C warming and right) difference between both. Bottom row is same as top row but for precipitation in %. Is Figure 3.3-1 from Hoegh-Guldberg et al. (2018).

is causing a deviation from observations. There is a clear global precipitation climate signal, with increased precipitation in warmer storylines. However, the impact of climate change on the precipitation patterns is somewhat less robust.

Regional attribution of seasonal precipitation as done for Mexico, Scandinavia, Australia and India is an example of continuous conditional attribution at these scales, which is a type of analysis that storylines introduce. It showcases that despite a global increase in precipitation, locally the precipitation characteristics can behave vastly different from the global trend. For the 2012 and 2014 Mexican monsoon there is a drying found, but the 2010 monsoon had no climate signal. The Indian monsoon of both 2011 and 2014 show a wetting, but the spatial location of the wetting inside the domain varies greatly between the two. Moreover, the robustness of the climate signal changes per year. The seasonal precipitation in Scandinavia was less for the summer of 2012 but more for the autumn of 2013. The seasonal precipitation event of summer 2011 and 2012 in Australia have become wetter and are expected to continue doing so in a +2 °C world; however, the signal is not very robust. The regional precipitation follows observations better than the global precipitation. The storylines, reanalysis and observations now show comparable results with excellently resolved seasonal variability but lose some robustness in differences between storylines. The signal-to-noise analysis shows that both regional drying and wetting is found with a robust signal,

though the effect is not always linear over time and not as clear-cut for all events. Peak precipitation, however, is systematically underestimated by the storylines. Moreover, regional precipitation attribution has to include several months, as the robustness in differences between storylines disappears with smaller time scales. These regional examples shown here are not meant to be exhaustive, but give an example of the new possibilities storylines offer in continuous precipitation attribution and year-to-year climate-change signal variability studies.

7

Event-based Temperature Extremes

To illustrate the application of the storylines method in event-based temperature extremes, two case studies are selected: The European heatwave of 2003 and the Russian heatwave of 2010. These events are considered the two strongest European heatwaves on record (Russo et al., 2014, 2015). The selected study domains are 10 °W-25 °E/35-50 °N as the domain for the European heatwave 2003, and 35-55 °E / 50-60 °N for the Russian heatwave 2010, in line with previous literature (Dole et al., 2011; García-Herrera et al., 2010; Otto et al., 2012; Rasmijn et al., 2018; Wehrli et al., 2019).

7.1 European heatwave 2003

The European summer of 2003 was exceptionally hot and exceptionally dry (Black et al., 2004; Schär et al., 2004; Stott et al., 2004). Two heatwaves occurred, a milder one in June and an extreme heatwave in August, with peak temperatures in France and Switzerland (Black et al., 2004; Schär et al., 2004; Trigo, 2005) but also affecting Portugal, northern Italy, western Germany and the UK (Feudale and Shukla, 2011a; Muthers et al., 2017). Temperatures exceeded the 1961-1990 average by 2.3–12.5°C, depending on location, without much cooling during the night (García-Herrera et al., 2010; Muthers et al., 2017; Schär et al., 2004; Stott et al., 2004). The 2003 summer was at that point in time not just the hottest on record (Bastos et al., 2014; Fink et al., 2004), it was the hottest summer in the past 500 years (Luterbacher et al., 2004). The

consequences were devastating. Estimates account for 22,000–40,000 heat-related deaths, $12-$14 billion in economic losses, 20-30 % decrease of Net Primary Productivity (NPP), 5-10 % of Alpine glacier loss and many more human health related issues due to increased surface ozone concentrations (Ciais et al., 2005; Fischer et al., 2007; García-Herrera et al., 2010).

Both the June and August heatwaves were caused by stationary anticyclonic circulations, or blocking (Black et al., 2004). The first block formed in June, broke and quickly reformed in July which then caused the second heatwave in August (García-Herrera et al., 2010). However, the extreme temperatures cannot be explained by atmospheric blocking alone. Due to large precipitation deficits in spring that year, the heatwaves happened in very dry conditions, enhancing the temperatures even further (Whan et al., 2015). The lack of clouds and soil moisture caused latent heat transfer to turn into sensible heat transfer, which dramatically increased surface temperatures (Bastos et al., 2014; Ciais et al., 2005; Fink et al., 2004; Fischer et al., 2007; Miralles et al., 2014). It is considered highly unlikely that the 2003 European heatwaves would have reached the temperatures they did without climate change. The probabilistic event attribution studies show an increased likelihood of the extreme temperatures from increased GHGs (Hannart et al., 2016; Schär et al., 2004; Stott et al., 2004). Other studies focused on the exceptionally high SSTs in the Mediterranean Sea and North Sea as a cause of reduced baroclinicity, providing an environment conducive to blocking (Black et al., 2004; Feudale and Shukla, 2011a,b). By applying the storyline approach, both causal factors are considered together which sheds some additional insight on this event. The dry spring leading up to the warm summer conditions was captured by initializing the simulations by 1st March at the latest.

In Figure 7.1a, the daily evolution of the domain-averaged temperature at two meters height for June, July and August for each of the ensemble members is plotted in comparison to the ECHAM_SN 5th-95th percentile (1985-2005) climatology. The ECHAM_SN 2010 temperature is also plotted for reference. The first thing to note is that the factual and counterfactual ensembles evolve very similarly in time but (except for the third week of June) are well separated, by approximately 0.6 °C, indicating a high signal-to-noise ratio at daily resolution for the domain average. This value of 0.6 °C is in line with the global mean warming. Also, the factual members and ECHAM_SN simulation are showing strong coherence. The factual temperatures exceed the 95th percentile several times in June, July and August. In August, the exceedance lasts for almost two weeks, whereas in June it does so for approximately one week. The counterfactual temperatures are not quite so extreme; they exceed the 95th percentile only for a few days at a time in June and August. Nevertheless, it is

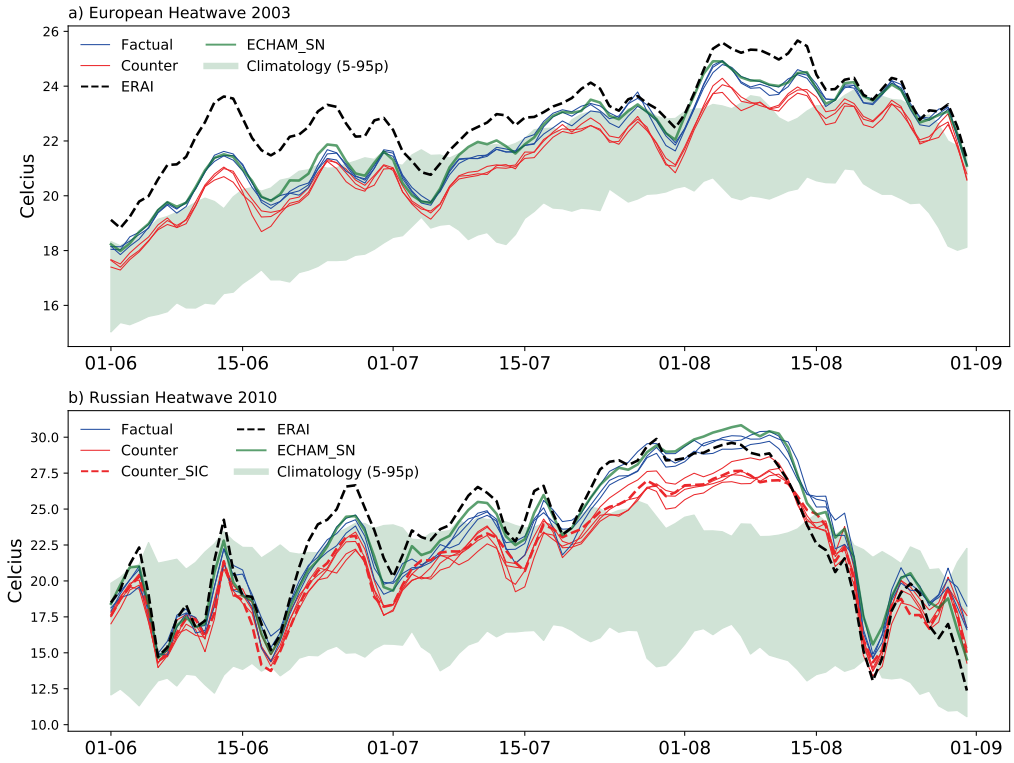

Figure 7.1: Daily mean temperature at two meters height [°C] averaged over a) Europe (10 °W-25 °E/35-50 °N) for summer 2003, and over b) Russia (35-55 °E/50-60 °N) for summer 2010, for the factual (blue), counterfactual (red) and ECHAM_SN (dashed black) simulations. The climatology (green shaded area) is the 5th-95th ranked percentile range between 1985-2015 calculated with ECHAM_SN (Schubert-Frisius et al., 2017).

clear that there would have been a European heatwave in 2003 even without climate change, albeit with less extreme temperatures. This analysis thus supports both of the perspectives on the event discussed earlier, whilst providing a daily resolution of the climate-change attribution.

The temperature differences between the factual and counterfactual ensembles are spatially non-uniform over Europe. In Figure 7.2a the factual members average of the two-meter temperature and geopotential height (z500) show the meteorological situation averaged over half-month periods following García-Herrera et al. (2010). Figure 7.2b shows the local differences in two meter temperatures between the counterfactual and factual ensemble averages. Stippling is added to each grid point where all the three factual members are at least 0.1 °C warmer than all the counterfactual members. There is strong local variance, especially during the heatwave in the first half of August, with differences of up to 2.5 °C. In the first period (1-15 July) the local

differences are generally modest, except in northern Spain where they reach 1.5-2 °C. In the second and third half-month periods (16-31 July, 1-15 August), the temperatures in the factual simulations can locally be up to 2-2.5 °C higher than in the counterfactual simulations, with the differences spread over a large area including Spain, Portugal, France, Germany, Hungary and Romania. During the period 1-15 August, which according to Figure 5a was the peak of the heat wave, the hottest area in Europe (Figure 7.2a) is located in south-west France and southern Iberia. However, the largest differences between the factual and counterfactual simulations (up to 2.5 °C) are found to the north of both of these regions, suggesting a shift of the peak temperature. In the second half of August, there are still some strong temperature differences visible over most of these regions, although the differences over western France have dampened.

As noted earlier, the dryness of the soil has been identified as an important contributing factor to the 2003 heatwave. The interest here, however, is on whether the soil wetness differed between factual and counterfactual. In Figure 7.3a a very similar decline in soil wetness for both the factual and counterfactual ensemble members from May until the end of August is seen. The counterfactual simulations start out with somewhat higher soil wetness than the factual simulations, but over the course of the summer the values of both sets of simulations move closer towards each other, so that by August the ensembles are close together. Thus, it does not appear that climate change had a first-order impact on soil wetness in this case.

7.2 Russian heatwave 2010

In August 2010 western Russia was hit by an unprecedented heatwave caused by a large quasi-stationary anticyclonic circulation, or blocking (Galarneau et al., 2012; Grumm, 2011; Matsueda, 2011). It was a heatwave that broke all records such as temperature anomalies during both day and night, temporal duration, and spatial extent. The effect of soil wetness, or rather the lack thereof, on the magnitude of the temperatures was profound (Bastos et al., 2014; Lau and Kim, 2012; Rasmijn et al., 2018; Wehrli et al., 2019). The 2010 Russian heatwave is considered the most extreme heatwave in Europe on record (Russo et al., 2015). Approximately 50,000 lives were lost, 5,000 km^2 forest burned, 25% of the crop failed and over 15 billion US dollars' worth of economic damage was recorded due to this heatwave (Barriopedro et al., 2011; Lau and Kim, 2012; Otto et al., 2012; Rasmijn et al., 2018). In some of the attribution studies, the heatwave was primarily attributed to internal variability as the dynamical situation strongly depended on ENSO being in a La Niña state (Dole et al., 2011;

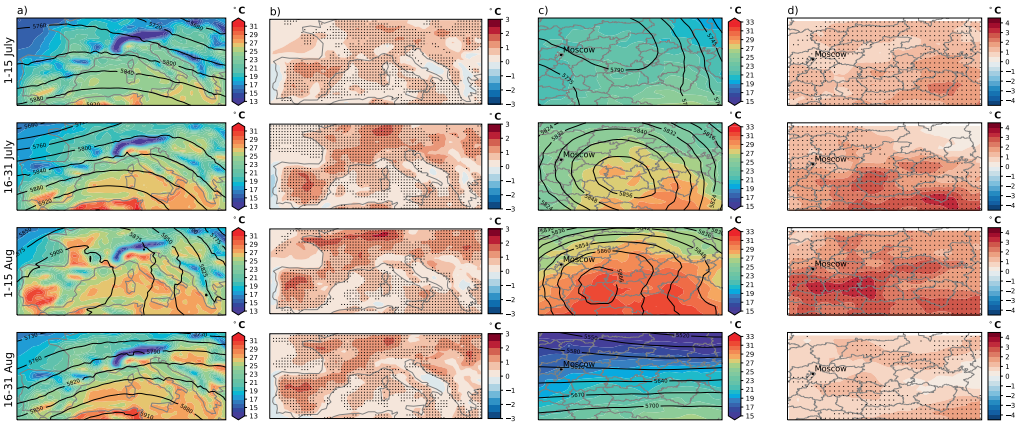

Figure 7.2: T2m maps where July and August are divided into four half-month periods. Columns a and b show the European heatwave 2003, while columns c and d show the Russian heatwave 2010. In columns a and c, the factual geopotential height at z500 [m] is shown as black contour lines, while temperatures at two meters height [°C] are shown as shaded fields. In columns b and d, the differences in two-meter temperature [°C] between the factual and counterfactual simulations are shown as shaded fields. Stippling shows where all the factual members are >0.1 °C above all the counterfactual members for that grid point. Note that the Russian domain is smaller, and therefore the stippling has a different spacing than in the European domain.

Russo et al., 2014; Schneider et al., 2012). However, the likelihood of the temperatures reaching such extreme values has also been assessed as being significantly exacerbated by climate change (Otto et al., 2012; Rahmstorf and Coumou, 2011). As with the previous example, the storyline approach can represent both of these perspectives. Moreover, it overcomes the general limitation of climate models to reproduce a complex blocking situation correctly (Trenberth and Fasullo, 2012; Watanabe et al., 2013).

In Figure 7.1b, the daily evolution of the domain-averaged temperature at two meters height for each of the ensemble members is shown in comparison to ECHAM_SN 2010 and the ECHAM_SN 5th-95th percentile climatological temperatures (1985-2015). Starting after the second half of July both the factual and counterfactual temperatures exceed the 95th percentile climatological temperature, peak around the 8th of August and return to climatological temperatures around the 17th of August. This analysis shows that this would have been an unprecedented event, even without climate change. The differences between the factual and counterfactual temperatures during the core of the heat wave are noticeably higher (about 2°C) than in the European heatwave 2003, as is the spread between the ensemble members. In contrast to the European case, the anthropogenic warming during the core of the heat wave is considerably higher than the global-mean warming. Both aspects are attributed — the greatly enhanced anthropogenic warming, and the larger internal variability — to

the fact that the Russian domain is much further inland than the European domain, and thus the blocking conditions cut off the influence of the SST forcing and allow a direct radiative effect of GHG increases (Wehrli et al., 2019). Note that western Russia is known for having large internal variability (Dole et al., 2011; Russo et al., 2014; Schneider et al., 2012), which is clearly apparent in the results. It is also the case that the Russian domain is smaller than the European domain by a factor of 3.4, which would furthermore tend to increase the variability in the domain-averaged temperature shown in Figure 7.1.

The range of temperature differences between factual and counterfactual simulations reached values up to 4 °C locally, as seen in Figure 7.2d. Note that the scale for the Russian heatwave reaches up to 4 °C, whereas the scale for the European heatwave reaches only 2.5 °C. In the first half-month period (1-15 July), when the heatwave had not yet started, the local temperature differences are between 0.5-2.5 °C, with the maximum differences in the south-east of the domain. The temperature differences are largest in the core of the blocking region, reaching up to 3.5 °C in the south-east in the second period (16-31 July) and up to 4 °C in the south, below Moscow, in the third period (1-15 August). The blocking broke in the fourth period (16-31 August) and resulted in a virtual elimination of the temperature difference. In contrast to the 2003 European heatwave, here the biggest temperature differences between factual and counterfactual are found in the regions with the highest temperatures.

As with the 2003 European heatwave, the differences in soil wetness does not appear to be of first-order importance to explain the temperature differences between the factual and counterfactual simulations. In Figure 7.3b the soil wetness in the factual simulations is seen to decrease somewhat more rapidly than in the counterfactual, which could be due to the higher surface temperature and thus greater evaporation of soil moisture. However, the soil wetness values are overlapping, and even cross each other in the beginning of August. It must be emphasized that this is not to downplay in any way the impact of soil wetness on the event itself, which has been well established in the literature. It is only to indicate that the impact would have been there even without climate change.

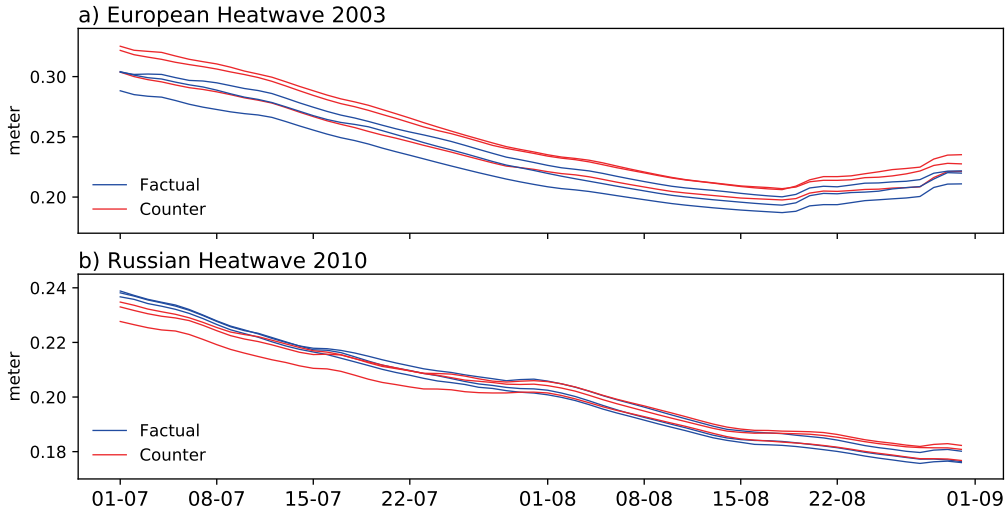

Figure 7.3: Average soil wetness in the root zone [m] averaged over Europe in 2003 and Russia in 2010, during July and August of each year. The factual simulations are shown in blue and the counterfactual simulations in red.

7.3 Signal-to-noise ratio

The found results only make sense if the signal of climate change can be distinguished from internal noise due to natural variability or inherent uncertainty in the method. As done with the regional seasonal precipitation events, the heatwaves are further studied using the signal-to-noise analysis in Figure 7.4. The half-monthly panels represent distributions of half-month averaged values, and the daily panels distributions of daily values within the half-month period.

The daily differences for the European heatwave (Figure 7.4a) show a median value of approximately 0.6 °C, irrespective of whether the timeframe is during the heatwave itself, directly before or directly after it, consistent with Figure 7.1a. Although these are not really probability distributions (since they include contributions from different locations within the domain), the inter-quartile ranges can be used as measures of signal and noise. The median difference for FC is above the 75th percentile of both CC and FF for daily values, giving confidence that our results are clearly above the noise level. Half-monthly time averages (Figure 7.4b) produce nearly identical median values, but the spread is much smaller, as expected. The 25th percentile of FC now lies above the 75th percentile of the CC and FF boxes.

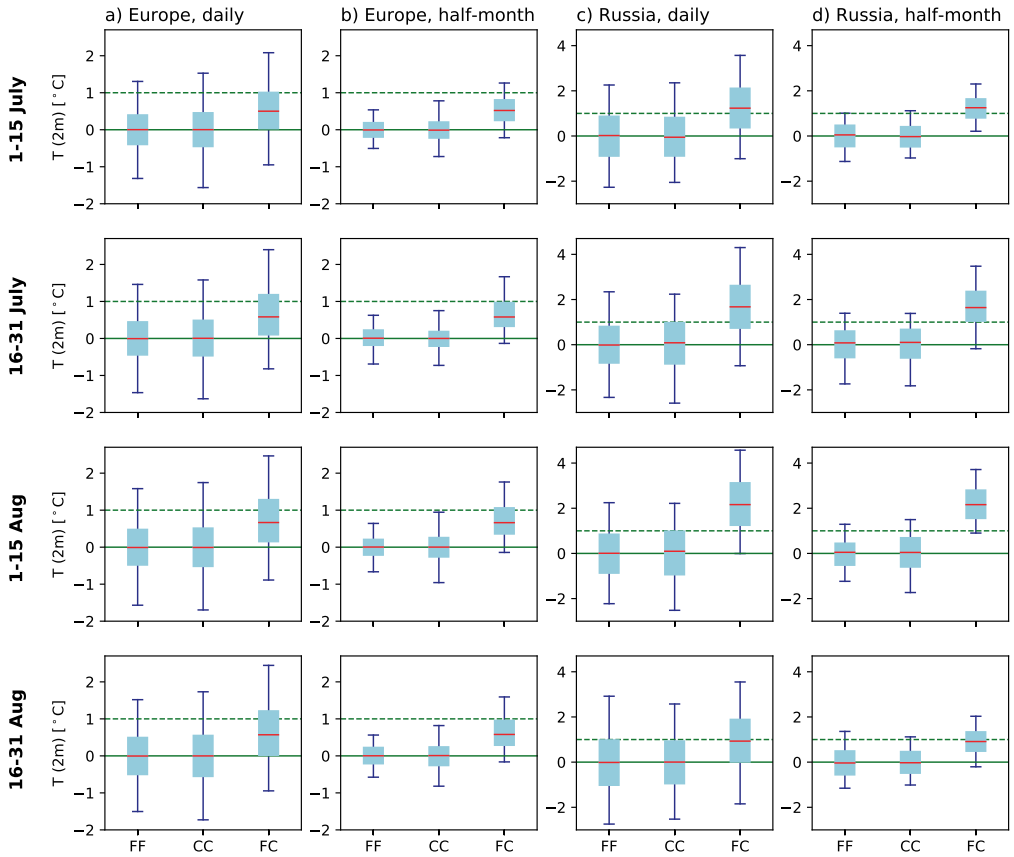

Figure 7.4: Distributions across grid points of differences between ensemble members in temperature at two meter height [°C], separated into the four half-monthly periods. FF = differences between pairs of factual members, CC = differences between pairs of counterfactual members, FC = differences between pairs of factual and counterfactual members. The boxes represent the 25th to 75th percentile range of the distributions, the red lines the 50th percentiles (the median), and the blue bars indicate the 5th to 95th percentile range. The dashed horizontal line indicates 1 °C for reference. Columns a and b are for the European 2010 heatwave, and columns c and d for the Russian 2010 heatwave. Columns a and c show the differences of daily averages, and columns b and d the differences of half-monthly averages.

The differences between CF and either FF or CC for the Russian heatwave (Figure 7.4c,d) are clearly larger than for the European heatwave, and in contrast to the European case vary substantially between the different periods. Consistent with Figure 5b, in the periods outside of the core of the heatwave (1-15 July; 16-31 August) the median difference between FC is about 1 °C. Inside the core heatwave period (16-31 July; 1-15 August), however, the median difference is more like 2 °C, reaching 2.2 °C for 1-15 August. During this latter period, the 5th percentile whisker of half-monthly FC differences is above the 75th percentile of FF and CC, which is a very strong signal

indeed. When looking at the results for individual members the larger internal variability within the Russian domain (apparent also in Figure 5b) is clearly visible (not shown), as compared with the European case.

7.4 Discussion and conclusion

Both heatwaves show an increased average daily temperature due to climate change and simultaneously show that without climate change the temperature would have been above the 95th percentile as well. This means that the heatwaves would have been there despite climate change, but were enhanced due to climate change. The analysis revealed a striking contrast between the two events. In the European heatwave of 2003, the effect of climate change was to increase temperatures across Europe by about the global-mean warming level throughout the summer, and the heat wave was simply the dynamical event riding on top of that. In the Russian heatwave of 2010, in contrast, the effect of climate change was much higher than the global warming level, and was particularly enhanced, by approximately three-fold, during the peak of the heatwave. When considering there is no noticeable soil-moisture feedback, this difference likely reflects the role of direct GHG radiative forcing, which can become apparent when air masses are cut off from marine influence. However, further analysis would be required to confirm this hypothesis.

The storylines allow for the climate signal to be determinable at both daily time scales and local spatial scales in both case studies. Difficult dynamical situations, such as the blocking in both these events, were shown not to hinder the signal-to-noise ratio analysis, which is a significant improvement in event attribution. Blocking is a large scale dynamical structure and well resolved by the model due to the nudging. Although the results are promising, they do not yet prove that the method will resolve smaller scale dynamical structures with the same high-quality results, as the method is limited by the resolution of the model. That said, the two case studies show that the method allows for a separation of natural variability and climate signal. Several studies concerning the Russian heatwave concluded that the event was dominantly steered by natural variability (Dole et al., 2011; Russo et al., 2014; Schneider et al., 2012). The results shown here indicate these conclusions were incomplete and there is a robust and quantifiable difference in temperature due to climate change.

8

Event-based Hydrological Extremes

8.1 Southeastern South America drought 2012

Often it is assumed that increased dryness will lead to increased droughts, the same for wetness and floods. Dryness refers to the climatological hydrological state of a region, whereas drought refers to an extreme event. However, in some regions climate change is expected to increase both wetness and the intensity of droughts (Ault, 2020). Southeastern South America (SESA) is a region of South America centered in the La Plata Basin which includes Uruguay, the southeast of Argentina, the southern tip of Brazil and the southeastern tip of Paraguay. The climate in SESA experienced a pronounced wetting in the second half of the 20th century. The regional precipitation trends are among the largest regional trends in the world (Vera and Díaz, 2015). This includes both an increase in mean annual rainfall (Doyle et al., 2011) and the frequency of extreme rainfall events (Penalba and Robledo, 2010). However, the SESA region also suffers from regular droughts, approximately every 5 to 10 years, which are part of the regional climate and are also to a large extent associated with strong La Niña events (Grimm et al., 2000). Both short-term (3 months) and long-term (10-12 months) droughts have impacts in SESA, the first affecting the agricultural sector and the second the water supplies.

Two examples of exceptionally severe droughts, in both extent and intensity, are the summer 1988/1989 and summer 2008/2009 droughts. In Uruguay, the 2008/2009

drought caused hydropower production, which normally accounts for roughly 80% of the national energy supply, to plummet to 20%. In Argentina, that same drought reduced grain production by 39%, and an estimated 1.5 million livestock were lost (Peterson and Baringer, 2009). The extent of agricultural impact depends on the timing of each drought. Soybean and corn production will be hampered if a drought occurs in summer (December-February). Wheat on the other hand is more sensitive to precipitation deficiency in spring (October-November). For this reason, shorter droughts may have equal impacts on crop loss as persistent droughts, if they occur in the critical growth periods. The 2011/2012 summer drought is an example of such a short but devastating event, with damages in corn and soybean production running up to USD 2.5 billion (Sgroi et al., 2021). Since the strongest climate-change signal in SESA is an increase in mean precipitation, drought impacts in this region have not received as much attention as might be needed for adaptation. However, one of the few studies available (Penalba and Rivera, 2013) showed that, under future scenarios, the frequency, duration and severity of these droughts are expected to increase in SESA. Thus, understanding the influence of a warmer climate on droughts in SESA is of clear societal relevance.

Despite the 2011/2012 SESA drought having a short three-month duration, neither as severe nor as persistent as e.g. the 2008/2009 drought, the timing of the event during crop sensitive months caused large yield losses. The November 2011 - February 2012 Standardized Precipitation Index (SPI) in the Argentinian part of SESA indicates moderate to extreme drought conditions. The 3-month Palmer Drought Severity Index (PDSI), for the same period and region, indicates a severe to extreme drought event (CREAN, 2017).

The dynamic situation, including La Niña and an intensified South Atlantic Convergence Zone (SACZ), favoured dry conditions. The event started in December 2011, during the second consecutive summer with a La Niña phase. The two-year La Niña event of 2010–2012 was one of the strongest La Niña events on record and caused extreme weather all over the globe (Blunden and Arndt, 2012). In the SESA region, the positive ENSO phases are characterized by increased precipitation anomalies, and negative ENSO phases by reduced precipitation anomalies (Grimm et al., 2000). The influence of La Niña on precipitation is strongest during the spring and summer following the event. Moreover, the SACZ intensified during the late spring - early summer season (NDJ) of 2011/2012, as shown using NCEP-R1 data in Figure 8.1a (negative outgoing long-wave radiation (OLR) indicating increased cloudiness). An intensified SACZ favours subsidence and clear sky conditions over SESA, hindering precipitation and increasing incoming short-wave radiation. Therefore, the state of the SACZ leads

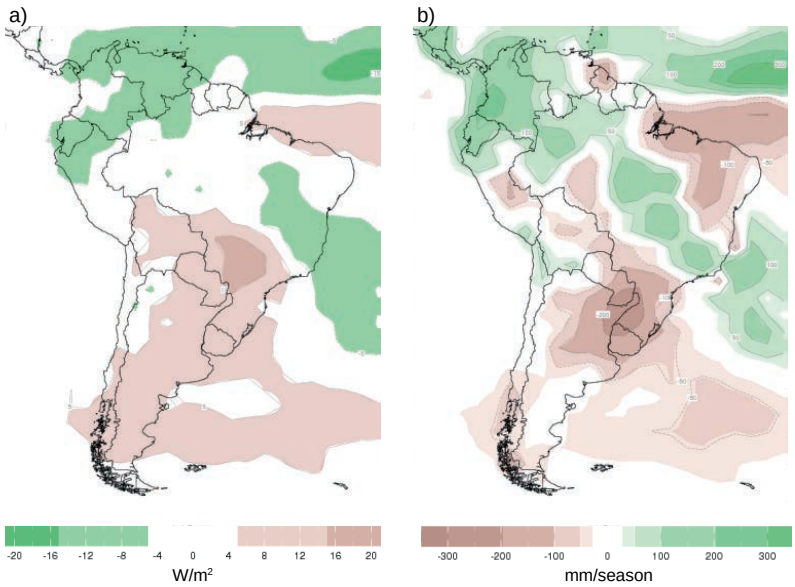

Figure 8.1: Drought characterization. Seasonal anomalies with respect to the 1979 - 2020 climatological average over Nov - Jan of a) Outgoing long-wave radiation (W/m^2) b) Precipitation (mm/season). The data is from the NOAA NCEP Climate Prediction Center and was plotted using the website: https://iridl.ldeo.columbia.edu/maproom/ (International Research Institute for Climate and Society, Columbia Climate School, New York, USA).

to anomalous high temperatures and dry conditions (Figure 8.1b). The atmospheric dynamical conditions for these types of droughts are well understood and explain a significant fraction of the summer variability. It is reasonable to expect events of this kind in the near future as La Niña events combined with an active SACZ are part of the local climatology (Cerne and Vera, 2011).

In Figure 8.2a the domain average time series of T2m for each storyline is visible, with ECHAM_SN climatology and ERA5 reanalysis (Hersbach et al., 2020) for comparison. The temperatures between the three storylines evolve comparably but are clearly separated in magnitude, revealing a strong climate-change signal. The factual temperatures do not exceed the ECHAM_SN (1981-2010) climatological 95th percentile, except for two instances in February. The plus2 storyline, however, peaks beyond the 95th percentile at nearly every six to twelve days, which is about three times more often than the factual storylines. The November to February average temperature differ-

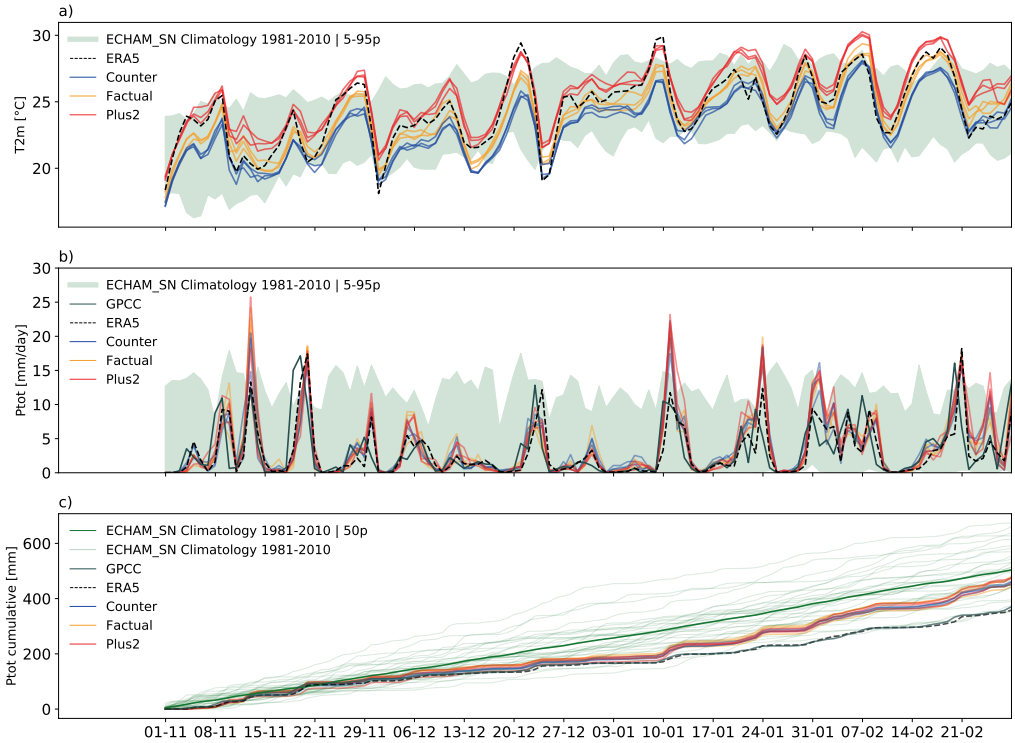

Figure 8.2: a) Daily 2-meter temperature (T2m) averaged over SESA from November 2011 until February 2012 for counterfactual, factual and plus2 storylines, climatology 1981-2010 5th-95th percentile and ERA5 reanalysis [°C], b) same as a), but for daily total precipitation over SESA [mm/day], c) Daily cumulative total precipitation over SESA [mm] for counterfactual, factual and plus2 storylines, climatology is taken from yearly ECHAM_SN values from 1981-2010 (Schubert-Frisius et al., 2017). ERA5 reanalysis and GPCC observations for comparison.

ence between counterfactual and factual is 1.0 °C; between factual and plus2, 1.4 °C; and between counterfactual and plus2, 2.4 °C, which is in line with the mean global warming over land. There is a strong intra-seasonal variability in the daily temperature signal (10-90-day period oscillations) with particularly strong and significant 10 – 15 day variability. Such variability has been found in various summer seasons that were dominated by an active SACZ (Cerne and Vera, 2011; Cerne et al., 2007).

Figure 8.2b shows the domain average of daily total precipitation for the three storylines, climatology and ERA5-reanalysis. For daily and cumulative precipitation the results match well with both ERA5 and Global Precipitation Climatology Centre (GPCC), up until the 10th of January. Following that period, the timing of precipitation events remains well simulated, however there is some mismatching of peak precipitation amounts. For this reason, there is an overestimation in cumulative pre-

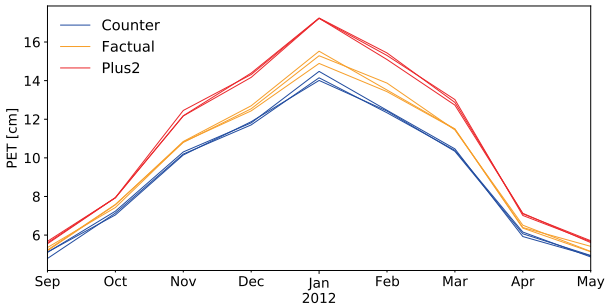

Figure 8.3: Monthly potential evapotranspiration (PET) [cm] over SESA according to Thornthwaite from September 2011 until April 2012.

cipitation starting in the second half of January and all the way through February. Just like temperature, the precipitation events can be explained by the intra-seasonal variability, where Rossby wave activity forces pulses of diagonally-aligned precipitation events (van der Wiel et al., 2015) controlling the wet and dry conditions over the SACZ and SESA regions respectively (Nogués-Paegle and Mo, 1997). However, there is no apparent climate-change signal between storylines. In Figure 8.2c, the cumulative precipitation of the different storylines, the climatological background and ERA5 reanalysis, confirms the lack of climate-change signal given the dynamic situation. It was a dry season in all storylines, with precipitation clearly below the climatological mean for December and January. The drought would have been there, with or without climate change.

The potential evapotranspiration (PET) according to Thornthwaite (1948), as shown in Figure 8.3, directly reflects the impact of increased temperatures between the storylines. Such increased temperatures causes a deficit in water vapour pressure, which in turn increases the PET. Higher PET values can be interpreted as a higher risk of drought, as the soil loses an increased amount of moisture to the atmosphere. In SESA the PET is peaking in January with values around 14 cm for counterfactual, 15 cm for factual and 17 cm for plus2. Between factual and counterfactual, the largest difference of 1.2 cm is found in February. The largest difference between plus2 and factual, 2 cm, and plus2 and counterfactual, 3 cm, is found in January. The highest difference in PET is thus found in the months with the largest PET values.

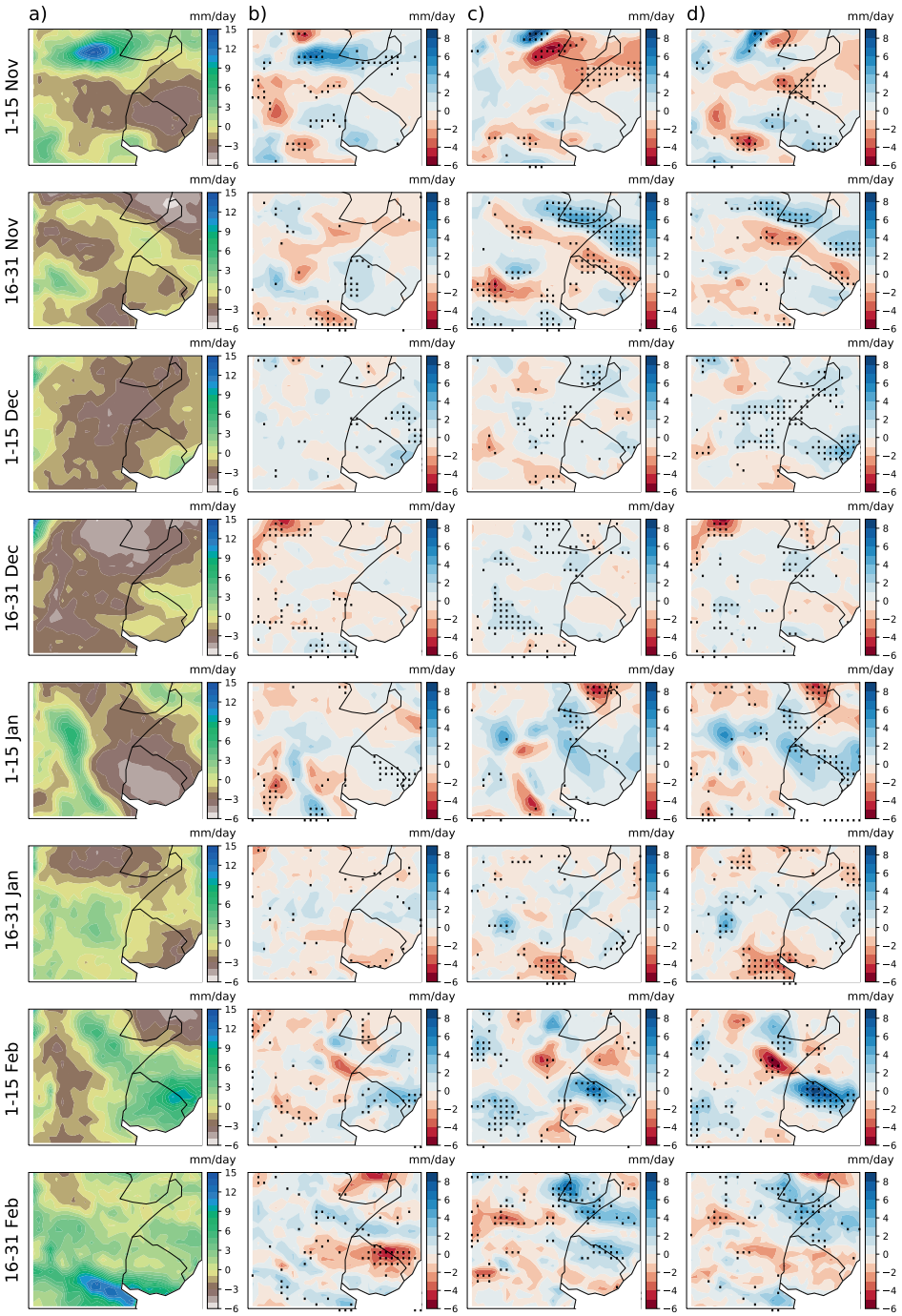

Figure 8.4: Half-month average water budget (precipitation - evaporation) [mm/day] between November 2011 and February 2012 for ensemble member averages of a) factual, b) difference between factual and counterfactual, c) difference between plus2 and factual and d) difference between plus2 and counterfactual. Stippling shows robustness, meaning a true split of the members between each world.

In Figure 8.4 the half-monthly averaged water budget (WB) for the factual, factual minus counterfactual, plus2 minus factual and plus2 minus counterfactual, shows the difference of input (precipitation) minus output (evapotranspiration) between the storylines. Especially in January, there are pockets of robust signal (stippling), meaning a true split between the members of each world, for both reduced and increased water budget. Nonetheless, in the water budget the effect of increased T2m and PET is not visible on a regional scale, as precipitation shows locally varying patterns. It is unexpected that with increased T and PET, in combination with an equal amount of precipitation, the water budget is not showing a clearer drought severity change between the different storylines.

To place the 2011/2012 SESA drought in a hydroclimatological context, the Budyko framework is applied (Budyko, 1951). The Budyko framework provides physical insight on the climatological dryness or wetness of a specific region by evaluating both the atmospheric demand and water balance. The Budyko graph (Figure 8.5) could be interpreted as a hydrological supply-and-demand graph. The atmospheric water 'demand' on the x-axis is the Budyko aridity index ($\varphi = (R/\lambda)/P$ where R is net surface radiation, λ is latent heat of vaporization (2.45*106 J/kg) and P is precipitation). The water 'supply' on the y-axis is the balance between precipitation and evapotranspiration (E/P). E/P is limited to 1 (marked with a horizontal black line), since input (P) limits output (E). Above the supply limit, other sources of water such as surface and groundwater are evaporated.

In Figure 8.5 is a Budyko graph that shows the hydrological state of SESA's climate for the counterfactual, factual and plus2 storylines. In the period between 2010–2014, SESA becomes slightly more humid in warmer storylines (round markers, average of 3 members, each 5 years). The plus2 storyline has increased wetness due to a decrease of E/P, meaning a larger water availability. Coincidently, there is a decrease in the aridity index, meaning the precipitation increase (i.e. plus2-counter 2010-2014 is 66 mm) is larger than the change in atmospheric water demand (i.e. plus2-counter 2010-2014 is 52 mm). This places the plus2 storyline left and below the counter and factual storylines (labelled with grey arrow), as was also found by Zaninelli et al. (2019). The 2011-2012 hydrological year (June 2011-May 2012, average of three members, each 1 year) (squared markers) is to the right and above the reference years, indicating a drier year than the reference. In other words, the Budyko aridity index increased towards a somewhat drier regime during the hydrological year of 2011/2012, but was counterbalanced by 10% due to climatological wetting and could be up to 15% reduction in drying in the plus2 storyline. The E/P balance also increased towards a drier regime in the hydrological year of the drought, but was counterbalanced back to a slightly wetter

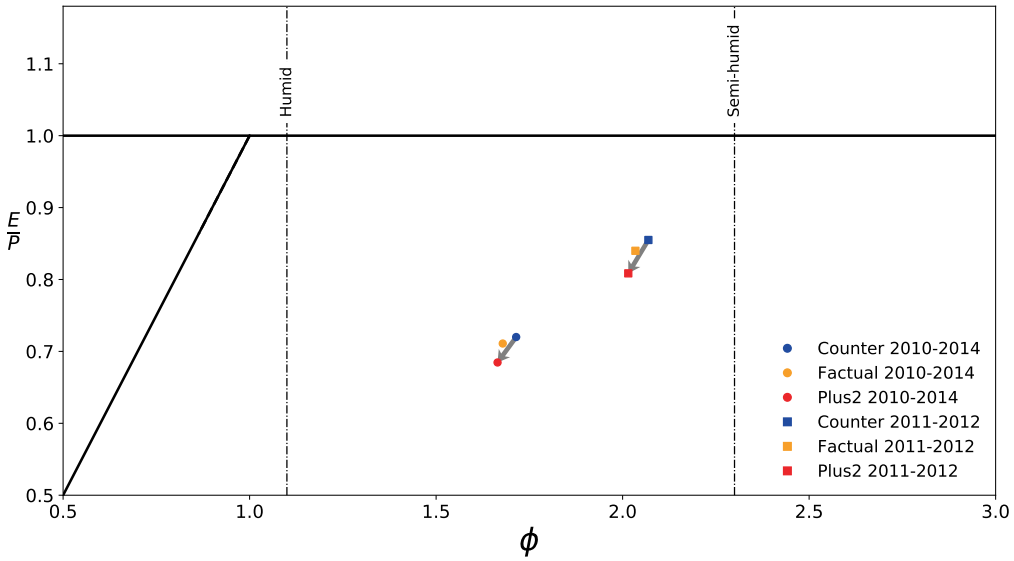

Figure 8.5: Budyko analysis over SESA for 2010-2014 (circles) averaged over the three members, and the hydrological year of 2011- 2012 (squares) averaged over the three members. Blue for counterfactual, yellow for factual and red for plus2. The Budyko aridity index (φ) is on the x-axis, evapotranspiration divided by total precipitation (E/P) on the y-axis. Grey arrows show the direction from the counterfactual towards the plus2 storyline.

regime by 11% in the factual and up to 34% in a world with 2 degrees warming. In this specific case, the natural variability shows a drying, where the climate signal shows a wetting which is in line with the known climatologically mean increase towards wetness.

8.2 South-England flood 2013/2014 - a case of limitations

The 2013/2014 winter was the wettest in the UK's observational record. Persistent storminess and precipitation, connected to a series of storms passing by in a short period of time, lasted for three months (Dec 2013 - Feb 2014) and caused storm damage and floods throughout southern-England and Wales (Kendon and McCarthy, 2015; Muchan et al., 2015). Over 700 floods were recorded, with an estimated €1.7 billion in economical losses (Fenn et al., 2016) for both privately owned goods and publicly owned infrastructure. The extreme was caused by two clusters of storms, one bridging over December and January, the second from the end of January until deep into February (Muchan et al., 2015). Despite the lack of a precipitation trend over the past 200 years (Huntingford et al., 2014), the longevity of the floods was likely increased by climate change (Kay et al., 2018). Oueslati et al. (2019) suggested separating the event

attribution to dynamic and thermodynamic drivers using storylines, and concluded that the climate signal is most likely to be found in the vertical moisture advection. There is, however, no clear results on how climate change has influenced this specific extreme event due to its dependence on dynamical conditions, and the large variability of the UK's winter climate (Huntingford et al., 2014; Kendon and McCarthy, 2015).

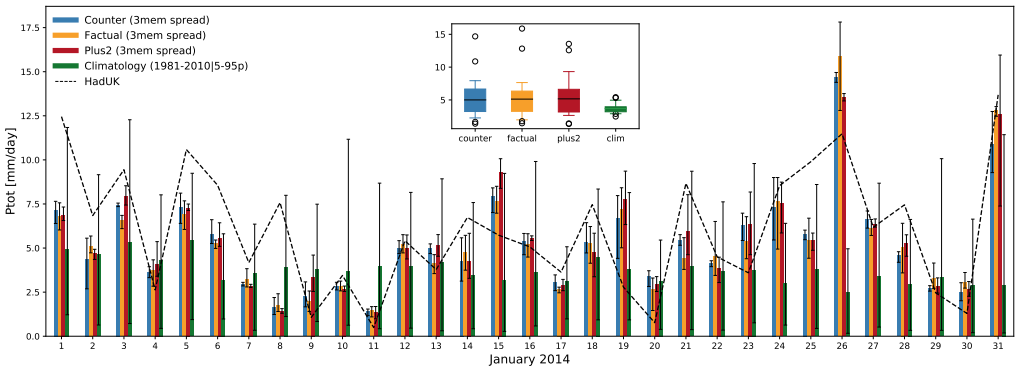

Figure 8.6: Daily averaged precipitation over the UK [mm/day] for January 2014. In blue the counterfactual, yellow the factual, red the plus2 and green the ECHAM_SN 1981-2010 climatology (5-95th percentile). In the box, the monthly average precipitation is given.

In Figure 8.6 the daily average UK precipitation for January 2014 (over land) for each storyline is compared to ECHAM_SN climatology and Met Office Hadley Centre United Kingdom gridded climate observations (HadUK-Grid) (Hollis et al., 2019) is shown. The precipitation in the storylines follow HadUK-Grid reasonably, though at the beginning of January the simulations underestimate the observed precipitation. The peak precipitation is found on January 26 and January 31, which is also comparable to HadUK-Grid observations. Between the different storylines there is no systematic difference, as which world has the largest precipitation volume differs per day. In Figure 8.7 the monthly precipitation anomalies with respect to ECHAM_SN 1981-2010 (panel a) and the difference between the factual and counter (panel b), between the plus2 and factual (panel c) and the plus and counter (panel d) is shown. Stippling is added to show robustness, where all the members of each storylines are truly split by 1% or more. The factual anomalies are dominantly wet, as expected. The difference between the storylines, however, do not show much robustness in southern-England or Wales (domain marked in panel b - December), especially in January. The precipitation patterns vary greatly between past and future, including a change of sign. When looking into the domain averaged precipitation specifically for southern-England (see domain box in Figure 8.7 b-December) in Figure 8.8, there is no increased robustness. The storylines are following the HadUK-grid observations well, except for the peak

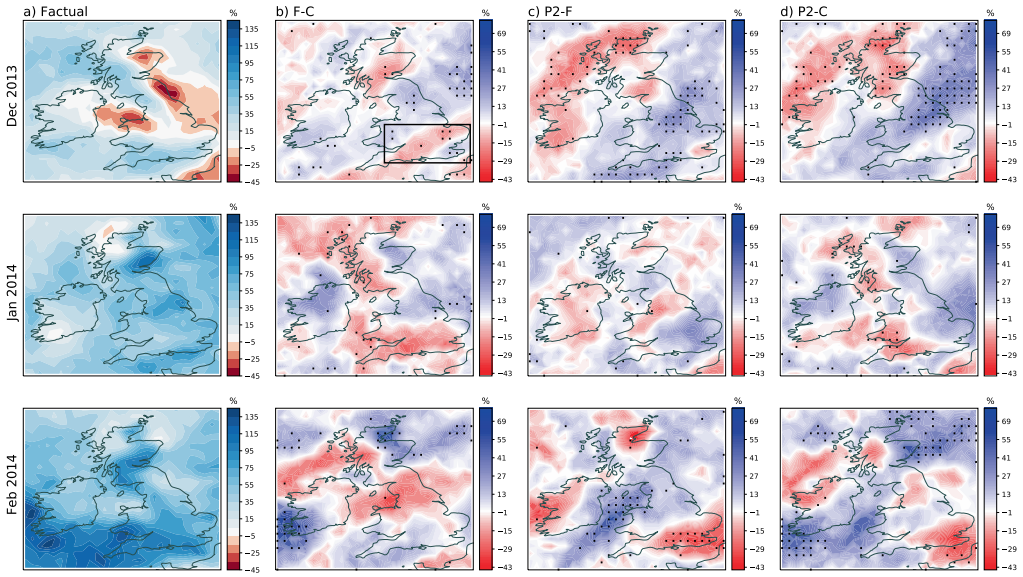

Figure 8.7: Monthly averaged precipitation anomalies for the UK for December 2013, January 2014 and February 2014, a) factual anomaly, b) difference between factual and counterfactual, c) difference between plus2 and factual, d) difference between plus2 and counterfactual. Stippling is robustness, where all the members of each storyline are truly split by 1% or more in comparison to the other storylines.

precipitation on the 23rd of January, which is underestimated by the storylines and ECHAM_SN.

Precipitation can be split up in two variables: the dynamical vertical velocity (ω) and the thermodynamic specific humidity (q). In Figure 8.9 the first row is the vertically averaged ω and the second is q for January 2014, the panels are organised as in Figure 8.7. The specific humidity graphs show a high level of robustness, with a local increase well above 1 g/kg when comparing plus2 with factual. The vertical velocity, on the other hand, shows a lot more variability, which explains the varying difference in the precipitation. Upward motion (negative values) is needed for precipitation to form. When looking at differences between worlds, a positive value means the uplift has decreased and less precipitation is expected. There is a reduction of vertical velocity visible over St. George's Channel and western Scotland. This is in agreement with a reduction in precipitation in Figure 8.7, but the signal in the precipitation is not robust. Neither is there a robust signal in southern-England or Wales. Note that it is unclear how the vertical velocity is influenced by the nudging in the higher atmosphere, and therefore the interpretation of ω should be done with care. The method in its current setup cannot contribute to conclusions concerning the conditional climate signal in the precipitation of this event.

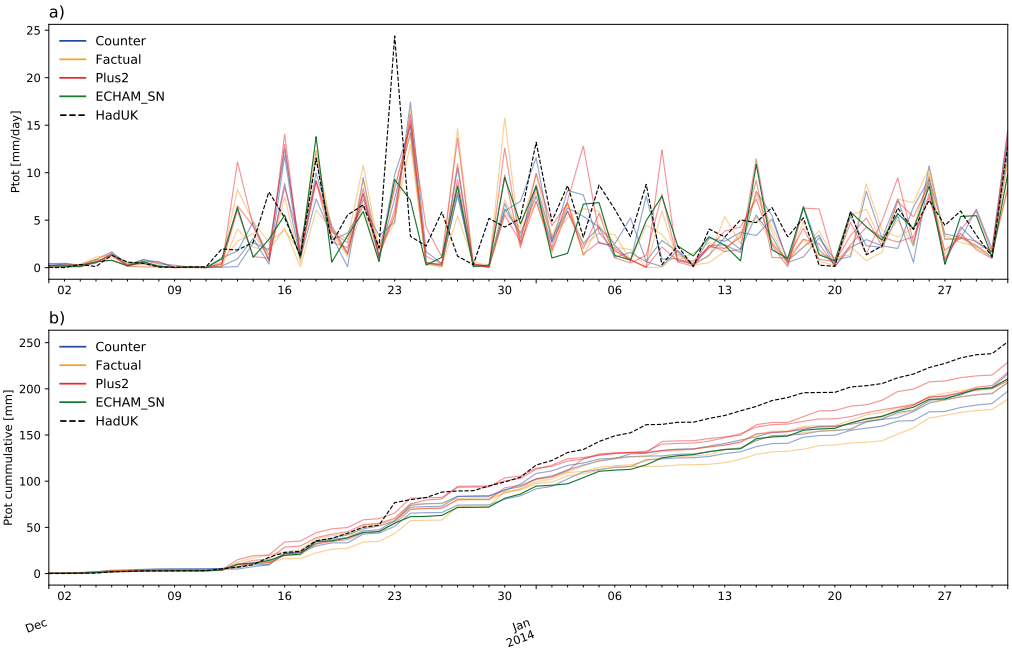

Figure 8.8: Precipitation in January 2014 southern-England for a) daily precipitation in mm/day, b) cumulative precipitation in mm. Blue is the counterfactual storyline, orange the factual, red is the plus2, green is the ECHAM_SN climatology and the black dashed line is the HadUK-Grid observations.

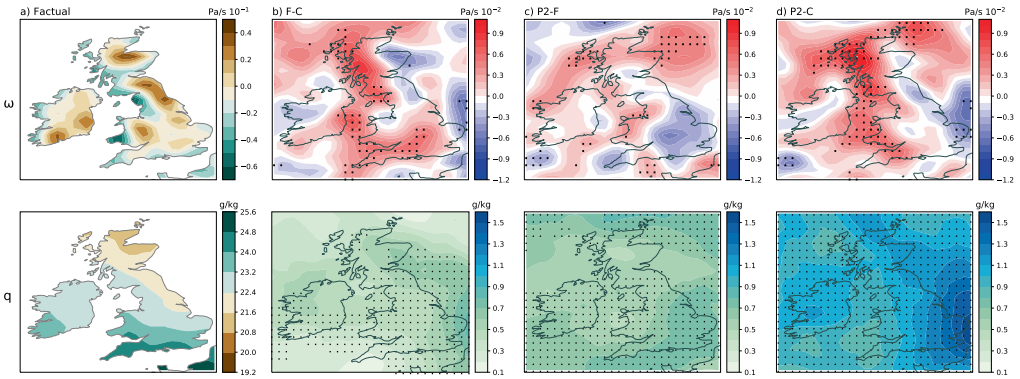

Figure 8.9: Monthly averaged vertical velocity (ω in Pa/s) and specific humidity (q in g/kg) for January 2014 a) factual, b) difference between factual and counter, c) difference between plus and factual, d) difference between plus2 and counter. Stippling indicates robustness where the members of each storylines are truly split by 0.1 Pa/s 10^{-2} or more for ω, and 0.1 g/kg or more for q.

8.3 Discussion and conclusion

The analysis of the 2011/2012 summer drought in Southeastern South America (SESA) was approached from an event attribution perspective, and additionally included a climatological background analysis to place the event in its climatological context. Understanding drought impacts in a region that exhibits a climatological wetting trend, like SESA, is relevant for decision-making and adaptation. The total precipitation compares well to GPCC and ERA5 (regridded to T255), although peak precipitation volume tends to be slightly overestimated. The 2011/2012 drought was connected to a large-scale pattern, namely the South Atlantic Convergence Zone (SACZ), which is well resolved by the model. Smaller scale precipitation events, either in space or time, would require a higher resolution model. In this study the temperature, potential evapotranspiration (PET) and precipitation are considered the main contributors to drought. For temperature, the counterfactual, factual and plus2 storylines show a climate change induced warming in line with the mean global warming over land. The temperature peaks, passing the 95th percentile, are more frequent in the plus2 storyline, compared to counter and factual. The impact and frequency of heat waves can thus be expected to increase with a plus2 degree warming in seasons with similar dynamical conditions (e.g. active SACZ conditions). The Thornthwaite method for calculating PET is temperature-based, and may have a non-linear temperature forcing bias when used in the light of climate change induced warming (Shaw and Riha, 2011). That said, PET is clearly higher in the factual and plus2 storylines, compared to the counterfactual. However, there are no differences in daily average nor cumulative precipitation between the storylines. Consequently, higher temperature and PET with equal amounts of precipitation place the region at a higher risk of drought. Be that as it may, no large-scale decrease or increase in the half-monthly water-budgets were found: the drought is actually not stronger in climate change impacted storylines.

These apparently contradictory results can be explained by taking into account the climatological hydrological background. The results show that the general climate change induced trend in SESA is wetting. In the 2011/2012 hydrological year, storylines with increased climate-change signal show increased precipitation amounts before and after the drought. When jointly considering the atmospheric water demand and the water balance it shows that the climate change induced precipitation increases in the region, and for this event, is large enough to outweigh the climate changed induced increased evapotranspiration and PET during the drought. Hence, the wetting background counters the increased T and PET, reducing the potential impact on agriculture. The climatological computations in the Budyko analysis were done using the 2010-2015 3 member average. This 15 year ensemble of data is suboptimal, and it

would be good to compare a 30-year average climatology with the hydrological year of 2011/2012. Whether under a different level of warming the effect of climate change on drought extremes would bypass the wetting background remains unclear. Other regions that experience a general drying due to climate change may therefore suffer even more during stronger droughts. More research using the event-based storylines is needed to understand these aspects fully.

The 2014 UK flooding showcased limitations that the current setup has to deal with. The simulated daily average precipitation for January 2014 followed the HadUK observations reasonably well, though there are some underestimations at the beginning of the month and the peak precipitation for the 16th of January is overestimated. Precipitation being a complicated variable, resulting from both dynamic and thermodynamic processes, the analysis was broadened by looking at specific humidity (q) and vertical velocity (ω) separately. Specific humidity is increasing due to climate change, with a strong and robust signal. The vertical velocity, however, shows a very different picture with little robustness over land and change of signal between past and future storylines. It is unclear how the spectral nudging of the horizontal flow influences the vertical velocity on pressure levels. However, this influence is considered to be limited since the nudged part of the atmospheric column represents a relatively small part of the total mass. Another point of uncertainty is lack of knowledge on the influence of the upper troposphere on precipitation (Trenberth, 2008). Beside these physical arguments there is a technical argument; precipitation is a hard to resolve variable due to its dependency on small-scale processes that are too small for the resolution of ECHAM6, and are thus parameterized. Such parameterization is an approximation, causing biases in the resulting precipitation and is significantly less accurate than convective-permitting regional models (IPCC, 2014).

Part IV

Interpretation

The spectrally nudged event storylines presented in this study are evaluated, and the climate change attribution of the individual case studies is discussed. The main findings are given and answers to the research questions are presented. Finally, in the outlook, improvements to the method and possible future applications are suggested.

9 Discussion

9.1 Spectrally nudged event storyline methodology

Global spectrally nudged event storylines have been applied to attribute extreme weather events conditionally to climate change. To enable thermodynamic attribution, the large-scale vorticity and divergence were spectrally nudged in the higher atmosphere of the ECHAM6 high-resolution atmospheric model towards NCEP1-R1 reanalysis data. Spectral nudging enables the reproduction of extreme events with their particular dynamical details, allowing the same dynamical events to be reproduced in simulations with different boundary conditions, and thereby achieving a higher signal-to-noise ratio of the climate change effect than in free running simulations. This ensures that each simulation has the same large-scale dynamic setup, but leaves other variables free to respond.

Three storylines were created, representing three worlds, 1) a world without climate change (counterfactual), 2) a world as is (factual) and 3) a world with two degrees of global warming (plus2). Each of the storylines have altered greenhouse gases (GHG) concentrations and sea surface temperature (SST). The GHG concentrations were set to pre-industrial times for the counterfactual, and to ssp585 scenario values corresponding to a 2 °C warmer world for the plus2 storyline. For the SSTs, different warming patterns were computed. The difference between the pre-industrial and present SST was deducted from the NCEP1-R1 SST model input to create the counterfactual

SST input. The plus2 SST warming pattern is the difference between the present and the ssp585 scenario SST corresponding to a 2 °C warmer world. This warming pattern was weighted and added to the NCEP1-R1 SST model input.

The simulations have resulted in 5-year continuous global storylines (2010-2014), analysed for seasonal weather trends and specific extreme events. A total of four case studies have been analysed in depth, two temperature extremes: the European heatwave of 2003, the Russian heatwave of 2010, and two hydrological extremes: the SESA drought of 2011/2012 and the South-England flood of 2014. In the following sections I will discuss the strengths and limitations of the spectrally nudged event storylines.

9.1.1 Strengths of spectrally nudged event storylines

Seven main strengths of using spectrally nudged event storylines for attributing climate change to extreme events are summarised below:

Continuous attribution
The nudged storylines provide a continuous climate attribution of global historic weather events. This means that within the time frame of the simulation, which in this study is 5 years, any historical weather event can potentially be attributed. The continuous nature of the method allows for both seasonal and multi-year event attribution, as well as short timescale events. Moreover, the method is independent of event location since the simulations are global. On a side note, attributable events are limited to those resolved by the reanalysis data that is used for nudging the simulations. In this study I have created 5-year simulations, but the method can be applied to any length of time for as long as nudging input data is available. Global precipitation and temperature analysis shows that the model can follow the seasonal variability well over the entire duration, which for precipitation is a larger challenge than for temperature (see Chapter 6).

Attributing specific events
The storyline method is capable of attributing climate change to one specific extreme event. There is no need for the definition of an event class with the connected arbitrary 'choice of events' and unavoidable blurring over event details. The European and Russian heatwave case studies show the events were well resolved compared to reanalysis and attributable on daily and regional time and spatial scales (see Chapter 7).

Small ensemble size
Due to the reduced uncertainties that comes with the nudged atmosphere, a small ensemble size will suffice. The noise range between members in the nudged simulation ensemble is small, as was shown with the time series of global temperature and precipitation, as well as the temperature time series of the heatwaves and the drought (see Chapter 6 and 7). However, for precipitation the three member ensemble might be expended to a somewhat larger number to deal with the variability and uncertainties inherent to the variable.

Robust separation of climate change from natural variability
Signal-to-noise ratio and robustness are pivotal to climate attribution. The results only makes sense when the signal is distinguishable from the noise, that is, the climate signal from the natural variability. Moreover, that signal should be robust in order to be reliable. The spectrally nudged event storylines are accurately able to do this on small time and spatial scales, especially for temperature related events. The attribution results of 0.6 °C average increase in T2m during the European heatwave, and 2 °C during the Russian heatwave, proves the method can isolate the climate-change signal despite the presence of a large natural variability element during each of these events. The temperature climate-change signal, in both the case studies and the global trends, is strongly robust. This is shown by the separation of members in the T2m time series both globally and heatwave-specific, as well as the signal-to-noise analysis of each of the heatwaves (see Chapter 8).

Distinguishing between opposing climate signals on different time scales
Climate change does not behave uniformly over the globe, but can influence extreme weather events very differently depending on the time and location. The method presented here is capable of separating between long-term and short-term climate influences, as well as competing climate signals, despite the complexity of the event under study. The southeastern South American drought analysis shows this pivotal quality of the storylines method. The drought event itself would clearly have been intensified due to climate change, with increased temperatures and evapotranspiration. The long-term wetting trend that climate change is causing in the background, however, is counterbalancing that. Analysing the specificity of this event, in combination with long-term background analysis, allows for this finding.

Widely applicable
Spectrally nudged storylines can be directly applied to any spectral model and indirectly to a non-spectral model using a Fourier transformation (or other comparable method) (Schaaf et al., 2017; von Storch et al., 2000). The method is widely applica-

ble and not too expensive in either model development or computing time (Schubert-Frisius et al., 2017). Moreover, nudging is not limited solely to NCEP1_R1, other datasets can be used allowing for flexibility in application.

Easy communication
Storylines offer a more straightforward and easy to understand result. As mentioned in the rationale (Part I), the challenge with extreme event attribution is more than just technical, it is also communication. Probabilistic attribution will often provide a return time which represents the chance of a type of extreme event happening with or without climate change. This kind of information can be challenging to understand for the non-climate-specialist (Patt and Schrag, 2003), though efforts are made to improve probability and uncertainty communication (Stephens et al., 2012). Storylines provide attribution statements that are more straightforward and easier to communicate. It is not possible to make a direct comparison between my findings and those from probabilistic attribution because they are answering different questions, and the conditions are quite different. However, from a methodological perspective, it is useful to contrast the nature of the attribution statements that can be made using the different methods. This is done in Table 9.1 for the case of the Russian 2010 heat wave. The 2010 Russian heatwave probabilistic analysis by Otto et al. (2012) showed the return time of this type of event in this region was 1-in-99-years and had become 1-in-33-years, meaning climate change triples the chance of an event such as the Russian heatwave to happen. The storyline result is an average 2 °C warmer heatwave due to climate change, with locally up to 4 °C warmer. A change in probability is extremely sensitive to the details of the event definition, which makes it difficult to understand in terms of the relevance to the event a person experienced. The storyline analysis is specific to the extreme event, which makes it independent of any event definition and does not require probabilities.

9.1.2 Limitations of spectrally nudged event storylines

Seven main limitations when using spectrally nudged event storylines for attributing climate change to extreme events are summarised below:

Aerosols
The plus2 storylines, with boundary conditions based on a 2 °C warmer world, in the end reached only 1.55 °C above the counterfactual. The most likely cause lies in the creation of the storyline boundary conditions. The GHG and SST changes are considered to create a storyline of a world that could be with plus 2 degrees warming,

Table 9.1: Example of attribution statements that are possible using the probabilistic and storyline approaches for the case of the 2010 Russian heatwave.

Probabilistic attribution (based on results from Otto et al. (2012))	Averaged over the Russian domain and over the month of July, shows temperatures in 2010 were 5 °C above the 1960s climatology, of which 4 °C was due to internal variability, and 1 °C was due to anthropogenic climate change. The heatwave represented a 1-in-33-year events, which was 3 times more likely than it would have been in the 1960s.
Storyline attribution (based on present results)	Averaged over the Russian domain, temperatures in 2010 steadily increased from the 1985-2015 climatology through the month of July up to approximately August 10th, then rapidly returned to climatology. The domain-averaged heatwave reached 10 °C above the 1985-2015 climatology in early August, of which 8 °C was due to internal variability, and 2 °C was due to anthropogenic climate change. The anthropogenic component of the warming reached 4 °C in the region to the south of Moscow during the first half of August, where it exacerbated the already warm temperatures there.

while aerosol settings were kept unchanged. Aerosols have, on average, a cooling effect on the climate (Samset et al., 2018). However, they are also damaging to the public's health and therefore action for cleaner air motivates a reduction of aerosols with a loss of their cooling effect since approximately the year 2000 (Smith et al., 2021). Moreover, aerosols are coemitted with GHGs and therefore any effort to reduce the GHG emissions will also reduce aerosols (Samset et al., 2018). As the aerosols are prescribed in ECHAM6 with the values from 2010-2014 (Stevens et al., 2013), which are the unchanged values, the level of aerosols is higher in ECHAM6 than in the RCP8.5 scenario at the point of 2 °C global warming (Westervelt et al., 2015), therefore the cooling due to aerosols is overestimated. Knowing the cooling effect of aerosols and how they are resolved in the model indicates that altering the aerosols in the plus2 world to the MPI-ESM ssp585 scenario values would enable the climate-change signal to reach the 2 °C. Storylines could be expanded to consider these factors. Even so, the results do give an insight in how a historic event would be different in a future world.

Prescribed boundary conditions

To regulate the climate signal in the sea surface temperature (SST) boundary conditions, warming patterns were computed for the past and future storylines. The patterns were made on a yearly timescale for the 2010-2014 simulations, which is suboptimal for seasonal variability. The sea ice concentration (SIC) boundary conditions were either not incorporated (2010-2014 simulation) or incorporated but resulted in large temperature issues around the poles (1948-2014 simulation) as result. The method of computing SIC concentrations based on SST caused an overestimation in the SIC values. Finding the proper way for altering SIC to remain self-consistent with the SST is complex, but the simulations would benefit. For the results presented in this work, the unaltered SIC is not considered a significant problem since the atmosphere is nudged and any overestimated pole-to-equator temperature gradient will have very limited influence on the large-scale dynamics.

Small-scale processes

The model used in this work is the ECHAM6 high resolution (T255L95) atmosphere only model. Despite this being the highest resolution available for ECHAM6, it is hydrostatic and too crude to resolve a large set of small processes. Convective processes, for instance, are too small scale for ECHAM6 to be resolved and are therefore parameterised. It is likely that the biases found in the precipitation, both globally and regionally, are related to this technical limitation. The South-England flood of the 2014 case study shows the difficulties of filtering a climate signal in such a small spatial- and timescale precipitation event (see Chapter 8). The parameterisation of precipitation produces relatively good results for longer time scales and for the average global

mean precipitation, with the exception of the tropical region. This makes sense as parameterisation aims only for a statistically correct value, and in smaller spatial and time resolutions those statistics can diverge significantly. Tropical precipitation is challenging for any model as summarised in Figure 9.1 where the largest bias and error for the CMIP5 multimodel mean precipitation is in the tropical regions. The difficulty lies in the dominantly convective precipitation and its dependence on a large set of small-scale processes in the atmosphere, the land-atmosphere interaction and topography, which are not resolvable or are problematic even for extremely high-resolution models (IPCC, 2014; Stevens and Bony, 2013). Since the challenges with small-scale processes is related to the models, they are the same for the storylines approach as they are for the probability approach. Most global models struggle with small-scale processes, though more recently developed non-hydrostatic global models now include convective permitting computations (e.g. ICON (Zängl et al., 2015)). However, these non-hydrostatic global models cannot be run for a longer period of time. To include small-scale processes in a simulation for a longer period of time would require a regional model. That said, any convective permitting model still struggles with the precipitation variable due to its complexity (IPCC, 2014).

One-model setup

The results are computed with ECHAM6 only; a comparison with several other models would clarify the influence of model bias uncertainties on the results. Also, the model was nudged towards NCEP-R1 only, which in itself should not be much of a problem as most reanalysis data sets are quite similar for large-scale vorticity and divergence, however the reanalysis data itself does have biases. Since the simulations are compared to each other, these biases should have a minimal impact.

Dynamical atmospheric situation

Event storylines incorporate the rationale that dynamical atmospheric situations can be seen as a given and the known thermodynamic aspects of climate change form the basis for the attribution. Thus, the effect of climate change on the likelihood of occurrence is not assessed. In that respect, this approach is complementary to the more widely-used probabilistic event attribution. To address changes in extremes due to altered circulation, which influence frequency and duration, dynamical storylines could be added to the attribution toolbox. However, since most results of probabilistic event attribution appeal in any case to the known thermodynamic aspects of climate change, it can be argued that not much is lost in the storyline approach, yet much is gained by its specificity. This is especially the case for extreme events whose dynamical conditions are not well represented in climate models, e.g. blocking.

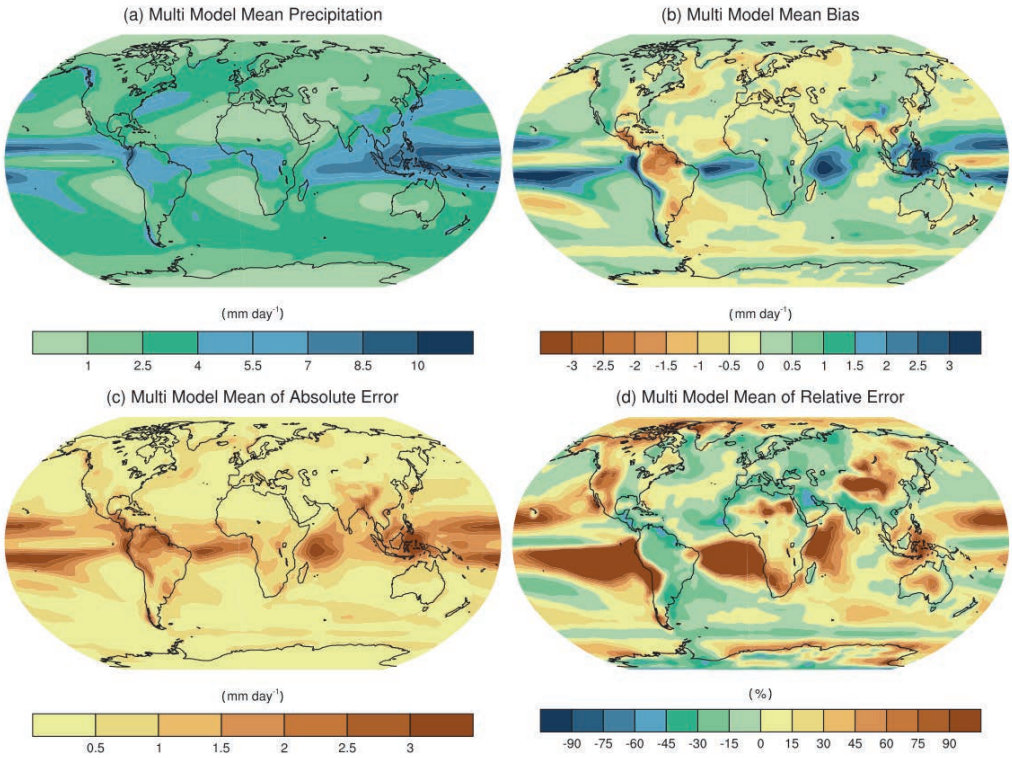

Figure 9.1: Global annual precipitation ($mm\ day^{-1}$) CMIP5 multimodel mean for a) Mean precipitation, b) difference between the mean precipitation and the Global Precipitation Climatology Project (GPCP) observations, c) mean absolute error in comparison to the GPCP observations and d) mean error based on the mean precipitation in a. Figure 9.4 from IPCC (2014).

Dynamic extreme events

Due to the conditionality of the analysis, there must be a thermodynamic aspect in the extreme under study to obtain meaningful results. For precipitation the specific humidity is a thermodynamic aspect, and the vertical velocity is dynamic. For storms, the distinction between dynamic and thermodynamic becomes more challenging. To understand extremes connected to dynamics, the attribution could be completed using dynamical storylines (Zappa and Shepherd, 2017). Nonetheless, such extremes remain complicated to model.

Epistemic uncertainty

Uncertainty, inconclusive results or lack of robustness is not always due to technical challenges. Many processes and causal relationships in the atmosphere are still unknown, or at least not completely understood. The processes that influence precipitation, for instance, are a topic of continuous research. The inconclusive results for

the 2014 UK flood could, for example, be related to the unknown role of the upper troposphere in relation to precipitation. Epistemic uncertainty is not unique to the method presented here, but is generally present. That said, it is important to keep in mind that processes might simply not be understood, which are most likely influenced by climate change as much as the understood processes, and therefore influencing the (un)certainty of the results.

The limitations mentioned above are all important to keep in mind when working with storylines, however not all of them are specific to the method. Epistemic uncertainty, one-model setup and prescribed boundary conditions are limitations common to most atmospheric modelling studies, or climate research as a whole. Small scale processes is an issue throughout studies that include a global model. Using the spectrally nudged setup might help reduce the uncertainties linked to small scale processes due to the prescribed dynamics, but it cannot solve the issue. The limitations concerning aerosols and dynamic extreme events are specific to the spectrally nudged storyline method presented in this thesis.

9.2 Comparison with other conditional attribution studies

During the completion of this research, nudged event storylines were developed by two other research groups as well, albeit it with either a different goal or a different technical setup. Wehrli et al. (2019) compared nudged simulations with free running simulations to perform a mechanism denial experiment and found the effect of soil moisture depletion on five different heatwaves, including the Russian heatwave in 2010. They used the Community Earth System Model (CESM) model with prescribed ocean settings and nudged towards ERA-Interim to create the storylines. The influence of recent GHG concentration increase, SST, soil moisture and circulation were compared to each other using the percentage of maximum temperature anomaly that could be explained with each. For the Russian heatwave roughly 10 % of the temperature anomaly could be attributed to recent increased GHG concentrations, representing an increase of 1.2 °C. Note that this is the difference between 2010-2016 (experimental time frame) and 1982-2008 (climatological reference). Roughly 35 % of the temperature anomaly was attributed to soil moisture depletion. Interestingly, they found that the SST pattern caused a reduction of -0.8 °C, roughly -6.5 %, in maximum temperature anomaly. The work presented here shows that for the Russian heatwave roughly 80 % (8 °C) of the average temperature anomaly was due to natural variability (which is a combination of circulation and soil moistures, as atmospheric nudging by definition constrains the soil moisture as well) and 20 % (2 °C) to climate change. Considering the differences in application, the results are comparable for the

climate change attribution. When comparing the findings of this current research to the results by Wehrli et al. (2019) it is important to keep in mind that their results does not span the full industrialised time period, but for a more recent set of years.

Recently Sánchez-Benítez et al. (2022) developed the spectrally nudged event storylines in the AWI-CM-1-1-MR coupled model with ECHAM6 (T127L95) for the atmosphere (CMIP6 setup) and spectrally nudged towards ERA5. Four storylines were created, namely pre-industrial, present day, +2 K and +4 K worlds. A coupled model could be beneficial for analyses such as ocean and sea-ice interaction or sea-ice extent. However, the trade-off is a lowering of the atmospheric resolution, which reduces spatial accuracy in extreme event attribution, and even more so when linking results to impact analysis. Reduced atmospheric resolution can lead to either dampening or overestimating of the maximum and minimum values in e.g. temperature and precipitation and struggles with biases, especially in a coupled setup (Moreno-Chamarro et al., 2022). The storylines were applied to the July 2019 European heatwave to showcase the method. An amplified global warming effect was found, on a daily timescale, reaching locally up to 5 °C and would, in a 4-K world, even reach up to 13 °C which would make the maximum temperature 50 °C. It is interesting to see that the 2003 European heatwave presented in this thesis did not show any amplified climate change effect, where the 2019 heatwave in Sánchez-Benítez et al. (2022) clearly does. Putting aside any possible technical differences that could lead to somewhat altered results, it shows the need for individual extreme event attribution, since similar events (in this case European summer heatwaves) may have undergone a very different influence by climate change.

The common denominator between the studies by Wehrli et al. (2019) and Sánchez-Benítez et al. (2022) and the work presented here, is a clear distinction between the climate-change signal and natural variability in heatwaves. This shows the capability of the storyline approach to isolate the climate-change signal and is not depending on a particular technical setup. Moreover, the method requires only a small ensemble size for robust results, which reduces costs. The extreme event type studies in these publications are heatwaves, which make sense as they are the most straightforward event to conditionally attribute (NASEM, 2016).

It is interesting to place the results found in the context of a different method that also focuses on thermodynamic attribution. The Russian heatwave of 2010 was also a case-study in Terray (2021), who applied the updated dynamical adjustment method. The dynamical adjustment method is based on analogues, finding the climate change effect between two very similar extreme events that happened in modern time with cli-

mate change and in older times with limited climate change using observational data. Using observations does, in fact, limit the application due to the observed data being non-uniform over the globe and not all variables of interest are included. That said, Terray (2021) found remarkably similar results to those presented here, despite the different method of analysing the conditional response. I found the natural variability and anthropogenic forcing of the Russian heatwave to be 8 °C and 2 °C respectively, as shown in Table 9.1. Terray (2021) found 8 °C internal variability and 1.9 °C anthropogenic influence. The similarity in results shows the validity of attributing the thermodynamic and dynamical elements separately.

10 Conclusions

10.1 Main findings

Based on the results presented in Part III, I summarize the main findings of the conditional climate attribution study below.

Conditional attribution has near identical global temperature climate-change signals as unconditional attribution.
Climate change causes a consistent increase in average global mean temperatures, which is a well known result (IPCC, 2021). However, that result was established with unconditional attribution and here the same results are found using a conditional setup. The conditional attribution is robust and spatially uniform which suggests that in that respect nothing is lost when attributing conditionally, but it does allow for a much shorter time period for integration. The maximum average temperature increase can differ per region and season. The strongest increase in maximum temperature is in the middle-east during June-July-August at 2.76 °C in the world as is and 3.67 °C in a world with +2 °C.

Conditional attribution has comparable precipitation climate-change signals as unconditional attribution.
The average global total precipitation has increased due to climate change, and would increase even more in a world with +2 °C warming. The spatial patterns and sign

of precipitation vary vastly over the globe, showing both wetting and drying. These conclusions are in agreement with known effects of climate change achieved through unconditional attribution (IPCC, 2021), showing that also with precipitation there is nothing much lost in attributing conditionally. The conditional climate signal is robust wetting for the Amazon, the east coast of North America, the Arctic and Antarctic, and drying for the west coast of Central and North America. That said, robustness is the strongest over sea and is less clear than in the global temperatures.

There are year to year variations in climate change induced alterations of regional seasonal precipitation characteristics.
The regional precipitation changes due to climate change are known to differ from the global trend, and the results in this study show how they can differ from year to year. For the 2012 and 2014 Mexican monsoon there is a drying found, but the 2010 monsoon had no climate signal. The Indian monsoon of both 2011 and 2014 show a wetting, but the spatial location of the wetting inside the domain varies greatly between the two. Moreover, the robustness of the climate signal is depending on season and location. The seasonal precipitation in Scandinavia was less for the summer of 2012 but more for the autumn of 2013. The seasonal precipitation event of summer 2011 and 2012 in Australia have become wetter and are expected to continue doing so in a +2 °C world; however, the signal is not very robust.

The European heatwave of 2003 was on average 0.6 °C warmer, in line with global warming, but local increases reached up to 2 °C.
The European heatwave in the first half of August 2003 was caused by an atmospheric blocking, which was semi-stationary and resulted in exceptionally hot and exceptionally dry conditions over central and Western Europe. The conditional attribution showed an increase of 0.6 °C between past and present storylines, which is in line with the average global mean warming in 2003. The warming is, however, not uniform over the domain. Local differences are between 0 °C and 2.5 °C, though over land the signal is robust and generally above 0.5 °C.

The Russian heatwave of 2010 had an amplified climate-change signal, on average 2 °C warmer, with local temperatures up to 4 °C warmer.
The exceptional Russian heatwave lasted three weeks, from the end of July until halfway through August, and was caused by a quasi-stationary atmospheric blocking. Climate change caused a robust amplified warming of 2 °C, which is about 1.4 °C above the average global mean warming in 2010. As with the European heatwave, the Russian heatwave climate-change signal is spatially non-uniform, varying between 1 °C and 4 °C.

The southeastern South American drought of 2011/2012 was at risk of intensification due to climate change, but was counter balanced by the general background wetting trend also due to climate change.
The short but devastating drought in southeastern South America during the summer of 2011/2012 was connected to the South Atlantic Convergence Zone (SACZ) large-scale pattern. Climate change caused the local temperature to increase and the potential evapotranspiration (PET) to increase as well, but left no quantifiable mark on the total precipitation. The combination of these three factors should cause the drought to become more intense. However, the water budget showed no climate signal. These apparently contradictory results are explained by an increased wetting in the background climate, meaning the average precipitation throughout the year increased. The increased wetting in the climate counter-balanced the potentially more extreme drought.

10.2 General conclusion

The main goal of the work presented here was to obtain high-quality conditional climate change attribution of singular extreme weather events. To achieve this goal, I have developed, applied and evaluated spectrally nudged event storylines using the ECHAM6 atmospheric model. Below I answer the individual research questions posed in Chapter 3.

To attribute individual extreme events, it is paramount to test if the method is capable of resolving individual extremes properly. The first research question to be answered is as follows:

How well can spectrally nudged storylines follow extreme events?

The timing of temperature extremes of individual extreme events are accurate and in agreement with reanalysis data on daily and monthly timescales, as well as local and regional spatial scales. Maximum temperatures can be somewhat under- or overestimated depending on the location. Precipitation extremes are simulated in correct daily timing and location. However, there is an overestimation compared to observations, especially in the tropics. Time and spatial scales need to be larger to capture the correct precipitation amounts, as shown with the seasonal precipitation over Scandinavia and India. Despite the bias found in precipitation, which was also visible in the southeastern South America drought analysis, the drought was resolved well. Droughts are more complicated than just lack of rain, and depend on variables such as temperature,

soil moisture and evaporative demand. These factors are well resolved to the detailed level that enables a separation of climatological wetting and strengthening of a drought in the same region in the same time frame.

Results found by applying spectrally nudged storylines are only meaningful if the climate-change signal is standing out from the noise of natural variability. Thus, the second research question is as follows:

How clearly can spectrally nudged storylines distinguish signal from noise?

By using a small ensemble of factual, counterfactual and plus2 simulations, the noise level for the analysis was determined. This revealed that the (conditional) signal of climate change is determinable at both daily timescales and local spatial scales when looking at temperature extremes. For the precipitation extremes there is more noise, and the daily and weekly resolution was therefore too small. Better signal-to-noise ratios are found for seasonal precipitation. Note that the signal-to-noise ratio analysis also confirms that a three member ensemble is sufficient to grasp the noise of the experiment, with a low noise around the median between members of the same ensemble. This confirms the visibly low noise of the ensemble in the time series of temperature (Figure 7.1 on page 67). These findings are in agreement with Wehrli et al. (2019) and Sánchez-Benítez et al. (2022).

The spectrally nudged event storylines method is applied to attribute a set of case-studies. Thus the third research question is as follows:

What is the relative role of climate change vs. natural variability in extreme weather events?

1. *For heatwaves?*
   From the case studies in both Europe and Russia, it follows that high-impact heatwaves would occur with or without climate change, but the extreme would have been less extreme without it. The climate change element is separable from natural variability and quantifiable. In the Russian heatwave, natural variability is responsible for 8 °C and climate change for 2 °C of the in total 10°C of anomalous temperature. Temperatures are shown to increase significantly due to climate change, despite the relatively large natural variability element in each of the case studies. These findings signal an increased impact of climate change on individual heatwaves.

2. *For precipitation extremes?*
   In global and large scale regions, climate change shows a clear increase in precipitation depending on season, in line with IPCC (2021). When narrowed down to smaller region and specific events, the climate-change signal can be reversed, as was shown with the Mexican monsoon case studies. Monsoons are complex, depending on many factors e.g. El Niño–Southern Oscillation (ENSO) and the Circumglobal Teleconnection Index (CGTI). Nonetheless, the storyline method showed that seasonal variability in the precipitation of several individual monsoons react differently to climate change by becoming either drier (Mexico 2012 and 2014 monsoon) or wetter (India 2011 and 2014 monsoon). The signal of change can also depend on season, as shown with the Scandinavian results, where wetting is found for the 2013 autumn and drying for the 2012 summer. For seasonal and regional scales, the method allows for a distinction of the climate signal from natural variability. Moreover, it allows for analysis of regional year-to-year climate-change signal variability. For a precipitation-based flood analysis with a small region and time frame, such as the southern England flood in early 2014, the method in its current setup is limited. The limitation is likely to be technical, based on model resolution and parametrization of important variables, but could also be related to epistemic uncertainty.

3. *For droughts?*
   Droughts are a more complex type of extreme event as they depend on a set of variables such as precipitation, temperature and evaporative demand at the same time. The method allows for separate analysis of each of these variables, as was shown for the southeastern South America drought. The temperatures have a clear climate-change element, separable from natural variability and quantifiable, as shown in the heatwave case studies. The same goes for the Budyko aridity index which showed that the hydrological year of 2011/2012 experienced a drying due to natural variability, but the effect of that on the drought was counterbalanced by climatological wetting and would be even more so for the plus2 world. From the case study it thus follows that climate change can increase temperatures and potential evapotranspiration (PET) during an event, but reduce the year-round aridity significantly at the same time. This illustrates the complexity of droughts, but also showcases the potential of the storyline method to separate the natural variability from the climate-change signal despite the complexity at hand.

The combination of both methods — global spectral nudging and the storyline method — presents a way to quantify, in great detail, the role of known thermodynamic aspects of climate change, together with the specific dynamical conditions, in selected extreme events which happened in the recent past. This can help reconcile the sometimes different perspectives on those events that appear in the literature (some emphasizing climate change, others emphasizing internal variability). Next to the attribution of climate change of the past events, the method provides a physically consistent view on what these extreme events would be like in a world with increased global warming. The nudged global storyline method is an important step towards a holistic approach and should be seen as an addition to dynamical attribution methods. The method can quantify the role of both dynamical variability and known thermodynamic aspects of climate change, and the interplay between them, for individual extreme weather events.

11 Outlook

The spectrally nudged event-based storylines can easily be expanded to a larger number of storylines for both past and future, as shown by Wehrli et al. (2019). The method could also be applied to other extreme events affected thermodynamically by climate change such as tropical cyclones (Feser and Barcikowska, 2012). Moreover, the method could be crucial to further understand compounding events, which have devastating impact on society. The future applications are, therefore, intended to cover a wide variety of extreme events over the historical record. To do so with a higher level of accuracy and for more recent events it follows to double nest a regional model that will allow for convection permitting high-resolution simulations. To analyse extreme events heavily depending on small-scale processes, the double nesting of a high resolution regional model will enable higher accuracy in conditional attribution studies. Extremes such as precipitation-based floods and tropical cyclones would require such an updated set-up to reduce dependency on parameterisation. Note that ECHAM6 is no longer further developed and therefore other models might be of interest to continue the implication of this method in the future.

A near-real-time system of storyline simulations could be set up depending on the release of reanalysis data needed for nudging. In this study NCEP-R1 was applied, but any reanalysis dataset could be used. Adding the near-real-time tool to complement the existing probabilistic fast attribution science, would give a detailed insight in the effect of climate change on recently occurred extreme events. After a high impact ex-

treme event, the general question asked is if, and how, climate change influenced the extreme. The near-real-time conditional attribution tool would enable a rapid answer of these types of questions with significantly higher certainty than in probabilistic attribution, albeit conditionally.

Spectrally nudged event storylines could be used to drive climate impact models, and thus perform realistic stress-testing of resilience strategies. Though some impacts such as storm damage are direct, often the impacts of meteorological extremes are not direct. For example, the effect of a drought or flood on agricultural yield will need an analysis of meteorological, hydrological and agricultural factors. In Figure 11.1 an example of a causal chain for yield losses due to drought is shown, adapted from Figure 7 in Lloyd and Shepherd (2020). Each arrow is the direction of a causal relationship, purple indicates the element is human influenced, blue indicates the element is not directly human influenced and yellow are the impacts of interest. Storylines can be set up for each of these relationships. The conditional storylines presented in this study can help answer questions concerning the climate change influence on rainfall and warming. The impact of those meteorological aspects on drought might be answered with a hydrological study (Chan et al., 2022), and the consequential yield loss impact with agricultural models. An example project of connecting fields of expertise to study such impacts can be found in the RECEIPT project (RECEIPT, 2022), and would benefit greatly from event-based storylines as presented here. The drought example is to show one of the many possibilities of using storylines in impact studies. Other possibilities are the study of compounding events that impact coastal regions, i.e. floods, by using the storyline atmospheric data in combination with a wave model. One could think of potentially attributing the 1953 North Sea flood with this setup. Traditional forms of modelling and data-analysis have been bypassed by hybrid machine learning methods, which can be used to analyse the storyline simulations to find the drivers behind historical extremes.

There is a need for operationalising extreme event attribution, and spectrally nudged storylines offers the best answer to that need. Leach et al. (2021) suggested to use conditioned weather forecast models in the process of operationalising event-based storylines. However, using conditioned weather forecast models would limit the lead times since a long lead-time would loosen the conditioning too much. Shorter lead times, on the other hand, would not be enough for the anthropogenic signal in the weather forecast model to build up. Moreover, the time series would not be statistically stationary. These are a set of challenges that are not part of the spectrally nudged event-based storylines as presented here. Operationalisation does not depend on ECHAM6, but it would be beneficial to start with the ECHAM6 spectrally nudged setup and

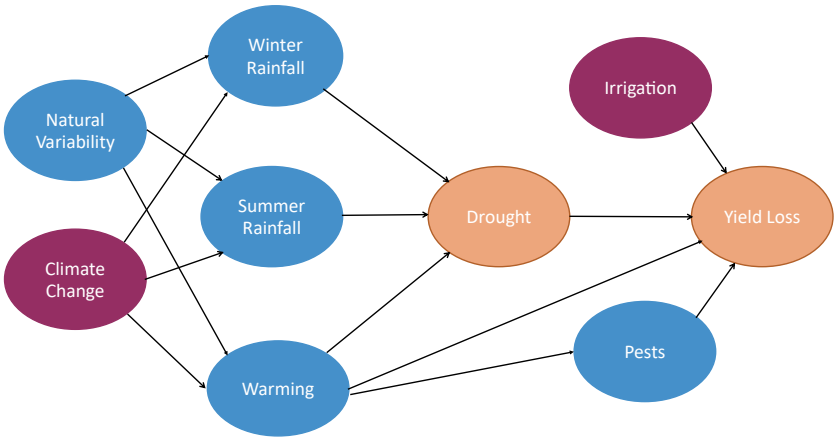

Figure 11.1: Causal chain of agricultural yield losses due to drought. The direction of causal influence is indicated with arrows. Purple coloured balloons indicate the element is human influenced, blue coloured balloons are not directly human influenced and yellow are the impacts of interest. Based on Figure 7 of Lloyd and Shepherd (2020).

broaden the scope from here by including more models, global and regionally nested, with different resolutions. Operationalised spectrally nudged event-based storylines can speed up extreme weather attribution and answer societal questions concerning climate-change influence on extremes to a higher certainty.

Acknowledgements

Many thanks to my supervisors Frauke Feser and Ted Shepherd. Frauke, thank you so much for your support and advice both about science and about academic life. Thank you for seeing potential in me and for encouraging me to develop my scientific skills without judgement. Ted, thank you for always being available, even during busier times, and for showing me how to be critical with my own work (which must have been tough since I am super excited about every graph I make).

Thank you to my wonderful colleagues at Hereon who have helped me out on a plethora of things, all the way from brainstorming on scientific ideas, to learning how to deal with German bureaucracy. I would like to especially mention Oliver Krüger, Benjamin Schaaf, Maria Pyrina, Marlene Klockmann, Sebastian Wagner, Sabine Billerbeck, Oliver Bothe, Birgit Hünicke, Eduardo Zorita, Felicitas Hansen, Nele Tim, Zeguo Zhang, Xing Yi, Julianna Carvalho Oliveira and Deboráh Benkort, you are the best! A special thanks to Corinna Schrum, your support for us as PhD students is priceless.

During my PhD, I was warmly welcomed as a guest student at Reading University for several months. So many lovely colleagues there made my Reading months unforgettable. Special thanks to my fellow visiting student, and my Reading flat mate, Julia Mindlin, for helping me get started in the first days and becoming not just my scientific brainstorm buddy but a close friend.

I am thrilled to have been part of the Hamburg Universität SICSS graduate school, with special thanks to Ingo Harms and Berit Hachfeld. You have made my PhD process so much more interesting and diverse. Thank you to my SICSS panel, Nedjeljka Žagar, Bernd Leitl, Richard Blender and Frauke Feser, for your scientific insight and general support throughout the PhD process. You helped me see the progress I made instead of only looking at the challenges I was facing. Many thanks to all my fellow SICSS PhD buddies for all the lunch meetings and encouraging conversations.

Getting started with global atmospheric modelling can be tricky, and therefore I was happy to receive technical support from Sebastian Rast (MPI) and Irina Fast (DKRZ) to get the model started and help me not to crash it (which I of course still managed to do). I am grateful to Beate Ratter and Gerhard Schmiedl for agreeing to be part of my PhD examination panel with such kindness and enthusiasm.

To my amazing family: when the going got tough, and it did, you were there for me! Marjanne van Nieuwkerk, Tanja de Ruijter, Trudy and Frenck Baksteen, Erik van Garderen, Annemarie Hoetmer, Gerda and Tonnie Kuiper and of course Opa and Oma van Garderen. It is impossible to tell you how much you mean to me and how lucky I feel to be part of our family. My dear friend Birthe Gratenau, when life was at its toughest you were there for me (every day!) and you helped me laugh again. To my husband Serge Gavras, you are my hero! It is such an honour and so much fun to be a team with you. In the last phase of my PhD you carried me through and took over all other responsibilities so I could focus on writing. I am so grateful (and astonished) that you manage to stick it out with me, a simple "thank you" does not do it justice. I love you a million books, stronger together!

In loving memory of my parents: Carola Deodate van Nieuwkerk (21.6.1958 - 15.7.2018) and Siet Cornelis van Garderen (22.5.1958 - 4.12.2018)

References

Ault, T. R. (2020). "On the essentials of drought in a changing climate". In: *Science* 368.6488, pp. 256–260. DOI: 10.1126/science.aaz5492.

Barriopedro, D., E. M. Fischer, J. Luterbacher, R. M. Trigo, and R. García-Herrera (2011). "The Hot Summer of 2010: Redrawing the Temperature Record Map of Europe". In: *Science* 332.6026, pp. 220–224. DOI: 10.1126/science.1201224.

Bastos, A., C. M. Gouveia, R. M. Trigo, and S. W. Running (2014). "Analysing the spatio-temporal impacts of the 2003 and 2010 extreme heatwaves on plant productivity in Europe". In: *Biogeosciences* 11.13, pp. 3421–3435. DOI: 10.5194/bg-11-3421-2014.

Bastos, A., R. Orth, M. Reichstein, P. Ciais, N. Viovy, S. Zaehle, P. Anthoni, A. Arneth, P. Gentine, E. Joetzjer, S. Lienert, T. Loughran, P. C. McGuire, S. O, J. Pongratz, and S. Sitch (2021). "Vulnerability of European ecosystems to two compound dry and hot summers in 2018 and 2019". In: *Earth System Dynamics* 12.4, pp. 1015–1035. DOI: 10.5194/esd-12-1015-2021.

Black, E., M. Blackburn, G. Harrison, B. Hoskins, and J. Methven (2004). "Factors contributing to the summer 2003 European heatwave". In: *Weather* 59.8, pp. 217–223. DOI: 10.1256/wea.74.04.

Blunden, J. and D. S. Arndt (2012). "State of the Climate in 2011". In: *Bulletin of the American Meteorological Society* 93.7, S1–S282. DOI: 10.1175/2012BAMSStateoftheClimate.1.

Bosilovich, M. G., J. Chen, F. R. Robertson, and R. F. Adler (2008). "Evaluation of Global Precipitation in Reanalyses". In: *Journal of Applied Meteorology and Climatology* 47.9, pp. 2279–2299. DOI: 10.1175/2008JAMC1921.1.

Budyko, M. I. (1951). "On climatic factors of runoff". In: *Prob. Fiz. Geogr.* 16, pp. 41–48.

Carvalho, L. M. V. (2020). "Assessing precipitation trends in the Americas with historical data: A review". In: *WIREs Climate Change* 11.2. DOI: 10.1002/wcc.627.

Cattiaux, J., R. Vautard, C. Cassou, P. Yiou, V. Masson-Delmotte, and F. Codron (2010). "Winter 2010 in Europe: A cold extreme in a warming climate". In: *Geophysical Research Letters* 37.20, n/a–n/a. DOI: 10.1029/2010GL044613.

Cerne, S. B. and C. S. Vera (2011). "Influence of the intraseasonal variability on heat waves in subtropical South America". In: *Climate Dynamics* 36.11, pp. 2265–2277. DOI: 10.1007/s00382-010-0812-4.

Cerne, S. B., C. S. Vera, and B. Liebmann (2007). "The Nature of a Heat Wave in Eastern Argentina Occurring during SALLJEX". In: *Monthly Weather Review* 135.3, pp. 1165–1174. DOI: 10.1175/MWR3306.1.

Chan, W. C. H., T. G. Shepherd, K. Facer-Childs, G. Darch, and N. W. Arnell (2022). "Storylines of UK drought based on the 2010–2012 event". In: *Hydrology and Earth System Sciences* 26.7, pp. 1755–1777. DOI: 10.5194/hess-26-1755-2022.

Chan, W. C. H., T. G. Shepherd, K. A. Smith, G. Darch, and N. W. Arnell (2021). *Storylines of UK drought based on the 2010–2012 event*. preprint. Catchment hydrology/Modelling approaches. DOI: 10.5194/hess-2021-123.

Ciais, P., M. Reichstein, N. Viovy, A. Granier, J. Ogée, V. Allard, M. Aubinet, N. Buchmann, C. Bernhofer, A. Carrara, F. Chevallier, N. De Noblet, A. D. Friend, P. Friedlingstein, T. Grünwald, B. Heinesch, P. Keronen, A. Knohl, G. Krinner, D. Loustau, G. Manca, G. Matteucci, F. Miglietta, J. M. Ourcival, D. Papale, K. Pilegaard, S. Rambal, G. Seufert, J. F. Soussana, M. J. Sanz, E. D. Schulze, T. Vesala, and R. Valentini (2005). "Europe-wide reduction in primary productivity caused by the heat and drought in 2003". In: *Nature* 437.7058, pp. 529–533. DOI: 10.1038/nature03972.

Cook, B. I. and R. Seager (2013). "The response of the North American Monsoon to increased greenhouse gas forcing". In: *Journal of Geophysical Research: Atmospheres* 118.4, pp. 1690–1699. DOI: 10.1002/jgrd.50111.

CREAN (2017). *Monitoreo de extremos hídricos*. Centro de Relevamiento y Evaluación de Recursos Agrícolas y Naturales. URL: https://www.crean.unc.edu.ar/monitoreo-de-sequias (visited on 11/10/2021).

Cuervo-Robayo, A. P., C. Ureta, M. A. Gómez-Albores, A. K. Meneses-Mosquera, O. Téllez-Valdés, and E. Martínez-Meyer (2020). "One hundred years of climate change in Mexico". In: *PLOS ONE* 15.7. Ed. by L. C. Silva, e0209808. DOI: 10.1371/journal.pone.0209808.

Dee, D. P., S. M. Uppala, A. J. Simmons, P. Berrisford, P. Poli, S. Kobayashi, U. Andrae, M. A. Balmaseda, G. Balsamo, P. Bauer, P. Bechtold, A. C. M. Beljaars, L. van de Berg, J. Bidlot, N. Bormann, C. Delsol, R. Dragani, M. Fuentes, A. J. Geer, L. Haimberger, S. B. Healy, H. Hersbach, E. V. Hólm, L. Isaksen, P. Kållberg, M. Köhler, M. Matricardi, A. P. McNally, B. M. Monge-Sanz, J.-J. Morcrette, B.-K. Park, C. Peubey, P. de Rosnay, C. Tavolato, J.-N. Thépaut, and F. Vitart (2011). "The ERA-Interim reanalysis: configuration and performance of the data assimilation system". In: *Quarterly Journal of the Royal Meteorological Society* 137.656, pp. 553–597. DOI: 10.1002/qj.828.

Deser, C., L. Terray, and A. S. Phillips (2016). "Forced and Internal Components of Winter Air Temperature Trends over North America during the past 50 Years: Mechanisms and Implications*". In: *Journal of Climate* 29.6, pp. 2237–2258. DOI: 10.1175/JCLI-D-15-0304.1.

Devasthale, A., T. Carlund, and K.-G. Karlsson (2022). "Recent trends in the agrometeorological climate variables over Scandinavia". In: *Agricultural and Forest Meteorology* 316, p. 108849. DOI: 10.1016/j.agrformet.2022.108849.

Di Capua, G., M. Kretschmer, R. V. Donner, B. van den Hurk, R. Vellore, R. Krishnan, and D. Coumou (2020). "Tropical and mid-latitude teleconnections interacting with the Indian summer monsoon rainfall: a theory-guided causal effect network approach". In: *Earth System Dynamics* 11.1, pp. 17–34. DOI: 10.5194/esd-11-17-2020.

Doblas-Reyes, F., A. A. Sörensson, M. Almazroui, A. Dosio, W. J. Gutowski, R. Haarsma, R. Hamdi, B. Hewitson, W.-T. Kwon, B. L. Lamptey, D. Maraun, T. S. Stephenson, I. Takayabu, L. Terray, A. Turner, and Z. Zuo (2021). *Linking Global to Regional Climate Change. In Climate Change 2021: The Physical Science Basis. Contribution of Working Group I to the Sixth Assessment Report of the Intergovernmental Panel on Climate Change*. Ed. by V. Masson-Delmotte, P. Zhai, A. Pirani, S. Connors, C. Péan, S. Berger, N. Caud, Y. Chen, L. Goldfarb, M. I. Gomis, M. Huang, K. Leitzell, E. Lonnoy, J. B. R. Matthews, T. K. Maycock, T. Waterfield, O. Yelekçi, R. Yu, and B. Zhou. In Press: Cambridge University Press.

Dole, R., M. Hoerling, J. Perlwitz, J. Eischeid, P. Pegion, T. Zhang, X.-W. Quan, T. Xu, and D. Murray (2011). "Was there a basis for anticipating the 2010 Russian heat wave?" In: *Geophysical Research Letters* 38.6, n/a–n/a. DOI: 10.1029/2010GL046582.

Douville, H., K. Raghavan, J. Renwick, R. P. Allan, P. Arias, M. Barlow, R. Cerezo-Mota, A. Cherchi, T. Y. Gan, D. Gergis, D. Jiang, A. Khan, W. Pokam Mba, D. Rosenfeld, J. Tierney, and O. Zolina (2021). *Water Cycle Changes. In Climate Change 2021: The Physical Science Basis. Contribution of Working Group I to the Sixth Assessment Report of the Intergovernmental Panel on Climate Change*. Cambridge University Press.

Dowdy, A. J. (2018). "Climatological Variability of Fire Weather in Australia". In: *Journal of Applied Meteorology and Climatology* 57.2, pp. 221–234. DOI: 10.1175/JAMC-D-17-0167.1.

Doyle, M. E., R. I. Saurral, and V. R. Barros (2011). "Trends in the distributions of aggregated monthly precipitation over the La Plata Basin". In: *International Journal of Climatology*, n/a–n/a. DOI: 10.1002/joc.2429.

Evans, J. P., G. Di Virgilio, A. L. Hirsch, P. Hoffmann, A. R. Remedio, F. Ji, B. Rockel, and E. Coppola (2021). "The CORDEX-Australasia ensemble: evaluation and

future projections". In: *Climate Dynamics* 57.5, pp. 1385–1401. DOI: 10.1007/s00382-020-05459-0.

Fenn, T., C. Clarke, L. Burgess-Gamble, E. Harding, F. Ogunyoye, E. Hick, S. Dawks, J. Morris, and J. Chatterton (2016). "The costs and impacts of the winter 2013/14 floods in England and Wales". In: *E3S Web of Conferences* 7. Ed. by M. Lang, F. Klijn, and P. Samuels, p. 05004. DOI: 10.1051/e3sconf/20160705004.

Feser, F. and M. Barcikowska (2012). "The influence of spectral nudging on typhoon formation in regional climate models". In: *Environmental Research Letters* 7.1, p. 014024. DOI: 10.1088/1748-9326/7/1/014024.

Feser, F., B. Rockel, H. von Storch, J. Winterfeldt, and M. Zahn (2011). "Regional Climate Models Add Value to Global Model Data: A Review and Selected Examples". In: *Bulletin of the American Meteorological Society* 92.9, pp. 1181–1192. DOI: 10.1175/2011BAMS3061.1.

Feudale, L. and J. Shukla (2011a). "Influence of sea surface temperature on the European heat wave of 2003 summer. Part I: an observational study". In: *Climate Dynamics* 36.9, pp. 1691–1703. DOI: 10.1007/s00382-010-0788-0.

— (2011b). "Influence of sea surface temperature on the European heat wave of 2003 summer. Part II: a modeling study". In: *Climate Dynamics* 36.9, pp. 1705–1715. DOI: 10.1007/s00382-010-0789-z.

Fink, A. H., T. Brücher, A. Krüger, G. C. Leckebusch, J. G. Pinto, and U. Ulbrich (2004). "The 2003 European summer heatwaves and drought -synoptic diagnosis and impacts: European heatwave - impacts". In: *Weather* 59.8, pp. 209–216. DOI: 10.1256/wea.73.04.

Fischer, E. M., S. I. Seneviratne, P. L. Vidale, D. Lüthi, and C. Schär (2007). "Soil Moisture–Atmosphere Interactions during the 2003 European Summer Heat Wave". In: *Journal of Climate* 20.20, pp. 5081–5099. DOI: 10.1175/JCLI4288.1.

Flato, G., J. Marotzke, B. Abiodun, P. Braconnot, S. C. Chou, W. Collins, P. Cox, F. Driouech, S. Emori, V. Eyring, C. Forest, P. Gleckler, E. Guilyardi, C. Jakob, V. Kattsov, C. Reason, and M. Rummukainen (2013). "Evaluation of Climate Models." In: *Climate Change 2013: The Physical Science Basis. Contribution of Working Group I to the Fifth Assessment Report of the Intergovernmental Panel on Climate Change*. Ed. by T. Stocker, D. Qin, G.-K. Plattner, M. Tignor, S. K. Allen, J. Boschung, A. Nauels, Y. Xia, V. Bex, and P. M. Midgley. Cambridge, United Kingdom and New York, NY, USA: Cambridge University Press.

Galarneau, T. J., T. M. Hamill, R. M. Dole, and J. Perlwitz (2012). "A Multiscale Analysis of the Extreme Weather Events over Western Russia and Northern Pakistan during July 2010". In: *Monthly Weather Review* 140.5, pp. 1639–1664. DOI: 10.1175/MWR-D-11-00191.1.

García-Herrera, R., J. Díaz, R. M. Trigo, J. Luterbacher, and E. M. Fischer (2010). "A Review of the European Summer Heat Wave of 2003". In: *Critical Reviews in Environmental Science and Technology* 40.4, pp. 267–306. DOI: 10.1080/10643380802238137.

Gelaro, R., W. McCarty, M. J. Suárez, R. Todling, A. Molod, L. Takacs, C. A. Randles, A. Darmenov, M. G. Bosilovich, R. Reichle, K. Wargan, L. Coy, R. Cullather, C. Draper, S. Akella, V. Buchard, A. Conaty, A. M. da Silva, W. Gu, G.-K. Kim, R. Koster, R. Lucchesi, D. Merkova, J. E. Nielsen, G. Partyka, S. Pawson, W. Putman, M. Rienecker, S. D. Schubert, M. Sienkiewicz, and B. Zhao (2017). "The Modern-Era Retrospective Analysis for Research and Applications, Version 2 (MERRA-2)". In: *Journal of Climate* 30.14, pp. 5419–5454. DOI: 10.1175/JCLI-D-16-0758.1.

Ghosh, R., A. Chakraborty, and R. S. Nanjundiah (2018). "Relative role of pre-monsoon conditions and intraseasonal oscillations in determining early-vs-late indian monsoon intensity in a GCM". In: *Theoretical and Applied Climatology* 131.1, pp. 319–333. DOI: 10.1007/s00704-016-1970-z.

Goulart, H. M. D., K. van der Wiel, C. Folberth, J. Balkovic, and B. van den Hurk (2021). "Storylines of weather-induced crop failure events under climate change". In: *Earth System Dynamics* 12.4, pp. 1503–1527. DOI: 10.5194/esd-12-1503-2021.

Grimm, A. M., V. R. Barros, and M. E. Doyle (2000). "Climate Variability in Southern South America Associated with El Niño and La Niña Events". In: *Journal of Climate* 13.1, pp. 35–58. DOI: 10.1175/1520-0442(2000)013<0035:CVISSA>2.0.CO;2.

Grumm, R. H. (2011). "The Central European and Russian Heat Event of July–August 2010". In: *Bulletin of the American Meteorological Society* 92.10, pp. 1285–1296. DOI: 10.1175/2011BAMS3174.1.

Hannart, A., J. Pearl, F. E. L. Otto, P. Naveau, and M. Ghil (2016). "Causal Counterfactual Theory for the Attribution of Weather and Climate-Related Events". In: *Bulletin of the American Meteorological Society* 97.1, pp. 99–110. DOI: 10.1175/BAMS-D-14-00034.1.

Hanssen-Bauer, I., C. Achberger, R. Benestad, D. Chen, and E. Førland (2005). "Statistical downscaling of climate scenarios over Scandinavia". In: *Climate Research* 29, pp. 255–268. DOI: 10.3354/cr029255.

He, C., T. Li, and W. Zhou (2020). "Drier North American Monsoon in Contrast to Asian–African Monsoon under Global Warming". In: *Journal of Climate* 33.22, pp. 9801–9816. DOI: 10.1175/JCLI-D-20-0189.1.

Hegdahl, T. J., K. Engeland, M. Müller, and J. Sillmann (2020). "An Event-Based Approach to Explore Selected Present and Future Atmospheric River–Induced

Floods in Western Norway". In: *Journal of Hydrometeorology* 21.9, pp. 2003–2021. DOI: 10.1175/JHM-D-19-0071.1.

Hersbach, H., B. Bell, P. Berrisford, S. Hirahara, A. Horányi, J. Muñoz-Sabater, J. Nicolas, C. Peubey, R. Radu, D. Schepers, A. Simmons, C. Soci, S. Abdalla, X. Abellan, G. Balsamo, P. Bechtold, G. Biavati, J. Bidlot, M. Bonavita, G. Chiara, P. Dahlgren, D. Dee, M. Diamantakis, R. Dragani, J. Flemming, R. Forbes, M. Fuentes, A. Geer, L. Haimberger, S. Healy, R. J. Hogan, E. Hólm, M. Janisková, S. Keeley, P. Laloyaux, P. Lopez, C. Lupu, G. Radnoti, P. Rosnay, I. Rozum, F. Vamborg, S. Villaume, and J.-N. Thépaut (2020). "The ERA5 global reanalysis". In: *Quarterly Journal of the Royal Meteorological Society* 146.730, pp. 1999–2049. DOI: 10.1002/qj.3803.

Hertwig, E., J.-S. von Storch, D. Handorf, K. Dethloff, I. Fast, and T. Krismer (2015). "Effect of horizontal resolution on ECHAM6-AMIP performance". In: *Climate Dynamics* 45.1, pp. 185–211. DOI: 10.1007/s00382-014-2396-x.

Hoegh-Guldberg, O., D. Jacob, M. Taylor, M. Bindi, S. Brown, I. Camilloni, A. Diedhiou, R. Djalante, K. L. Ebi, F. Engelbrecht, J. Guiot, Y. Hijioka, S. Mehrotra, A. Payne, S. I. Seneviratne, A. Thomas, R. Warren, and G. Zhou (2018). *Impacts of 1.5ºC Global Warming on Natural and Human Systems. In: Global Warming of 1.5°C. An IPCC Special Report on the impacts of global warming of 1.5°C above pre-industrial levels and related global greenhouse gas emission pathways, in the context of strengthening the global response to the threat of climate change, sustainable development, and efforts to eradicate poverty*. Ed. by V. Masson-Delmotte, P. Zhai, H.-O. Pörtner, D. Roberts, J. Skea, P. R. Shukla, A. Pirani, W. Moufouma-Okia, C. Péan, R. Pidcock, S. Connors, J. B. R. Matthews, Y. Chen, X. Zhou, M. I. Gomis, E. Lonnoy, T. Maycock, M.Tignor, and T.Waterfield. In Press: Cambridge University Press.

Hollis, D., M. McCarthy, M. Kendon, T. Legg, and I. Simpson (2019). "HadUK-Grid—A new UK dataset of gridded climate observations". In: *Geoscience Data Journal* 6.2, pp. 151–159. DOI: 10.1002/gdj3.78.

Hoskins, B. and T. Woollings (2015). "Persistent Extratropical Regimes and Climate Extremes". In: *Current Climate Change Reports* 1.3, pp. 115–124. DOI: 10.1007/s40641-015-0020-8.

Huffman, G. J., R. F. Adler, D. T. Bolvin, and G. Gu (2009). "Improving the global precipitation record: GPCP Version 2.1". In: *Geophysical Research Letters* 36.17, p. L17808. DOI: 10.1029/2009GL040000.

Huntingford, C., T. Marsh, A. A. Scaife, E. J. Kendon, J. Hannaford, A. L. Kay, M. Lockwood, C. Prudhomme, N. S. Reynard, S. Parry, J. A. Lowe, J. A. Screen, H. C. Ward, M. Roberts, P. A. Stott, V. A. Bell, M. Bailey, A. Jenkins, T. Legg, F. E. L. Otto, N. Massey, N. Schaller, J. Slingo, and M. R. Allen (2014). "Poten-

tial influences on the United Kingdom's floods of winter 2013/14". In: *Nature Climate Change* 4.9, pp. 769–777. DOI: 10.1038/nclimate2314.

Hurrell, J. W., J. J. Hack, D. Shea, J. M. Caron, and J. Rosinski (2008). "A New Sea Surface Temperature and Sea Ice Boundary Dataset for the Community Atmosphere Model". In: *Journal of Climate* 21.19, pp. 5145–5153. DOI: 10.1175/2008JCLI2292.1.

IPCC (2014). "Evaluation of Climate Models". In: *Inter-governmental Panel on Climate Change: Climate Change 2013 - The Physical Science Basis*. Ed. by IPCC. Cambridge: Cambridge University Press, pp. 741–866. DOI: 10.1017/CBO9781107415324.020.

— (2018). *Summary for Policymakers. In: Global Warming of 1.5°C. An IPCC Special Report on the impacts of global warming of 1.5°C above pre-industrial levels and related global greenhouse gas emission pathways, in the context of strengthening the global response to the threat of climate change, sustainable development, and efforts to eradicate poverty*. Ed. by V. Masson-Delmotte, P. Zhai, H. Pörtner, D. Roberts, J. Skea, P. Shukla, A. Pirani, W. Moufouma-Okia, C. Péan, R. Pidcock, S. Connors, J. Matthews, Y. Chen, X. Zhou, M. Gomis, E. Lonnoy, T. Maycock, M. Tignor, and T. Waterfield. Geneva, Switzerland: World Meteorological Organization.

— (2021). *Climate Change 2021: The Physical Science Basis. Contribution of Working Group I to the Sixth Assessment Report of the Intergovernmental Panel on Climate Change*. Ed. by V. Masson-Delmotte, P. Zhai, A. Pirani, S. L. Connors, C. Péan, S. Berger, Y. C. N. Caud, L. Goldfarb, M. H. M.I. Gomis, E. L. K. Leitzell, J. B. R. Matthews, T. K. Maycock, T. Waterfield, O. Yelekçi, R. Yu, and B. Zhou. Cambridge University Press.

Jeuken, A. B. M., P. C. Siegmund, L. C. Heijboer, J. Feichter, and L. Bengtsson (1996). "On the potential of assimilating meteorological analyses in a global climate model for the purpose of model validation". In: *Journal of Geophysical Research: Atmospheres* 101 (D12), pp. 16939–16950. DOI: 10.1029/96JD01218.

Kalnay, E., M. Kanamitsu, R. Kistler, W. Collins, D. Deaven, L. Gandin, M. Iredell, S. Saha, G. White, J. Woollen, Y. Zhu, A. Leetmaa, R. Reynolds, M. Chelliah, W. Ebisuzaki, W. Higgins, J. Janowiak, K. C. Mo, C. Ropelewski, J. Wang, R. Jenne, and D. Joseph (1996). "The NCEP/NCAR 40-Year Reanalysis Project". In: *Bulletin of the American Meteorological Society* 77.3, pp. 437–471. DOI: 10.1175/1520-0477(1996)077<0437:TNYRP>2.0.CO;2.

Kay, A. L., N. Booth, R. Lamb, E. Raven, N. Schaller, and S. Sparrow (2018). "Flood event attribution and damage estimation using national-scale grid-based modelling: Winter 2013/2014 in Great Britain". In: *International Journal of Climatology* 38.14, pp. 5205–5219. DOI: 10.1002/joc.5721.

Keil, P., T. Mauritsen, J. Jungclaus, C. Hedemann, D. Olonscheck, and R. Ghosh (2020). "Multiple drivers of the North Atlantic warming hole". In: *Nature Climate Change* 10.7, pp. 667–671. DOI: 10.1038/s41558-020-0819-8.

Kendon, M. and M. McCarthy (2015). "The UK's wet and stormy winter of 2013/2014". In: *Weather* 70.2, pp. 40–47. DOI: 10.1002/wea.2465.

Kennedy, J. J., N. A. Rayner, R. O. Smith, D. E. Parker, and M. Saunby (2011a). "1. Reassessing biases and other uncertainties in sea surface temperature observations measured in situ since 1850: 1. Measurement and sampling uncertainties". In: *Journal of Geophysical Research* 116 (D14), p. D14103. DOI: 10.1029/2010JD015218.

— (2011b). "2. Reassessing biases and other uncertainties in sea surface temperature observations measured in situ since 1850: 2. Biases and homogenization". In: *Journal of Geophysical Research* 116 (D14), p. D14104. DOI: 10.1029/2010JD015220.

Kim, J.-E. and S.-Y. Hong (2012). "A Global Atmospheric Analysis Dataset Downscaled from the NCEP–DOE Reanalysis". In: *Journal of Climate* 25.7, pp. 2527–2534. DOI: 10.1175/JCLI-D-11-00534.1.

KNMI (2014). *KNMI'14: Climate Change scenarios for the 21st Century – A Netherlands perspective*. Ed. by B. v. d. Hurk, P. Siegmund, A. K. Tank (Eds), J. Attema, A. Bakker, J. Beersma, J. Bessembinder, R. Boers, T. Brandsma, H. v. d. Brink, S. Drijfhout, H. Eskes, R. Haarsma, W. Hazeleger, R. Jilderda, C. Katsman, G. Lenderink, J. Loriaux, E. v. Meijgaard, T. v. Noije, G. J. v. Oldenborgh, F. Selten, P. Siebesma, A. Sterl, H. d. Vries, M. v. Weele, R. de Winter, and G.-J. v. Zadelhoff. Scientific Report WR2014-01. KNMI,De Bilt, The Netherlands.

Kreienkamp, F., S. Y. Philip, J. S. Tradowsky, S. F. Kew, P. Lorenz, J. Arrighi, A. Belleflamme, T. Bettmann, S. Caluwaerts, S. C. Chan, A. Ciavarella, L. De Cruz, H. de Vries, N. Demuth, A. Ferrone, E. M. Fischer, H. J. Fowler, K. Goergen, D. Heinrich, Y. Henrichs, G. Lenderink, F. Kaspar, E. Nilson, F. E. L. Otto, F. Ragone, S. I. Seneviratne, R. K. Singh, A. Skålevåg, P. Termonia, L. Thalheimer, M. van Aalst, J. Van den Bergh, H. Van de Vyver, S. Vannitsem, G. J. van Oldenborgh, B. Van Schaeybroeck, R. Vautard, D. Vonk, and N. Wanders (2021). *Rapid attribution of heavy rainfall events leading to the severe flooding in Western Europe during July 2021*. world weather attribution, p. 54.

Lau, W. K. M. and K.-M. Kim (2012). "The 2010 Pakistan Flood and Russian Heat Wave: Teleconnection of Hydrometeorological Extremes". In: *Journal of Hydrometeorology* 13.1, pp. 392–403. DOI: 10.1175/JHM-D-11-016.1.

Leach, N. J., A. Weisheimer, M. R. Allen, and T. Palmer (2021). "Forecast-based attribution of a winter heatwave within the limit of predictability". In: *Proceedings of the National Academy of Sciences* 118.49, e2112087118. DOI: 10.1073/pnas.2112087118.

Lloyd, E. A. and N. Oreskes (2018). "Climate Change Attribution: When Is It Appropriate to Accept New Methods?" In: *Earth's Future* 6.3, pp. 311–325. DOI: 10.1002/2017EF000665.

Lloyd, E. A. and T. G. Shepherd (2020). "Environmental catastrophes, climate change, and attribution". In: *Annals of the New York Academy of Sciences* 1469.1, pp. 105–124. DOI: 10.1111/nyas.14308.

— (2021). "Climate change attribution and legal contexts: evidence and the role of storylines". In: *Climatic Change* 167.3, p. 28. DOI: 10.1007/s10584-021-03177-y.

Luterbacher, J., D. Dietrich, E. Xoplaki, M. Grosjean, and H. Wanner (2004). "European Seasonal and Annual Temperature Variability, Trends, and Extremes Since 1500". In: *Science* 303.5663, pp. 1499–1503. DOI: 10.1126/science.1093877.

Matsueda, M. (2011). "Predictability of Euro-Russian blocking in summer of 2010". In: *Geophysical Research Letters* 38.6, n/a–n/a. DOI: 10.1029/2010GL046557.

Meinshausen, M., S. J. Smith, K. Calvin, J. S. Daniel, M. L. T. Kainuma, J.-F. Lamarque, K. Matsumoto, S. A. Montzka, S. C. B. Raper, K. Riahi, A. Thomson, G. J. M. Velders, and D. P. van Vuuren (2011). "The RCP greenhouse gas concentrations and their extensions from 1765 to 2300". In: *Climatic Change* 109.1, pp. 213–241. DOI: 10.1007/s10584-011-0156-z.

Meredith, E. P., V. A. Semenov, D. Maraun, W. Park, and A. V. Chernokulsky (2015). "Crucial role of Black Sea warming in amplifying the 2012 Krymsk precipitation extreme". In: *Nature Geoscience* 8.8, pp. 615–619. DOI: 10.1038/ngeo2483.

Miguez-Macho, G., G. L. Stenchikov, and A. Robock (2004). "Spectral nudging to eliminate the effects of domain position and geometry in regional climate model simulations". In: *Journal of Geophysical Research: Atmospheres* 109 (D13), n/a–n/a. DOI: 10.1029/2003JD004495.

Mindlin, J., T. G. Shepherd, C. S. Vera, M. Osman, G. Zappa, R. W. Lee, and K. I. Hodges (2020). "Storyline description of Southern Hemisphere midlatitude circulation and precipitation response to greenhouse gas forcing". In: *Climate Dynamics* 54.9, pp. 4399–4421. DOI: 10.1007/s00382-020-05234-1.

Miralles, D. G., A. J. Teuling, C. C. van Heerwaarden, and J. Vilà-Guerau de Arellano (2014). "Mega-heatwave temperatures due to combined soil desiccation and atmospheric heat accumulation". In: *Nature Geoscience* 7.5, pp. 345–349. DOI: 10.1038/ngeo2141.

Moreno-Chamarro, E., L.-P. Caron, S. Loosveldt Tomas, J. Vegas-Regidor, O. Gutjahr, M.-P. Moine, D. Putrasahan, C. D. Roberts, M. J. Roberts, R. Senan, L. Terray, E. Tourigny, and P. L. Vidale (2022). "Impact of increased resolution on long-standing biases in HighResMIP-PRIMAVERA climate models". In: *Geoscientific Model Development* 15.1, pp. 269–289. DOI: 10.5194/gmd-15-269-2022.

Muchan, K., M. Lewis, J. Hannaford, and S. Parry (2015). "The winter storms of 2013/2014 in the UK: hydrological responses and impacts". In: *Weather* 70.2, pp. 55–61. DOI: 10.1002/wea.2469.

Müller, W. A., J. H. Jungclaus, T. Mauritsen, J. Baehr, M. Bittner, R. Budich, F. Bunzel, M. Esch, R. Ghosh, H. Haak, T. Ilyina, T. Kleine, L. Kornblueh, H. Li, K. Modali, D. Notz, H. Pohlmann, E. Roeckner, I. Stemmler, F. Tian, and J. Marotzke (2018). "A Higher-resolution Version of the Max Planck Institute Earth System Model (MPI-ESM1.2-HR)". In: *Journal of Advances in Modeling Earth Systems* 10.7, pp. 1383–1413. DOI: 10.1029/2017MS001217.

Muthers, S., G. Laschewski, and A. Matzarakis (2017). "The Summers 2003 and 2015 in South-West Germany: Heat Waves and Heat-Related Mortality in the Context of Climate Change". In: *Atmosphere* 8.11, p. 224. DOI: 10.3390/atmos8110224.

NASEM (2016). *Attribution of extreme weather events in the context of climate change*. Ed. by National Academies of Sciences, Engineering, and Medicine. OCLC: ocn956661423. Washington, DC: The National Academies Press. 165 pp. DOI: 10.17226/21852.

Nese, J. M., G. M. Lee, and D. Babb (2018). *A World of Weather: Fundamentals of Meteorology*. 6th ed. Kendall Hunt.

NFRR (2016). *UK National flood Resilience Review*. United Kingdom.

Nogués-Paegle, J. and K. C. Mo (1997). "Alternating Wet and Dry Conditions over South America during Summer". In: *Monthly Weather Review* 125.2, pp. 279–291. DOI: 10.1175/1520-0493(1997)125<0279:AWADCO>2.0.CO;2.

O'Neill, B. C., E. Kriegler, K. Riahi, K. L. Ebi, S. Hallegatte, T. R. Carter, R. Mathur, and D. P. van Vuuren (2014). "A new scenario framework for climate change research: the concept of shared socioeconomic pathways". In: *Climatic Change* 122.3, pp. 387–400. DOI: 10.1007/s10584-013-0905-2.

Olsson, L., H. Thorén, D. Harnesk, and J. Persson (2022). "Ethics of Probabilistic Extreme Event Attribution in Climate Change Science: A Critique". In: *Earth's Future* 10.3. DOI: 10.1029/2021EF002258.

Otto, F. E. L., N. Massey, G. J. van Oldenborgh, R. G. Jones, and M. R. Allen (2012). "Reconciling two approaches to attribution of the 2010 Russian heat wave". In: *Geophysical Research Letters* 39.4, n/a–n/a. DOI: 10.1029/2011GL050422.

Otto, F. E. (2017). "Attribution of Weather and Climate Events". In: *Annual Review of Environment and Resources* 42.1, pp. 627–646. DOI: 10.1146/annurev-environ-102016-060847.

Oueslati, B., P. Yiou, and A. Jézéquel (2019). "Revisiting the dynamic and thermodynamic processes driving the record-breaking January 2014 precipitation in the southern UK". In: *Scientific Reports* 9.1, p. 2859. DOI: 10.1038/s41598-019-39306-y.

Pascale, S., L. M. V. Carvalho, D. K. Adams, C. L. Castro, and I. F. A. Cavalcanti (2019). "Current and Future Variations of the Monsoons of the Americas in a Warming Climate". In: *Current Climate Change Reports* 5.3, pp. 125–144. DOI: 10.1007/s40641-019-00135-w.

Patricola, C. M. and M. F. Wehner (2018). "Anthropogenic influences on major tropical cyclone events". In: *Nature* 563.7731, pp. 339–346. DOI: 10.1038/s41586-018-0673-2.

Patt, A. G. and D. P. Schrag (2003). "Using Specific Language to Describe Risk and Probability". In: *Climatic Change* 61.1, pp. 17–30. DOI: 10.1023/A:1026314523443.

Pearl, J. and D. Mackenzie (2018). *The book of Why: The new science of cause and effect*. New York: Basic Books.

Penalba, O. C. and J. A. Rivera (2013). "Future Changes in Drought Characteristics over Southern South America Projected by a CMIP5 Multi-Model Ensemble". In: *American Journal of Climate Change* 02.3, pp. 173–182. DOI: 10.4236/ajcc.2013.23017.

Penalba, O. C. and F. A. Robledo (2010). "Spatial and temporal variability of the frequency of extreme daily rainfall regime in the La Plata Basin during the 20th century". In: *Climatic Change* 98.3, pp. 531–550. DOI: 10.1007/s10584-009-9744-6.

Peterson, T. C. and M. O. Baringer (2009). "State of the Climate in 2008". In: *Bulletin of the American Meteorological Society* 90.8, S1–S196. DOI: 10.1175/BAMS-90-8-StateoftheClimate.

Pirtle, K. (2021). *The December 2021 tornado outbreak, explained*. noaa.gov. URL: https://www.noaa.gov/news/december-2021-tornado-outbreak-explained (visited on 02/16/2021).

Pulkkinen, K., S. Undorf, F. Bender, P. Wikman-Svahn, F. Doblas-Reyes, C. Flynn, G. C. Hegerl, A. Jönsson, G.-K. Leung, J. Roussos, T. G. Shepherd, and E. Thompson (2022). "The value of values in climate science". In: *Nature Climate Change* 12.1, pp. 4–6. DOI: 10.1038/s41558-021-01238-9.

Rahmstorf, S. and D. Coumou (2011). "Increase of extreme events in a warming world". In: *Proceedings of the National Academy of Sciences* 108.44, pp. 17905–17909. DOI: 10.1073/pnas.1101766108.

Rasmijn, L. M., G. van der Schrier, R. Bintanja, J. Barkmeijer, A. Sterl, and W. Hazeleger (2018). "Future equivalent of 2010 Russian heatwave intensified by weakening soil moisture constraints". In: *Nature Climate Change* 8.5, pp. 381–385. DOI: 10.1038/s41558-018-0114-0.

Rayner, N. A., P. Brohan, D. E. Parker, C. K. Folland, J. J. Kennedy, M. Vanicek, T. J. Ansell, and S. F. B. Tett (2006). "Improved Analyses of Changes and Uncer-

tainties in Sea Surface Temperature Measured In Situ since the Mid-Nineteenth Century: The HadSST2 Dataset". In: *Journal of Climate* 19.3, pp. 446–469. DOI: 10.1175/JCLI3637.1.

RECEIPT (2022). *RECEIPT*. RECEIPT. URL: https://climatestorylines.eu/ (visited on 03/21/2022).

Reick, C. H., T. Raddatz, V. Brovkin, and V. Gayler (2013). "Representation of natural and anthropogenic land cover change in MPI-ESM: Land Cover in MPI-ESM". In: *Journal of Advances in Modeling Earth Systems* 5.3, pp. 459–482. DOI: 10.1002/jame.20022.

Russo, S., A. Dosio, R. G. Graversen, J. Sillmann, H. Carrao, M. B. Dunbar, A. Singleton, P. Montagna, P. Barbola, and J. V. Vogt (2014). "Magnitude of extreme heat waves in present climate and their projection in a warming world". In: *Journal of Geophysical Research: Atmospheres* 119.22. DOI: 10.1002/2014JD022098.

Russo, S., J. Sillmann, and E. M. Fischer (2015). "Top ten European heatwaves since 1950 and their occurrence in the coming decades". In: *Environmental Research Letters* 10.12, p. 124003. DOI: 10.1088/1748-9326/10/12/124003.

Samset, B. H., M. Sand, C. J. Smith, S. E. Bauer, P. M. Forster, J. S. Fuglestvedt, S. Osprey, and C.-F. Schleussner (2018). "Climate Impacts From a Removal of Anthropogenic Aerosol Emissions". In: *Geophysical Research Letters* 45.2, pp. 1020–1029. DOI: 10.1002/2017GL076079.

Sánchez-Benítez, A., H. Goessling, F. Pithan, T. Semmler, and T. Jung (2022). "The July 2019 European Heat Wave in a Warmer Climate: Storyline Scenarios with a Coupled Model Using Spectral Nudging". In: *Journal of Climate* 35.8, pp. 2373–2390. DOI: 10.1175/JCLI-D-21-0573.1.

Schaaf, B., H. von Storch, and F. Feser (2017). "Does Spectral Nudging Have an Effect on Dynamical Downscaling Applied in Small Regional Model Domains?" In: *Monthly Weather Review* 145.10, pp. 4303–4311. DOI: 10.1175/MWR-D-17-0087.1.

Schär, C., C. Frei, D. Lüthi, and H. C. Davies (1996). "Surrogate climate-change scenarios for regional climate models". In: *Geophysical Research Letters* 23.6, pp. 669–672. DOI: 10.1029/96GL00265.

Schär, C., P. L. Vidale, D. Lüthi, C. Frei, C. Häberli, M. A. Liniger, and C. Appenzeller (2004). "The role of increasing temperature variability in European summer heatwaves". In: *Nature* 427.6972, pp. 332–336. DOI: 10.1038/nature02300.

Schneider, D. P., C. Deser, and Y. Okumura (2012). "An assessment and interpretation of the observed warming of West Antarctica in the austral spring". In: *Climate Dynamics* 38.1, pp. 323–347. DOI: 10.1007/s00382-010-0985-x.

Schneider, U., A. Becker, P. Finger, A. Meyer-Christoffer, and M. Ziese (2015). *GPCC Monitoring Product Version 5.0 at 1.0°: Near Real-Time Monthly Land-Surface*

Precipitation from Rain-Gauges based on SYNOP and CLIMAT Data: Gridded Monthly Totals. Artwork Size: 200 KB per monthly gzip file Medium: gzip NetCDF Pages: 200 KB per monthly gzip file Version Number: 5.0 Type: dataset. DOI: 10.5676/DWD_GPCC/MP_M_V5_100.

Schubert-Frisius, M., F. Feser, H. von Storch, and S. Rast (2017). "Optimal Spectral Nudging for Global Dynamic Downscaling". In: *Monthly Weather Review* 145.3, pp. 909–927. DOI: 10.1175/MWR-D-16-0036.1.

Scinocca, J. F., V. V. Kharin, Y. Jiao, M. W. Qian, M. Lazare, L. Solheim, G. M. Flato, S. Biner, M. Desgagne, and B. Dugas (2016). "Coordinated Global and Regional Climate Modeling". In: *Journal of Climate* 29.1, pp. 17–35. DOI: 10.1175/JCLI-D-15-0161.1.

Sgroi, L. C., M. A. Lovino, E. H. Berbery, and G. V. Müller (2021). "Characteristics of droughts in Argentina's core crop region". In: *Hydrology and Earth System Sciences* 25.5, pp. 2475–2490. DOI: 10.5194/hess-25-2475-2021.

Shaw, S. B. and S. J. Riha (2011). "Assessing temperature-based PET equations under a changing climate in temperate, deciduous forests". In: *Hydrological Processes* 25.9, pp. 1466–1478. DOI: 10.1002/hyp.7913.

Shepherd, T. G. (2014). "Atmospheric circulation as a source of uncertainty in climate change projections". In: *Nature Geoscience* 7.10, pp. 703–708. DOI: 10.1038/ngeo2253.

— (2016). "A Common Framework for Approaches to Extreme Event Attribution". In: *Current Climate Change Reports* 2.1, pp. 28–38. DOI: 10.1007/s40641-016-0033-y.

— (2019). "Storyline approach to the construction of regional climate change information". In: *Proceedings of the Royal Society A: Mathematical, Physical and Engineering Sciences* 475.2225, p. 20190013. DOI: 10.1098/rspa.2019.0013.

Shepherd, T. G., E. Boyd, R. A. Calel, S. C. Chapman, S. Dessai, I. M. Dima-West, H. J. Fowler, R. James, D. Maraun, O. Martius, C. A. Senior, A. H. Sobel, D. A. Stainforth, S. F. B. Tett, K. E. Trenberth, B. J. J. M. van den Hurk, N. W. Watkins, R. L. Wilby, and D. A. Zenghelis (2018). "Storylines: an alternative approach to representing uncertainty in physical aspects of climate change". In: *Climatic Change* 151.3, pp. 555–571. DOI: 10.1007/s10584-018-2317-9.

Sillmann, J., V. V. Kharin, X. Zhang, F. W. Zwiers, and D. Bronaugh (2013). "Climate extremes indices in the CMIP5 multimodel ensemble: Part 1. Model evaluation in the present climate". In: *Journal of Geophysical Research: Atmospheres* 118.4, pp. 1716–1733. DOI: 10.1002/jgrd.50203.

Sillmann, J., T. G. Shepherd, B. van den Hurk, W. Hazeleger, O. Martius, J. Slingo, and J. Zscheischler (2021). "Event-Based Storylines to Address Climate Risk". In: *Earth's Future* 9.2. DOI: 10.1029/2020EF001783.

Singh, D., S. Ghosh, M. K. Roxy, and S. McDermid (2019). "Indian summer monsoon: Extreme events, historical changes, and role of anthropogenic forcings". In: *WIREs Climate Change* 10.2. DOI: 10.1002/wcc.571.

Smith, C. J., G. R. Harris, M. D. Palmer, N. Bellouin, W. Collins, G. Myhre, M. Schulz, J.-C. Golaz, M. Ringer, T. Storelvmo, and P. M. Forster (2021). "Energy Budget Constraints on the Time History of Aerosol Forcing and Climate Sensitivity". In: *Journal of Geophysical Research: Atmospheres* 126.13. DOI: 10.1029/2020JD033622.

Sousa, P. M., D. Barriopedro, R. García-Herrera, C. Ordóñez, P. M. M. Soares, and R. M. Trigo (2020). "Distinct influences of large-scale circulation and regional feedbacks in two exceptional 2019 European heatwaves". In: *Communications Earth & Environment* 1.1, p. 48. DOI: 10.1038/s43247-020-00048-9.

Stammer, D., A. Engels, J. Marotzke, E. Gresse, C. Hedemann, and J. Petzold (2021). *Hamburg Climate Futures Outlook 2021: Assessing the plausibility of deep decarbonization by 2050*. Version Number: 1/2021. Universität Hamburg. DOI: 10.25592/UHHFDM.9104.

Stephens, E. M., T. L. Edwards, and D. Demeritt (2012). "Communicating probabilistic information from climate model ensembles-lessons from numerical weather prediction: Communicating probabilistic information from climate model ensembles". In: *Wiley Interdisciplinary Reviews: Climate Change* 3.5, pp. 409–426. DOI: 10.1002/wcc.187.

Stevens, B. and S. Bony (2013). "What Are Climate Models Missing?" In: *Science* 340.6136, pp. 1053–1054. DOI: 10.1126/science.1237554.

Stevens, B., M. Giorgetta, M. Esch, T. Mauritsen, T. Crueger, S. Rast, M. Salzmann, H. Schmidt, J. Bader, K. Block, R. Brokopf, I. Fast, S. Kinne, L. Kornblueh, U. Lohmann, R. Pincus, T. Reichler, and E. Roeckner (2013). "Atmospheric component of the MPI-M Earth System Model: ECHAM6". In: *Journal of Advances in Modeling Earth Systems* 5.2, pp. 146–172. DOI: 10.1002/jame.20015.

Stott, P. A., N. Christidis, F. E. L. Otto, Y. Sun, J.-P. Vanderlinden, G. J. van Oldenborgh, R. Vautard, H. von Storch, P. Walton, P. Yiou, and F. W. Zwiers (2016). "Attribution of extreme weather and climate-related events". In: *WIREs Climate Change* 7.1, pp. 23–41. DOI: 10.1002/wcc.380.

Stott, P. A., D. A. Stone, and M. R. Allen (2004). "Human contribution to the European heatwave of 2003". In: *Nature* 432.7017, pp. 610–614. DOI: 10.1038/nature03089.

Tamarin-Brodsky, T., K. Hodges, B. J. Hoskins, and T. G. Shepherd (2019). "A Dynamical Perspective on Atmospheric Temperature Variability and Its Response to Climate Change". In: *Journal of Climate* 32.6, pp. 1707–1724. DOI: 10.1175/JCLI-D-18-0462.1.

Tapiador, F., A. Navarro, V. Levizzani, E. García-Ortega, G. Huffman, C. Kidd, P. Kucera, C. Kummerow, H. Masunaga, W. Petersen, R. Roca, J.-L. Sánchez, W.-K. Tao, and F. Turk (2017). "Global precipitation measurements for validating climate models". In: *Atmospheric Research* 197, pp. 1–20. DOI: 10.1016/j.atmosres.2017.06.021.

Terray, L. (2021). "A dynamical adjustment perspective on extreme event attribution". In: *Weather and Climate Dynamics* 2.4, pp. 971–989. DOI: 10.5194/wcd-2-971-2021.

Thornthwaite, C. W. (1948). "An Approach toward a Rational Classification of Climate". In: *Geographical Review* 38.1, p. 55. DOI: 10.2307/210739.

Trenberth, K. E. (2008). "The Impact of Climate Change and Variability on Heavy Precipitation, Floods, and Droughts". In: *Encyclopedia of Hydrological Sciences*. Ed. by M. G. Anderson and J. J. McDonnell. Chichester, UK: John Wiley & Sons, Ltd, hsa211. DOI: 10.1002/0470848944.hsa211.

Trenberth, K. E. and J. T. Fasullo (2012). "Climate extremes and climate change: The Russian heat wave and other climate extremes of 2010". In: *Journal of Geophysical Research: Atmospheres* 117 (D17), n/a–n/a. DOI: 10.1029/2012JD018020.

Trenberth, K. E., J. T. Fasullo, and T. G. Shepherd (2015). "Attribution of climate extreme events". In: *Nature Climate Change* 5.8, pp. 725–730. DOI: 10.1038/nclimate2657.

Trigo, R. M. (2005). "How exceptional was the early August 2003 heatwave in France?" In: *Geophysical Research Letters* 32.10, p. L10701. DOI: 10.1029/2005GL022410.

Van der Wiel, K., G. Lenderink, and H. de Vries (2021). "Physical storylines of future European drought events like 2018 based on ensemble climate modelling". In: *Weather and Climate Extremes* 33, p. 100350. DOI: 10.1016/j.wace.2021.100350.

Van der Wiel, K., A. J. Matthews, D. P. Stevens, and M. M. Joshi (2015). "A dynamical framework for the origin of the diagonal South Pacific and South Atlantic Convergence Zones". In: *Quarterly Journal of the Royal Meteorological Society* 141.691, pp. 1997–2010. DOI: 10.1002/qj.2508.

Van der Wiel, K., F. M. Selten, R. Bintanja, R. Blackport, and J. A. Screen (2020). "Ensemble climate-impact modelling: extreme impacts from moderate meteorological conditions". In: *Environmental Research Letters* 15.3, p. 034050. DOI: 10.1088/1748-9326/ab7668.

Van Garderen, L., F. Feser, and T. G. Shepherd (2021). "A methodology for attributing the role of climate change in extreme events: a global spectrally nudged storyline". In: *Natural Hazards and Earth System Sciences* 21.1, pp. 171–186. DOI: 10.5194/nhess-21-171-2021.

Van Niekerk, A., T. G. Shepherd, S. B. Vosper, and S. Webster (2016). "Sensitivity of resolved and parametrized surface drag to changes in resolution and parametrization". In: *Quarterly Journal of the Royal Meteorological Society* 142.699, pp. 2300–2313. DOI: 10.1002/qj.2821.

Van Oldenborgh, G. J., F. Krikken, S. Lewis, N. J. Leach, F. Lehner, K. R. Saunders, M. van Weele, K. Haustein, S. Li, D. Wallom, S. Sparrow, J. Arrighi, R. K. Singh, M. K. van Aalst, S. Y. Philip, R. Vautard, and F. E. L. Otto (2021a). "Attribution of the Australian bushfire risk to anthropogenic climate change". In: *Natural Hazards and Earth System Sciences* 21.3, pp. 941–960. DOI: 10.5194/nhess-21-941-2021.

Van Oldenborgh, G. J., K. van der Wiel, S. Kew, S. Philip, F. Otto, R. Vautard, A. King, F. Lott, J. Arrighi, R. Singh, and M. van Aalst (2021b). "Pathways and pitfalls in extreme event attribution". In: *Climatic Change* 166.1, p. 13. DOI: 10.1007/s10584-021-03071-7.

Vautard, R., P. Yiou, F. Otto, P. Stott, N. Christidis, G. J. van Oldenborgh, and N. Schaller (2016). "Attribution of human-induced dynamical and thermodynamical contributions in extreme weather events". In: *Environmental Research Letters* 11.11, p. 114009. DOI: 10.1088/1748-9326/11/11/114009.

Vautard, R., M. van Aalst, O. Boucher, A. Drouin, K. Haustein, F. Kreienkamp, G. J. van Oldenborgh, F. E. L. Otto, A. Ribes, Y. Robin, M. Schneider, J.-M. Soubeyroux, P. Stott, S. I. Seneviratne, M. M. Vogel, and M. Wehner (2020). "Human contribution to the record-breaking June and July 2019 heatwaves in Western Europe". In: *Environmental Research Letters* 15.9, p. 094077. DOI: 10.1088/1748-9326/aba3d4.

Vera, C. S. and L. Díaz (2015). "Anthropogenic influence on summer precipitation trends over South America in CMIP5 models: preccipitation trends over South America in CMIP5 models". In: *International Journal of Climatology* 35.10, pp. 3172–3177. DOI: 10.1002/joc.4153.

Vincent, C. L. and A. N. Hahmann (2015). "The Impact of Grid and Spectral Nudging on the Variance of the Near-Surface Wind Speed". In: *Journal of Applied Meteorology and Climatology* 54.5, pp. 1021–1038. DOI: 10.1175/JAMC-D-14-0047.1.

Von Storch, H., L. Cavicchia, F. Feser, and D. Li (2018). "The Concept of Large-Scale Conditioning of Climate Model Simulations of Atmospheric Coastal Dynamics: Current State and Perspectives". In: *Atmosphere* 9.9, p. 337. DOI: 10.3390/atmos9090337.

Von Storch, H., H. Langenberg, and F. Feser (2000). "A Spectral Nudging Technique for Dynamical Downscaling Purposes". In: *Monthly Weather Review* 128.10, pp. 3664–3673. DOI: 10.1175/1520-0493(2000)128<3664:ASNTFD>2.0.CO;2.

Waldron, K. M., J. Paegle, and J. D. Horel (1996). "Sensitivity of a Spectrally Filtered and Nudged Limited-Area Model to Outer Model Options". In: *Monthly Weather Review* 124.3, pp. 529–547. DOI: 10.1175/1520-0493(1996)124<0529:SOASFA>2.0.CO;2.

Wang, B., M. Biasutti, M. P. Byrne, C. Castro, C.-P. Chang, K. Cook, R. Fu, A. M. Grimm, K.-J. Ha, H. Hendon, A. Kitoh, R. Krishnan, J.-Y. Lee, J. Li, J. Liu, A. Moise, S. Pascale, M. K. Roxy, A. Seth, C.-H. Sui, A. Turner, S. Yang, K.-S. Yun, L. Zhang, and T. Zhou (2021). "Monsoons Climate Change Assessment". In: *Bulletin of the American Meteorological Society* 102.1, E1–E19. DOI: 10.1175/BAMS-D-19-0335.1.

Watanabe, M., H. Shiogama, Y. Imada, M. Mori, M. Ishii, and M. Kimoto (2013). "Event Attribution of the August 2010 Russian Heat Wave". In: *SOLA* 9.0, pp. 65–68. DOI: 10.2151/sola.2013-015.

Wehrli, K., B. P. Guillod, M. Hauser, M. Leclair, and S. I. Seneviratne (2019). "Identifying Key Driving Processes of Major Recent Heat Waves". In: *Journal of Geophysical Research: Atmospheres* 124.22, pp. 11746–11765. DOI: 10.1029/2019JD030635.

Westervelt, D. M., L. W. Horowitz, V. Naik, J.-C. Golaz, and D. L. Mauzerall (2015). "Radiative forcing and climate response to projected 21st century aerosol decreases". In: *Atmospheric Chemistry and Physics* 15.22, pp. 12681–12703. DOI: 10.5194/acp-15-12681-2015.

Whan, K., J. Sillmann, N. Schaller, and R. Haarsma (2020). "Future changes in atmospheric rivers and extreme precipitation in Norway". In: *Climate Dynamics* 54.3, pp. 2071–2084. DOI: 10.1007/s00382-019-05099-z.

Whan, K., J. Zscheischler, R. Orth, M. Shongwe, M. Rahimi, E. O. Asare, and S. I. Seneviratne (2015). "Impact of soil moisture on extreme maximum temperatures in Europe". In: *Weather and Climate Extremes* 9, pp. 57–67. DOI: 10.1016/j.wace.2015.05.001.

Yoshimura, K. and M. Kanamitsu (2008). "Dynamical Global Downscaling of Global Reanalysis". In: *Monthly Weather Review* 136.8, pp. 2983–2998. DOI: 10.1175/2008MWR2281.1.

Young, H. R., T. G. Shepherd, J. Acidri, R. J. Cornforth, C. Petty, J. Seaman, and L. C. Todman (2021). "Storylines for decision-making: climate and food security in Namibia". In: *Climate and Development* 13.6, pp. 515–528. DOI: 10.1080/17565529.2020.1808438.

Žagar, N., M. Blaauw, B. Jesenko, and L. Magnusson (2016). "Diagnosing model performance in the tropics". In: *ECMWF Newsletter* 147, pp. 26–33.

Zängl, G., D. Reinert, P. Rípodas, and M. Baldauf (2015). "The ICON (ICOsahedral Non-hydrostatic) modelling framework of DWD and MPI-M: Description of the

non-hydrostatic dynamical core". In: *Quarterly Journal of the Royal Meteorological Society* 141.687, pp. 563–579. DOI: 10.1002/qj.2378.

Zaninelli, P. G., C. G. Menéndez, M. Falco, N. López-Franca, and A. F. Carril (2019). "Future hydroclimatological changes in South America based on an ensemble of regional climate models". In: *Climate Dynamics* 52.1, pp. 819–830. DOI: 10.1007/s00382-018-4225-0.

Zappa, G. and T. G. Shepherd (2017). "Storylines of Atmospheric Circulation Change for European Regional Climate Impact Assessment". In: *Journal of Climate* 30.16, pp. 6561–6577. DOI: 10.1175/JCLI-D-16-0807.1.

Part V

Appendices

A

Paper nr.1: A methodology for attributing the role of climate change in extreme events: a global spectrally nudged storyline

Nat. Hazards Earth Syst. Sci., 21, 171–186, 2021
https://doi.org/10.5194/nhess-21-171-2021

Natural Hazards and Earth System Sciences
Open Access
EGU

A methodology for attributing the role of climate change in extreme events: a global spectrally nudged storyline

Linda van Garderen[1], **Frauke Feser**[1], **and Theodore G. Shepherd**[2]

[1]Institute for Coastal Research – Analysis and Modelling, Helmholtz-Zentrum Geesthacht, Max-Planck-Straße 1, 21502 Geesthacht, Germany
[2]Department of Meteorology, University of Reading, Reading RG6 6BB, United Kingdom

Correspondence: Linda van Garderen (linda.vangarderen@hzg.de)

Received: 5 June 2020 – Discussion started: 26 June 2020
Revised: 25 September 2020 – Accepted: 26 November 2020 – Published: 18 January 2021

Abstract. Extreme weather events are generally associated with unusual dynamical conditions, yet the signal-to-noise ratio of the dynamical aspects of climate change that are relevant to extremes appears to be small, and the nature of the change can be highly uncertain. On the other hand, the thermodynamic aspects of climate change are already largely apparent from observations and are far more certain since they are anchored in agreed-upon physical understanding. The storyline method of extreme-event attribution, which has been gaining traction in recent years, quantitatively estimates the magnitude of thermodynamic aspects of climate change, given the dynamical conditions. There are different ways of imposing the dynamical conditions. Here we present and evaluate a method where the dynamical conditions are enforced through global spectral nudging towards reanalysis data of the large-scale vorticity and divergence in the free atmosphere, leaving the lower atmosphere free to respond. We simulate the historical extreme weather event twice: first in the world as we know it, with the events occurring on a background of a changing climate, and second in a "counterfactual" world, where the background is held fixed over the past century. We describe the methodology in detail and present results for the European 2003 heatwave and the Russian 2010 heatwave as a proof of concept. These show that the conditional attribution can be performed with a high signal-to-noise ratio on daily timescales and at local spatial scales. Our methodology is thus potentially highly useful for realistic stress testing of resilience strategies for climate impacts when coupled to an impact model.

1 Introduction

There is increasing interest in understanding and quantifying the impact of climate change on individual extreme weather and climate events. This is to be distinguished from detecting the effect of climate change on the statistics of extreme events (IPCC, 2012). In the most commonly used approach, changes in the probability distribution of an event class, whose definition is motivated by a historical event, are calculated by simulating large ensembles with an atmosphere-only climate model (Watanabe et al., 2013). The changes are computed between the "factual" ensemble, corresponding to observed forcings (e.g. sea-surface temperatures (SSTs) and greenhouse-gas (GHG) concentrations), and a "counterfactual" ensemble, corresponding to an imagined world without climate change. The latter is usually constructed by removing an estimate of the forced changes in SSTs and imposing pre-industrial GHG concentrations. As discussed by Shepherd (2016), this probabilistic approach has two prominent limitations. The first is that every extreme event is unique, but the construction of a general event class blurs the connection to the actual event and makes it difficult to link the event attribution to climate impacts. This is important because extreme impacts are not always associated with extreme meteorology (van der Wiel et al., 2020). The second limitation is that extreme events are generally associated with extreme dynamical conditions, and there is little understanding, let alone agreement, on how those dynamical conditions might respond to climate change (Hoskins and Woollings, 2015; Shepherd, 2014). This represents an uncertainty in the probabilistic estimates that is difficult to quantify.

Published by Copernicus Publications on behalf of the European Geosciences Union.

On the other hand, thermodynamic aspects of climate change such as warming and increasing specific humidity are robust in sign, anchored in agreed-upon physical understanding, and clearly emerging in observations (IPCC, 2018). Moreover in many cases the signal-to-noise ratio of the forced dynamical changes appears likely to be small (Deser et al., 2016; Schneider et al., 2012). Thus, although dynamical and thermodynamic processes are interwoven in the real climate system, it can be useful to regard the *uncertainties* in their forced response to climate change as being separable, at least to a first approximation. This has been a growing theme in climate change attribution over the past few decades. The distinction between thermodynamic and dynamical changes is not precise, and various ways of implementing the separation diagnostically have been used in different contexts. For extratropical regional climate, it has been common to regard the component of change congruent with large-scale internal variability (e.g. as defined by empirical orthogonal functions or by self-organizing maps) as "dynamical" (Deser et al., 2016; Horton et al., 2015) and the residual as "thermodynamic". For tropical climate or for extratropical storms, dynamical changes are instead commonly identified with changes in vertical velocity (Bony et al., 2013; Pfahl et al., 2017). In the absence of evidence to the contrary, a reasonable hypothesis is that the forced dynamical changes are undetectable; this hypothesis is implemented explicitly in the "pseudo global warming" methodology used for regional climate studies (Schär et al., 1996) and in the "dynamical adjustment" methodology used to study observed climate trends (Wallace et al., 2012).

Trenberth et al. (2015) suggested that the same thinking could be usefully applied to the attribution of individual extreme events. Specifically, the extreme dynamical circumstances leading to the event could be regarded as given, i.e. arising by chance, and the question posed of how the event was modified by the known thermodynamic aspects of climate change. This conditional framing of the attribution question was subsequently dubbed the "storyline" approach (Shepherd, 2016) and has a precedent in the application of dynamical adjustment to extreme seasonal climate anomalies (Cattiaux et al., 2010). As emphasized by Shepherd (2016) and NAS (2016), there is actually a continuum between the storyline and probabilistic approaches: storylines are highly conditioned probabilities, and probabilistic approaches generally involve some form of dynamical conditioning too, through the imposed SST patterns. However, the extent of conditioning imposed by constraining the atmospheric state is so severe that in practice the storyline approach can be regarded as deterministic, just as weather forecasts, whilst probabilistic in principle, are interpreted deterministically when the ensemble spread is sufficiently narrow.

By focusing on the known effects of climate change, the storyline approach seeks to avoid "Type 2" errors or missed warnings, in contrast to the probabilistic approach, which, by needing to reject the null hypothesis of no climate change whatsoever, seeks to avoid "Type 1" errors or false alarms (Lloyd and Oreskes, 2018; Trenberth et al., 2015). A colloquial way of putting this is that rather than asking what extreme events can tell us about climate change, we ask what known aspects of climate change can tell us about particular extreme events. Although its results are not expressed probabilistically, the storyline approach enables a quantitative estimate of climate change with a clear causal interpretation (Pearl and Mackenzie, 2018). Notwithstanding the need for asking both kinds of questions as they provide different kinds of information (Lloyd and Shepherd, 2020), the storyline approach is a new development, and there are as yet not so many studies employing this approach.

In previous applications of the storyline approach, individual extreme weather events have been dynamically constrained through boundary conditions applied to a regional model (Meredith et al., 2015) or by controlling the initial conditions in a weather forecast model (Patricola and Wehner, 2018). More recently, nudging the free atmosphere to reanalysis data (leaving the boundary layer free to respond) has been applied in a global medium-resolution atmospheric model to constrain the dynamical conditions leading to heatwaves, first to determine the effect of soil moisture changes on selected recent heatwaves (Wehrli et al., 2019) and subsequently to determine the effect of past and projected future warming on the 2018 Northern Hemisphere heatwave (Wehrli et al., 2020). The concept of nudging the atmospheric circulation in order to impose the dynamical conditions has a long history. In particular, spectral nudging (von Storch et al., 2000; Waldron et al., 1996) allows for scale-selective nudging so that only the large spatial scales of the model are constrained, while the smaller scales, including those relevant to extreme events, are free to be simulated by the high-resolution model. The climate model can thus potentially add value and regional detail to the coarser-resolution forcing dataset. Spectral nudging has been used in regional climate modelling (Feser and Barcikowska, 2012; Scinocca et al., 2015) and in boundary-layer sensitivity studies (van Niekerk et al., 2016). Note that in all these modelling approaches, the dynamical constraint is imposed "remotely" from the phenomenon of interest (in space, time, and/or spatial scale) in contrast to the diagnostic approaches mentioned earlier and thus preserves the physical interplay between dynamics and thermodynamics within the extreme event itself.

The purpose of this paper is to provide a methodological underpinning for the application of large-scale spectral nudging of divergence and vorticity in a global high-resolution atmospheric model for the purpose of attributing the role of thermodynamic aspects of climate change (or other conditional perturbations) in extreme events of various types and timescales. A key question is to determine what level of refinement of the attribution, in both space and time, is possible. The outline of the paper is as follows. In Sect. 2, we elaborate on the technicalities of spectral nudging within the ECHAM6 model and its parameter sensitiv-

ities as well as the construction of the counterfactual simulations. In Sect. 3, we exemplify the method by applying it to two well-studied heatwaves: the European 2003 heatwave and the Russian 2010 heatwave. As well as identifying some important differences between the two events, we examine the signal-to-noise ratio of our attribution. A concluding discussion follows in Sect. 4.

2 Method

2.1 Spectral nudging

The spectral-nudging technique is well established within the context of regional climate modelling (Miguez-Macho et al., 2004; von Storch et al., 2000, 2018; Waldron et al., 1996). In this approach, so-called "nudging terms" are added to the large-scale part of the climate model trajectory, which draws the model towards reanalysis data. Global spectral nudging (Kim and Hong, 2012; Schubert-Frisius et al., 2017; Yoshimura and Kanamitsu, 2008) works in a similar way. It constrains large-scale weather patterns of the climate model, such as high- and low-pressure systems or fronts, to stay close to reanalysis data in order to derive a global high-resolution weather reconstruction. The general idea is that the realistic large-scale state of the reanalysis data is followed by the global climate model (GCM), while at smaller scales the model provides additional detail to improve high-resolution weather patterns. Another merit of the approach is the potential to reduce inhomogeneities in the dataset by using only a very limited number of variables from the reanalysis data, although this is less of an issue for our application because we compare factual and counterfactual simulations for the same large-scale conditions, so any inhomogeneity in the reanalysis would apply equally to both. For the same reason, our approach can be expected to be robust to any differences between reanalyses. In order to define a noise level for our analysis, we construct small ensembles of three factual and three counterfactual simulations. Although such small ensembles are clearly inadequate for quantifying conditional probabilities, they have been successfully used in the past (e.g. Shepherd, 2008) to identify robust differences between the two ensembles from a deterministic perspective, which is our interest here.

2.2 ECHAM6 application

For this study, we use the high-resolution T255L95 GCM ECHAM6 (Stevens et al., 2013) with the JSBACH land component sub-model (Reick et al., 2013); however the method is applicable to any atmospheric GCM. SSTs and sea ice concentrations (SICs) are prescribed from NCEP1 reanalysis data (Kalnay et al., 1996). ECHAM6 is globally spectrally nudged towards the NCEP1 reanalysis data to achieve realistic weather patterns and extreme events of the past. However, any other reanalysis should provide similar results since only the large-scale fields are nudged. We chose NCEP1 due to its starting date in 1948, which is earlier than any of the other reanalysis data, enabling application of our method over a longer period of time. It is conceivable that for certain kinds of extreme events involving a tight coupling between resolved and parameterized processes, ensuring consistency between the reanalysis and the model would be beneficial. In a previous application nudging was applied for pressure, temperature, vorticity, and divergence (Jeuken et al., 1996) with a constant height profile throughout the entire atmosphere. However, we want to reproduce only the large-scale atmospheric circulation and in particular leave the thermodynamic fields (temperature and moisture) free to respond; hence we only nudge vorticity and divergence in the free atmosphere. The aim is to constrain the model as little as possible so that it can freely develop small-scale meteorological processes and extreme events while still achieving an effective control of the large-scale weather situation.

The nudging of variable X over time is applied in the spectral domain as follows (adapted from Jeuken et al., 1996):

$$\frac{\partial X}{\partial t} = \begin{cases} F_X + G\,(X_{\mathrm{NCEP}} - X) & \text{for } n \leq 20,\ p < 750\,\mathrm{hPa} \\ F_X & \text{otherwise} \end{cases}, \quad (1)$$

where X is the variable to be nudged (either vorticity or divergence), F_X is the model tendency for variable X, and X_{NCEP} is the state of that variable in NCEP1. The thresholds p and n need to be met for nudging to happen, namely pressure p must be below 750 hPa, and the spherical harmonic index n must not exceed 20. G is the relaxation coefficient in units of $10^{-5}\,\mathrm{s}^{-1}$ determining the nudging strength. Nudging is performed at every time step.

We applied most settings according to Schubert-Frisius et al. (2017), including the usage of spectral nudging in both meridional and zonal directions. We use a plateau nudging-strength height profile (see Fig. 1a), which starts at 750 hPa, then quickly increases up to its maximum nudging strength, and stays there for higher tropospheric and lower and medium stratospheric levels until it again quickly tapers back to 0 at a height corresponding to 5 hPa. The reason for the latter choice is that above 5 hPa there is no NCEP1 reanalysis data available.

The strength of nudging is determined by the relaxation coefficient (G; in $10^{-5}\,\mathrm{s}^{-1}$); see Eq. (1). The relaxation coefficient is often described using the e-folding time (G^{-1}; in 10^5 s) which represents the simulated time necessary for nudging to dampen out a model-introduced disturbance. For example, if the e-folding time is 10 h then the nudged model will dampen out that disturbance (with an assumed amplitude of 1) to a value of $1/e$ and thus greatly reduce it within 10 h. A larger relaxation coefficient implies a stronger nudging and translates into a shorter e-folding time or dampening time (von Storch et al., 2000). We have tested several e-folding times to see if the settings could be further relaxed and still reproduce the large-scale weather conditions. In Fig. 1b the impact of the tested e-folding time settings on the temporal

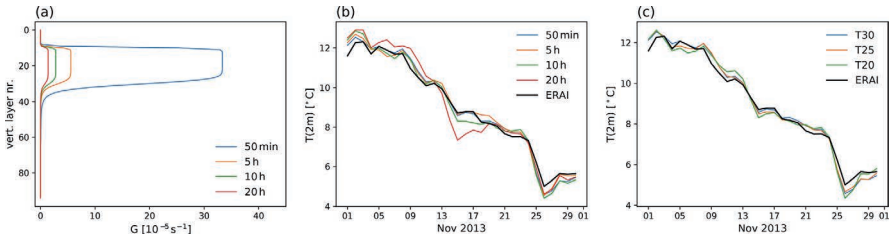

Figure 1. **(a)** Nudging strength G [10^{-5} s^{-1}] as a function of model level for different choices of minimum e-folding time as indicated. **(b)** Daily mean temperatures at 2 m height [°C] of ECHAM6 in November 2013 averaged over the European domain (35–60° N, 10° W–35° E) using the different e-folding times shown in **(a)** in comparison to ERA-Interim. **(c)** Daily mean temperatures as in **(b)** but with a 50 min nudging timescale at different truncations again in comparison to ERA-Interim.

evolution of the 2 m temperature averaged over Europe (35–60° N, 10° W–30° E) in comparison to ERA-Interim is shown through November 2013. There is little difference visible between the 50 min and 5 h e-folding times. The 10 h results start to show small deviations, whilst the 20 h results deviate even more noticeably. On the basis of this sensitivity study, we conclude that the e-folding time can safely be relaxed from 50 min to 5 h without losing the accuracy of the results.

We similarly aim to limit the range of spatial scales being nudged as much as possible. In Fig. 1c we show the 2 m temperature results for the different nudging wavelengths in comparison to ERA-Interim. The original T_{30} settings used by Schubert-Frisius et al. (2017), which translate to a minimum wavelength of approximately 1300 km (360°/30 × 111 km), show comparable results to the T_{25} and T_{20} resolutions. The nudging was therefore relaxed to the T_{20} resolution, which translates to a minimum wavelength of approximately 2000 km (360°/20 × 111 km). This should be sufficient to resolve the large-scale circulation while allowing smaller-scale processes related to local weather events to develop freely. In Fig. 2 the geopotential height anomalies for summer 2010 in the factual and counterfactual simulations show a strong resemblance. Even though the background conditions of the two simulations are different (which is further explained in Sect. 2.3), the blocking pattern formed over Russia in 2010 is clearly present in both simulations, demonstrating the capability of our nudging method to reproduce the complex dynamical situation.

We used ECHAM_SN throughout this paper to calculate climatological data for comparison to our own findings. The ECHAM_SN dataset is a spectrally nudged global historical simulation from 1948–2015 (Schubert-Frisius et al., 2017). It nudged vorticity and divergence towards NCEP1 in a vertical plateau-shaped profile, equal to the profile we use, at spatial scales corresponding to T_{30} or larger, with an e-folding time of 50 min.

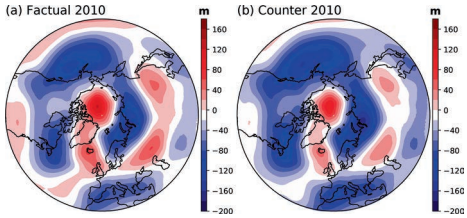

Figure 2. Geopotential height (z_{500}) June–July–August (JJA) anomalies [m] for the Northern Hemisphere showing the averaged spectrally nudged dynamic situation over **(a)** factual members and **(b)** counterfactual members of the summer 2010 blocking. Anomalies were calculated relative to the ECHAM_SN 1980–2014 JJA climatology.

2.3 Simulating the counterfactual

In this study, as in probabilistic event attribution, counterfactual and factual climate simulations are used to assess the effect of climate change on extreme events. Factual is defined as the world as we know it or a historical simulation. Counterfactual is defined as an imagined modern world without climate change. In our simulations, land use and volcanic activity as well as aerosol forcing and sea ice concentration are unchanged between factual and counterfactual. The differences between the two worlds are created by altering two important aspects of the simulation: (a) sea-surface temperature (SST) and (b) greenhouse gases (GHG). Both worlds are spectrally nudged in the same way. A potential way to check the results of the counterfactual simulation, especially for simulations over a longer time span, is to study the consistency between the inferred signals of climate change for smaller climate forcings (e.g. since mid-century) and the attributed changes in the observational record. Our simulations are 5 years each and therefore cannot be tested in this way.

However for longer simulations such a test would be beneficial.

SST patterns such as the Atlantic Multidecadal Oscillation or El Niño greatly influence weather extremes. Therefore, as with probabilistic event attribution, we impose the same SST variability for both the factual and counterfactual simulation, based on the observed SST pattern. (However, this is expected to be less critical in our case since we are imposing the large-scale atmospheric circulation.) We create the counterfactual SST conditions by subtracting a climatological warming pattern from the observed pattern, which is a standard procedure in probabilistic event attribution studies (Otto, 2017; Vautard et al., 2016; Stott et al., 2016). Although it is common to consider different climatological warming patterns as a means of exploring uncertainty, this is not so relevant in our case since the large-scale circulation is imposed. The climatological warming pattern is computed using the ECHAM6 CMIP6 (MPI-ESM1.2-HR) control and historical simulations at an atmospheric resolution of T_{127} (Müller et al., 2018). The procedure is shown in Eq. (2):

$$\mathrm{SST}_{t,\mathrm{c}} = \mathrm{SST}_t^{\mathrm{NCEP1}} - \left(\mathrm{SST}_{t,\mathrm{h}}^{\mathrm{CMIP6}} - \mathrm{SST}_{t,\mathrm{pi}}^{\mathrm{CMIP6}}\right), \tag{2}$$

where $\mathrm{SST}_{t,\mathrm{c}}$ is the counterfactual SST at time t, $\mathrm{SST}_t^{\mathrm{NCEP1}}$ is the NCEP1 SST at time t, $\mathrm{SST}_{t,\mathrm{h}}^{\mathrm{CMIP6}}$ is the CMIP6 historical SST at time t, and $\mathrm{SST}_{t,\mathrm{pi}}^{\mathrm{CMIP6}}$ is the CMIP6 pre-industrial SST at time t (for the latter, the only relevant time dependence would be seasonal). In our present implementation, which targets boreal summer only and concerns only a fairly short time period, the seasonal time dependence is suppressed, and the historical CMIP SSTs are taken to be the 2000–2009 average. For a simulation covering a full year the warming pattern should be made seasonal, and for one covering several decades it would furthermore need to be weighted over time. In Fig. 3 the CMIP6 SST warming pattern shows a good resemblance to the observed HadSST3 warming pattern. The HadSST3 pattern is obtained by subtracting the 1880–1890 average from the 1980–1990 average SST values. The general warming and cooling patches in the Pacific Ocean and Atlantic Ocean south of Greenland agree well. Also, the warming north of Scandinavia is clearly visible in both warming patterns. Despite the observational data-void region east of Greenland and north of Iceland, there is a good resemblance of our modelled warming pattern with observations. Note that pre-industrial SST observations were dependent upon ship records, which in the polar region were very few (Rayner et al., 2006), causing this part of the observational dataset to be incomplete.

For technical reasons, we did not alter the SIC in the counterfactual simulations. Given that the atmospheric circulation is nudged, changes in SIC are not expected to be relevant for summertime heatwaves as Arctic amplification from sea ice loss is a wintertime phenomenon (Screen and Simmonds, 2010). In Fig. 4 the counterfactual SSTs for July 2003 and July 2010 are shown together with the factual SIC. This shows that the sea ice edge is well away from the European and western Russian domains. Moreover, even under counterfactual conditions the SST remains almost completely physically self-consistent with the SIC according to the constraints of Hurrell et al. (2008); in particular, there are only a very few isolated regions where the SST falls below −2 °C. Nevertheless, we tested the impact of altering SIC in a counterfactual simulation of the Russian heatwave based on the counterfactual SSTs, using the linear relation found by Hurrell et al. (2008). Specifically, SIC was set to 100 % for SSTs below −1.7 °C and to 0 % for SSTs above 3 °C, with a linear interpolation in between. The results show no differences compared to the unaltered SIC counterfactual members (see Fig. 5b). However, to apply our method to other seasons or regions in close proximity to areas of sea ice loss, the counterfactual simulations would benefit from including SIC changes in the same way as was done with SST.

Table 1. Greenhouse-gas concentrations for the ECHAM6 counterfactual simulations.

Greenhouse gas	Concentration
Carbon dioxide (CO_2)	285 ppmv
Methane (CH_4)	790 ppbv
Nitrous oxide (N_2O)	275 ppbv
Chlorofluorocarbons (CFCs)	0

In the factual simulation the GHGs change according to observed values (Meinshausen et al., 2011). In the counterfactual simulation, GHGs remain at their 1890 values as listed in Table 1. This means that, strictly speaking, our attribution is to the combined effects of anthropogenic climate change (including aerosol forcing) recorded in the SSTs as well as the direct radiative effects of GHG forcing.

The default initial atmospheric state of the ECHAM6 model is a random state during the simulated mid-1990s. Changing that initial state to a counterfactual initial state requires a spin-up time to allow the atmosphere and land surface enough time to reach a new equilibrium state with their new boundary conditions. To accomplish this we run a non-nudged counterfactual spin-up ensemble for 3 model years with three members. We chose a 3-year spin-up after confirming the soil moisture was adapted to the new counterfactual situation (not shown). Each member was initiated at a different starting date (January–March 1995). The results of these spin-ups are three random atmospheric counterfactual states, which are used as initial conditions for the counterfactual experiments. Although in principle both the factual and counterfactual conditions define conditional probabilities, our three-member ensembles are certainly not sufficient to estimate those probabilities. As noted earlier, our goal here is simply to determine the robustness of the deterministic differences between the factual and counterfactual ensembles.

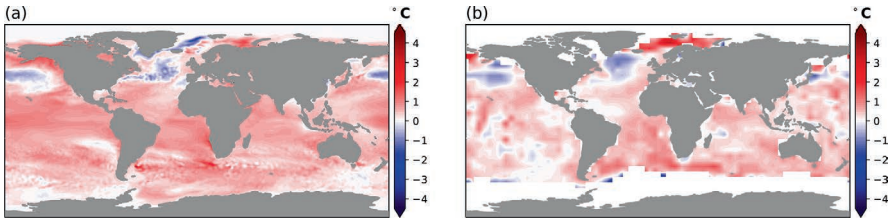

Figure 3. Sea-surface temperature (SST) warming pattern [°C] calculated **(a)** from ECHAM6 CMIP6 modelled data and **(b)** from HadSST3 observed data.

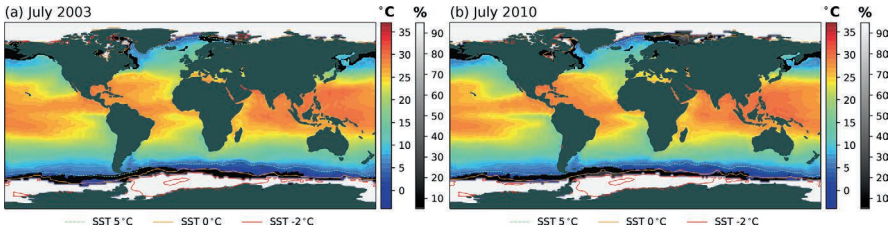

Figure 4. Counterfactual SST [°C] in shaded colours and factual SIC [%] in greyscale for **(a)** July 2003 and **(b)** July 2010. The SST 5 °C (dashed green), 0 °C (orange), and −2 °C (red) contours are marked for reference.

The ECHAM_SN simulation and the altered SIC simulation provide out-of-sample tests of robustness for the factual and counterfactual ensembles, respectively. Figure 5 shows that in both cases, these simulations fall largely within the range of the three-member ensembles.

For the European 2003 heatwave the three counterfactual members run from 1 March and are initialized with the spin-up counterfactual atmospheric state members (year 3, March). The three factual members are started 1 month apart from each other (in January–March 2003), and initialized with the corresponding atmospheric state from the ECHAM_SN dataset. For the Russian 2010 heatwave the three counterfactual members run instead from 1 January because of the known importance of soil preconditioning for this event (Wehrli et al., 2019). The three factual members again run with 1-month differences in their starting dates, but here from November 2009, December 2009, and January 2010, again initialized with the corresponding state from the ECHAM_SN dataset. For analysis regions we select 35–50° N, 10° W–25° E as the domain for the European heatwave 2003 and 50–60° N, 35–55° E for the Russian heatwave 2010, in line with previous literature (Dole et al., 2011; García-Herrera et al., 2010; Otto et al., 2012; Rasmijn et al., 2018; Wehrli et al., 2019).

For the summer of 2003, the global temperature difference between factual and counterfactual simulations is 0.64 °C, while for the summer of 2010 the difference is 0.66 °C. From observations we know that the earth has experienced a global warming of approximately 0.7–0.8 °C between preindustrial times and 2010 (IPCC, 2018). Our modelled global warming, found through the difference between the factual and counterfactual simulations, thus represents this difference well, albeit with a slight underestimation.

3 Results

To illustrate our method, we provide two examples, namely the European heatwave of 2003 and the Russian heatwave of 2010. These events are considered the two strongest European heatwaves on record (Russo et al., 2014, 2015). In Sect. 3.3 we look deeper into the signal-to-noise ratio of each of the examples and how they compare to each other.

3.1 European heatwave 2003

The European summer of 2003 was exceptionally hot and exceptionally dry (Black et al., 2004; Schär et al., 2004; Stott et al., 2004). Two heatwaves occurred, a milder one in June and an extreme heatwave in August, with peak temperatures in France and Switzerland (Black et al., 2004; Schär et al., 2004; Trigo et al., 2005) but also affecting Portugal, northern Italy, western Germany, and the UK (Feudale and Shukla, 2011a; Muthers et al., 2017). Temperatures exceeded the 1961–1990 average by 2.3–12.5 °C, depending on loca-

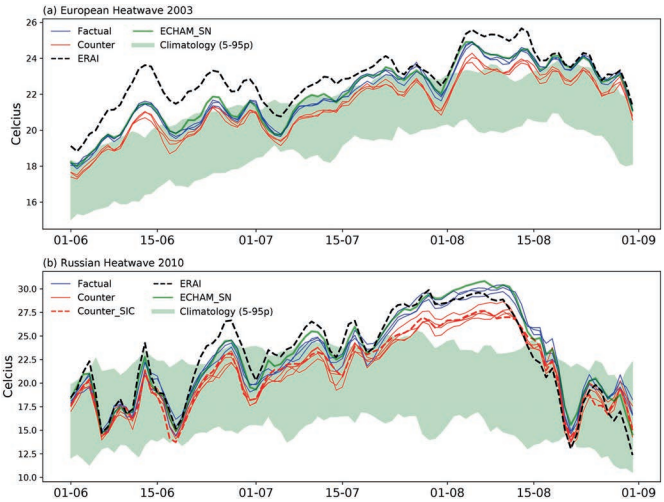

Figure 5. Daily mean temperature at 2 m height [°C] averaged over **(a)** Europe (35–50° N, 10° W–25° E) for summer 2003 and over **(b)** Russia (50–60° N, 35–55° E) for summer 2010 for the factual (blue), counterfactual (red), and ECHAM_SN (green) simulations and ERA-Interim (dashed black) reanalysis data. The climatology (green shaded area) is the 5th–95th ranked percentile range between 1985–2015 calculated with ECHAM_SN (Schubert-Frisius et al., 2017). The dashed red line in **(b)** shows the simulation with SIC changed in one of the counterfactual simulations (see text for details).

tion, without much cooling during the night (García-Herrera et al., 2010; Schär et al., 2004; Stott et al., 2004; Muthers et al., 2017). The 2003 summer was at that point in time not just the hottest on record (Bastos et al., 2014; Fink et al., 2004), it was the hottest summer in the past 500 years (Luterbacher et al., 2004). The consequences were devastating. Estimates account for 22 000–40 000 heat-related deaths, USD 12–14 billion in economic losses, 20 %–30 % decrease in net primary productivity (NPP), 5 %–10 % of Alpine glacier loss, and many more human-health-related issues due to increased surface ozone concentrations (Ciais et al., 2005; Fischer et al., 2007; García-Herrera et al., 2010).

Both the June and August heatwaves were caused by stationary anticyclonic circulations or blocking (Black et al., 2004). The first block formed in June, then broke and quickly reformed in July, which then caused the second heatwave in August (García-Herrera et al., 2010). However, the extreme temperatures cannot be explained by atmospheric blocking alone. Due to large precipitation deficits in spring that year, the heatwaves happened in very dry conditions. The lack of clouds and soil moisture caused latent heat transfer to turn into sensible heat transfer, which dramatically increased surface temperatures (Bastos et al., 2014; Ciais et al., 2005; Fischer et al., 2007; Fink et al., 2004; Miralles et al., 2014). It is considered highly unlikely that the 2003 European heatwaves would have reached the temperatures they did without climate change (Hannart et al., 2016; Schär et al., 2004; Stott et al., 2004). The probabilistic event attribution studies show an increased likelihood of the extreme temperatures from increased GHGs (Hannart et al., 2016; Schär et al., 2004; Stott et al., 2004). Other studies focused on the exceptionally high SSTs in the Mediterranean Sea and North Sea as a cause of reduced baroclinicity, providing an environment conducive to blocking (Black et al., 2004; Feudale and Shukla, 2011a, b). By applying the storyline approach, we can consider both causal factors together and shed some additional insight on this event. The dry spring leading up to the warm summer conditions was captured by initializing the simulations by 1 March at the latest.

In Fig. 5a, the daily evolution of the domain-averaged temperature at 2 m height for June–August for each of the ensemble members is plotted in comparison to the ECHAM_SN 5th–95th-percentile (1985–2005) climatology and ERA-Interim (Dee et al., 2011). The ECHAM_SN 2003 temperature is also plotted for reference and shows a strong coherence with the factual ensemble, confirming the appropriateness of using the ECHAM_SN climatology as a reference for our factual simulations. The first thing to note is that the factual and counterfactual ensembles evolve very similarly in time but (except for the third week of June) are well separated, by approximately 0.6 °C, indicating a high signal-to-noise ratio at daily resolution for the domain av-

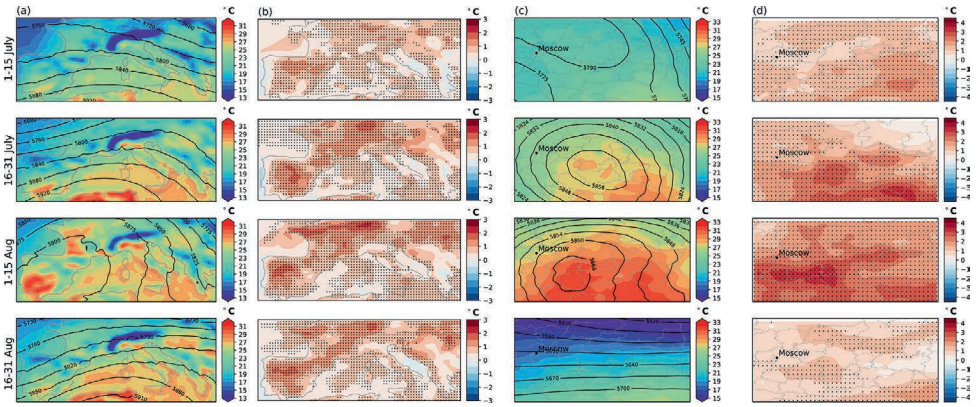

Figure 6. July and August divided into four half-month periods. Columns **(a)** and **(b)** show the European heatwave 2003, while columns **(c)** and **(d)** show the Russian heatwave 2010. In columns **(a)** and **(c)**, the factual geopotential height at z_{500} [m] is shown as black contour lines, while temperatures at 2 m height [°C] are shown as shaded fields. In columns **(b)** and **(d)**, the differences in 2 m temperature [°C] between the factual and counterfactual simulations are shown as shaded fields. Stippling shows where all the factual members are > 0.1 °C above all the counterfactual members for that grid point. Note that the Russian domain is smaller; therefore the stippling has a different spacing than in the European domain.

erage. This value of 0.6 °C is in line with the global-mean warming. ERA-Interim and the factual members show a strong correlation in time, although the ERA-Interim temperatures are higher especially in June and during the heatwave in the first half of August. The factual temperatures exceed the 95th percentile several times in June–August. In August, the exceedance lasts for almost 2 weeks, whereas in June it does so for approximately 1 week. The counterfactual temperatures are not quite so extreme; they exceed the 95th percentile only for a few days at a time in June and August. Nevertheless, it is clear that there would have been a European heatwave in 2003 even without climate change, albeit with less extreme temperatures. This analysis thus supports both of the perspectives on the event discussed earlier whilst providing a daily resolution of the climate change attribution.

The temperature differences between the factual and counterfactual ensembles are spatially nonuniform over Europe. In Fig. 6a the factual members' average of the 2 m temperature and of the geopotential height (z_{500}) show the meteorological situation averaged over half-month periods following García-Herrera et al. (2010). Figure 6b shows the local differences in 2 m temperatures between the counterfactual and factual ensemble averages. Stippling is added to each grid point where all the three factual members are at least 0.1 °C warmer than all the counterfactual members. There is strong local variance, especially during the heatwave in the first half of August, with differences of up to 2.5 °C. In the first period (1–15 July) the local differences are generally modest, except in northern Spain, where they reach 1.5–2 °C. In the second and third half-month periods (16–31 July, 1–15 August), the temperatures in the factual simulations can locally be up to 2–2.5 °C higher than in the counterfactual simulations, with the differences spread over a large area including Spain, Portugal, France, Germany, Hungary, and Romania. During the period 1–15 August, which according to Fig. 5a was the peak of the heatwave, the hottest area in Europe (Fig. 6a) is located in south-west France and southern Iberia. However the largest differences between the factual and counterfactual simulations (up to 2.5 °C) are found to the north of both of these regions, suggesting a shift in the peak temperature. In the second half of August, there are still some strong temperature differences visible over most of these regions, although the differences over western France have dampened.

As noted earlier, the dryness of the soil has been identified as an important contributing factor to the 2003 heatwave. Our interest here, however, is on whether the soil wetness differed between factual and counterfactual conditions. In Fig. 7a we see a very similar decline in soil wetness for both the factual and counterfactual ensemble members from May until the end of August. The counterfactual simulations start out with somewhat higher soil wetness than the factual simulations, but over the course of the summer the values of both sets of simulations move closer towards each other so that by August the ensembles are close together. Thus it does not appear that climate change had a first-order impact on soil wetness in this case.

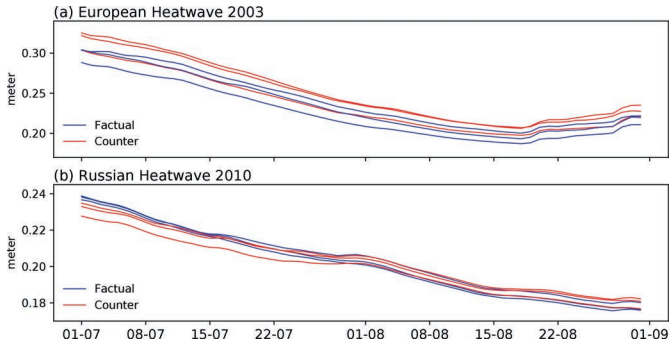

Figure 7. Average soil wetness in the root zone [m] averaged over Europe in 2003 and Russia in 2010 during July and August of each year. The factual simulations are shown in blue and the counterfactual simulations in red.

3.2 Russian heatwave 2010

In August 2010 western Russia was hit by an unprecedented heatwave caused by a large quasi-stationary anticyclonic circulation, or blocking (Galarneau et al., 2012; Grumm, 2011; Matsueda, 2011). It was a heatwave that broke all records such as temperature anomalies during both day and night, temporal duration, and spatial extent. The effect of soil wetness, or rather the lack thereof, on the magnitude of the temperatures was profound (Lau and Kim, 2012; Rasmijn et al., 2018; Wehrli et al., 2019; Bastos et al., 2014). The 2010 Russian heatwave is considered the most extreme heatwave in Europe on record (Russo et al., 2015). Approximately 50 000 lives were lost, 5000 km^2 forest burned, 25 % of the crop failed and over USD 15 billion worth of economic damage was recorded due to this heatwave (Barriopedro et al., 2011; Lau and Kim, 2012; Otto et al., 2012; Rasmijn et al., 2018). In some of the attribution studies, the heatwave was primarily attributed to internal variability as the dynamical situation strongly depended on the El Niño–Southern Oscillation (ENSO) being in a La Niña state (Dole et al., 2011; Russo et al., 2014; Schneidereit et al., 2012). However, the likelihood of the temperatures reaching such extreme values has also been assessed as being significantly exacerbated by climate change (Otto et al., 2012; Rahmstorf and Coumou, 2011). As with the previous example, the storyline approach can represent both of these perspectives. Moreover, it overcomes the limitation that the climate models used to perform probabilistic event attribution generally have trouble reproducing a blocking situation correctly (Trenberth and Fasullo, 2012; Watanabe et al., 2013).

In Fig. 5b, the daily evolution of the domain-averaged temperature at 2 m height for each of the ensemble members is shown in comparison to ECHAM_SN 2010, the ECHAM_SN 5th–95th-percentile climatological temperatures (1985–2015), and ERA-Interim. ERA-Interim temperatures correlate highly with the counterfactual members, though are somewhat higher at the end of June and beginning of July, and decline much more rapidly following the heatwave halfway through August. Starting after the second half of July, both the factual and counterfactual temperatures exceed the 95th-percentile climatological temperature, peak around 8 August, and return to climatological temperatures around 17 August. This analysis shows that this would have been an unprecedented event even without climate change. The differences between the factual and counterfactual temperatures during the core of the heatwave are noticeably higher (about 2 °C) than in the European heatwave 2003, as is the spread between the ensemble members. In contrast to the European case, the anthropogenic warming during the core of the heatwave is considerably higher than the global-mean warming. We attribute both aspects – the greatly enhanced anthropogenic warming and the larger internal variability – to the fact that the Russian domain is much farther inland than the European domain, and thus the blocking conditions cut off the influence of the SST forcing and allow a direct radiative effect of GHG increases (Wehrli et al., 2019). Note that western Russia is known for having large internal variability (Dole et al., 2011; Russo et al., 2014; Schneidereit et al., 2012), which is clearly apparent in our results. It is also the case that the Russian domain is smaller than the European domain by a factor of 3.4, which would furthermore tend to increase the variability in the domain-averaged temperature shown in Fig. 5.

The range of temperature differences between factual and counterfactual simulations reach values up to 4 °C locally, as seen in Fig. 6d. Note that the scale for the Russian heatwave reaches up to 4.5 °C, whereas the scale for the European heatwave reaches only 3 °C. In the first half-month period (1–15 July), when the heatwave had not yet started, the local temperature differences are between 0.5–2.5 °C, with the maximum differences in the south-east of the domain.

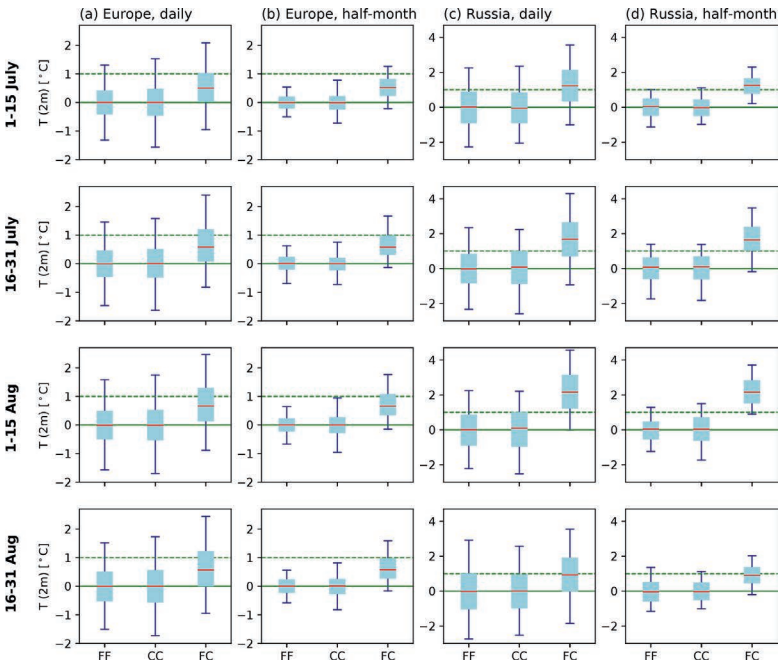

Figure 8. Distributions across grid points of differences between ensemble members in temperature at 2 m height [°C], separated into the four half-monthly periods. FF: differences between pairs of factual members; CC: differences between pairs of counterfactual members; FC: differences between pairs of factual and counterfactual members. The boxes represent the 25th-to-75th-percentile range of the distributions, the red lines represent the 50th percentiles (the median), and the blue bars indicate the 5th-to-95th-percentile range. The dashed horizontal line indicates 1 °C for reference. Columns **(a)** and **(b)** are for the European 2010 heatwave, and columns **(c)** and **(d)** for the Russian 2010 heatwave. Note the different vertical scales for the two events. Columns **(a)** and **(c)** show the differences in daily averages, and columns **(b)** and **(d)** show the differences in half-monthly averages.

The temperature differences are largest in the core of the block region, reaching up to 3.5 °C in the south-east in the second period (16–31 July) and up to 4 °C in the south, below Moscow, in the third period (1–15 August). The block broke in the fourth period (16–31 August) and resulted in a virtual elimination of the temperature difference. In contrast to the European heatwave 2003, here the biggest temperature differences between factual and counterfactual are found in the regions with the highest temperatures.

As with the European heatwave 2003, the differences in soil wetness do not appear to be of first-order importance to explain the temperature differences between the factual and counterfactual simulations. In Fig. 7b the soil wetness in the factual simulations is seen to decrease somewhat more rapidly than in the counterfactual, which could be due to the higher surface temperature and thus greater evaporation of soil moisture. However, the soil wetness values are overlapping and even cross each other in the beginning of August. These findings are in agreement with those of Hauser et al. (2016), who reproduced the Russian heatwave under 1960 conditions and found that the dry conditions occurred there too, thus concluding they found no direct link between the drought conditions and climate change. It must be emphasized that this is not to downplay in any way the impact of soil wetness on the event itself, which has been well established in the literature. It is only to indicate that the impact would have been there even without climate change.

3.3 Signal-to-noise analysis

The temperature differences found between the factual and counterfactual simulations are meaningful if they are outside of the internal variability within each ensemble. A different way of saying this is that the differences are meaningful if the two ensembles are distinguishable from each other. To assess

this in a statistical manner, temperature differences between pairs of factual members (FF), pairs of counterfactual members (CC), and factual–counterfactual pairs (FC) are plotted for each half-month period in Fig. 8. The FF and CC pairs have a median close to 0 and represent the noise level; in both cases there are three pairs (F1–F2, F2–F3, F3–F1; C1–C2, C2–C3, C3–C1). The FC pairs contain the signal; here there are nine pairs (F1–C1, F2–C2, F3–C3, F2–C1, F3–C2, F1–C3, F3–C1, F1–C2, F2–C3). Each box plot represents the distribution of 2 m temperature differences across the pairs and across all grid points. The half-monthly panels represent distributions of half-month-averaged values, and the daily panels represent distributions of daily values within the half-month period.

The daily differences for the European heatwave (Fig. 8a) show a median value of about 0.6 °C, irrespective of whether the time frame is during the heatwave itself or directly before or directly after it, consistent with Fig. 5a. Although these are not really probability distributions (since they include contributions from different locations within the domain), we can use the inter-quartile ranges as measures of signal and noise. The median difference for FC is above the 75th percentile of both CC and FF for daily values, giving confidence that our results are clearly above the noise level. Half-monthly time averages (Fig. 8b) produce nearly identical median values, but we see that the spread is much smaller, as expected. The 25th percentile of FC now lies above the 75th percentile of the CC and FF boxes.

The differences between CF and either FF or CC for the Russian heatwave (Fig. 8c and d) are clearly larger than for the European heatwave and in contrast to the European case vary substantially between the different periods. Consistent with Fig. 5b, in the periods outside of the core of the heatwave (1–15 July, 16–31 August) the median difference between FC is about 1 °C. Inside the core heatwave period (16–31 July, 1–15 August), however, the median difference is more like 2 °C, reaching 2.2 °C for 1–15 August. During this latter period the 5th-percentile whisker of half-monthly FC differences is above the 75th percentile of FF and CC, which is a very strong signal indeed. When looking at the results for individual members, the larger internal variability within the Russian domain (apparent also in Fig. 5b) is clearly visible (not shown), as compared with the European case.

4 Discussion and conclusion

We have presented a detailed description and assessment of a global spectrally nudged storyline methodology to quantify the role of known thermodynamic aspects of climate change in specific extreme weather events. In this methodology, the particular dynamical conditions leading to the event are taken as given, i.e. are regarded as random, and the attribution is therefore highly conditional. Thus, as with all such storyline approaches to extreme-event attribution, the effect of climate change on the occurrence likelihood of those dynamical conditions is not assessed. In that respect, this approach is complementary to the more widely used probabilistic event attribution. However, since most results of probabilistic event attribution appeal in any case to the known thermodynamic aspects of climate change, it can be argued that not much is lost in the storyline approach, yet much is gained by the specificity. This is especially the case for extreme events whose dynamical conditions are not well represented in climate models, e.g. blocking. Spectral nudging enables the reproduction of extreme events with their particular dynamical details, allowing the same dynamical events to be reproduced in simulations with different boundary conditions and thereby achieving a high signal-to-noise ratio of the climate change effect. The combination of both methods – global spectral nudging and the storyline method – thus presents a way to quantify, in great detail, the role of known thermodynamic aspects of climate change, together with the specific dynamical conditions, in selected extreme events which happened in the recent past. This can help reconcile the sometimes different perspectives on those events that appear in the literature (some emphasizing climate change, others emphasizing internal variability).

We illustrated the method by applying it to two extreme events that have been the subject of much study: the European heatwave of 2003 and the Russian heatwave of 2010. By using a small ensemble of both factual and counterfactual simulations, we were able to determine a noise level for our analysis. This revealed that the (conditional) signal of climate change is determinable at both daily timescales and local spatial scales. It follows that our methodology could be used to drive climate impact models and thus perform realistic stress-testing of resilience strategies. With regard to the two heatwave examples, our analysis revealed a striking contrast between the two events. In the European heatwave of 2003, the effect of climate change was to increase temperatures across Europe by about the global-mean warming level throughout the summer, and the heatwave was simply the dynamical event riding on top of that. In the Russian heatwave of 2010, in contrast, the effect of climate change was much higher than the global warming level and was particularly enhanced, approximately threefold, during the peak of the heatwave. We interpret this difference as reflecting the role of direct GHG radiative forcing, which can become apparent when air masses are cut off from marine influence. However, further analysis would be required to confirm this hypothesis.

It is not possible to make a direct comparison between our results and probabilistic attribution of these heatwaves because they are answering different questions, and the conditionalities are quite different. However, from a methodological perspective it is useful to contrast the *nature* of the attribution statements that can be made using the different methods. We do this in Table 2 for the case of the Russian 2010

Table 2. Example of attribution statements that are possible using the probabilistic and storyline approaches for the case of the 2010 Russian heatwave.

Probabilistic attribution (based on results from Otto et al., 2012)	Averaged over the Russian domain and over the month of July, temperatures in 2010 were 5 °C above the 1960s climatology, of which 4 °C was due to internal variability, and 1 °C was due to anthropogenic climate change. The heatwave represented a 1-in-33-year event, which was 3 times more likely than it would have been in the 1960s.
Storyline attribution (based on present results)	Averaged over the Russian domain, temperatures in 2010 steadily increased from the 1985–2015 climatology through the month of July until about 10 August, then rapidly returned to climatology. The domain-averaged heatwave reached 10 °C above the 1985–2015 climatology in early August, of which 8 °C was due to internal variability, and 2 °C was due to anthropogenic climate change. The anthropogenic component of the warming reached 4 °C in the region to the south of Moscow during the first half of August, where it exacerbated the already warm temperatures there.

heatwave. Having said that, there is a continuum between storyline and probabilistic approaches (Shepherd, 2016), and it is possible to imagine intermediate set-ups which would provide a seamless connection between event attribution and probabilistic weather prediction (NAS, 2016). These would need to involve large ensembles (to calculate conditional probabilities) and pay more attention to the self-consistency of how the counterfactual conditions are imposed. An example is the recent use of an operational subseasonal-to-seasonal prediction system, which involves modifying the atmospheric state and land surface conditions as well as the SSTs in generating the counterfactual (Wang et al., 2020).

The nudged global storyline method is an important step towards a holistic approach within the attribution of individual extreme events, which can quantify the role of both dynamical variability and known thermodynamic aspects of climate change and the interplay between them in great spatio-temporal detail. As shown by Wehrli et al. (2020), the method can easily be expanded to a larger number of storylines for both past and future. The method could also be applied to other extreme events affected thermodynamically by climate change such as tropical cyclones (Feser and Barcikowska, 2012). Our future applications are, therefore, intended to cover a wide variety of extreme events over the historical record.

Code and data availability. The ECHAM6.1 global atmospheric model is available from the Max Planck Institute for Meteorology (MPI-M) website: https://code.mpimet.mpg.de/projects/mpi-esm-users/files (last access: 15 January 2021) (Giorgetta et al., 2021). The CMIP6 historical simulation data are archived at the World Data Centre for Climate (WDCC): https://cera-www.dkrz.de/WDCC/ui/cerasearch/entry?acronym=RCM_CMIP6_Historical-HR (last access: 15 January 2021) (Schupfner, 2021). For analysis we have used the open-access Python packages.

Author contributions. LvG wrote the article, ran the simulations, and analysed their results. FF and TGS conceived the study and contributed to the writing and the interpretation of the results.

Competing interests. The authors declare that they have no conflict of interest.

Acknowledgements. We would like to thank Sebastian Rast from the Max Planck Institute for Meteorology (MPI-M) in Hamburg for his technical support in applying spectral nudging in the ECHAM6 model and Matthias Bittner and Wolfgang Müller from MPI-M for providing ECHAM6 CMIP6 data. Simulations were carried out on the MISTRAL supercomputer at the German Climate Computing Centre (DKRZ), with technical support from Irina Fast. This work is a contribution to the "Helmholtz Climate Initiative REKLIM" (Regional Climate Change), a joint research project of the Helmholtz Association of German Research Centres (HGF), as well as to the European Research Council advanced grant "Understanding the atmospheric circulation response to climate change" (grant no. 339390). The authors would like to thank Francis Zwiers and an anonymous reviewer for their thoughtful and constructive comments which helped improve the manuscript.

Financial support. This research has been supported by the European Research Council (grant no. 339390).

The article processing charges for this open-access publication were covered by a Research Centre of the Helmholtz Association.

Review statement. This paper was edited by Joaquim G. Pinto and reviewed by Francis Zwiers and one anonymous referee.

References

Barriopedro, D., Fischer, E. M., Luterbacher, J., Trigo, R., and Garcia-Herrera, R.: The Hot Summer of 2010: Redrawing the Temperature Record Map of Europe, Science, 332, 220–224, https://doi.org/10.1126/science.1201224, 2011.

Bastos, A., Gouveia, C. M., Trigo, R. M., and Running, S. W.: Analysing the spatio-temporal impacts of the 2003 and 2010 extreme heatwaves on plant productivity in Europe, Biogeosciences, 11, 3421–3435, https://doi.org/10.5194/bg-11-3421-2014, 2014.

Black, E., Blackburn, M., Harrison, G., Hoskins, B., and Methven, J.: Factors contributing to the summer 2003 European heatwave, Weather, 59, 217–223, https://doi.org/10.1256/wea.74.04, 2004.

Bony, S., Bellon, G., Klocke, D., Sherwood, S., Fermepin, S., and Denvil, S.: Robust direct effect of carbon dioxide on tropical circulation and regional precipitation, Nat. Geosci., 6, 447–451, https://doi.org/10.1038/ngeo1799, 2013.

Cattiaux, J., Vautard, R., Cassou, C., Yiou, P., Masson-Delmotte, V., and Codron, F.: Winter 2010 in Europe: A cold extreme in a warming climate, Geophys. Res. Lett., 37, L20704, https://doi.org/10.1029/2010GL044613, 2010.

Ciais, P., Reichstein, M., Viovy, N., Granier, A., Ogee, J., Allard, V., Aubinet, M., Buchmann, N., Bernhofer, C., Carrara, A., Chevallier, F., De Noblet, N., Friend, A. D., Friedlingstein, P., Grunwald, T., Heinesch, B., Keronen, P., Knohl, A., Krinner, G., Loustau, D., Manca, G., Matteucci, G., Miglietta, F., Ourcival, J. M., Papale, D., Pilegaard, K., Rambal, S., Seufert, G., Soussana, J. F., Sanz, M. J., Schulze, E. D., Vesala, T., and Valentini, R.: Europe-wide reduction in primary productivity caused by the heat and drought in 2003, Nature, 437, 529–533, https://doi.org/10.1038/nature03972, 2005.

Dee, D. P., Uppala, S. M., Simmons, A. J., Berrisford, P., Poli, P., Kobayashi, S., Andrae, U., Balmaseda, M. A., Balsamo, G., Bauer, P., Bechtold, P., Beljaars, A. C. M., van de Berg, L., Bidlot, J., Bormann, N., Delsol, C., Dragani, R., Fuentes, M., Geer, A. J., Haimberger, L., Healy, S. B., Hersbach, H., Holm, E. V., Isaksen, L., Kallberg, P., Kohler, M., Matricardi, M., McNally, A. P., Monge-Sanz, B. M., Morcrette, J. J., Park, B. K., Peubey, C., de Rosnay, P., Tavolato, C., Thepaut, J. N., and Vitart, F.: The ERA-Interim reanalysis: configuration and performance of the data assimilation system, Q. J. Roy. Meteorol. Soc., 137, 553–597, https://doi.org/10.1002/qj.828, 2011.

Deser, C., Terray, L., and Phillips, A. S.: Forced and Internal Components of Winter Air Temperature Trends over North America during the past 50 Years: Mechanisms and Implications, J. Climate, 29, 2237–2258, https://doi.org/10.1175/jcli-d-15-0304.1, 2016.

Dole, R., Hoerling, M., Perlwitz, J., Eischeid, J., Pegion, P., Zhang, T., Quan, X. W., Xu, T. Y., and Murray, D.: Was there a basis for anticipating the 2010 Russian heat wave?, Geophys. Res. Lett., 38, L06702, https://doi.org/10.1029/2010gl046582, 2011.

Feser, F. and Barcikowska, M.: The influence of spectral nudging on typhoon formation in regional climate models, Environ. Res. Lett., 7, 014024, https://doi.org/10.1088/1748-9326/7/1/014024, 2012.

Feudale, L. and Shukla, J.: Influence of sea surface temperature on the European heat wave of 2003 summer. Part I: an observational study, Clim. Dynam., 36, 1691–1703, https://doi.org/10.1007/s00382-010-0788-0, 2011a.

Feudale, L. and Shukla, J.: Influence of sea surface temperature on the European heat wave of 2003 summer. Part II: a modeling study, Clim. Dynam., 36, 1705–1715, https://doi.org/10.1007/s00382-010-0789-z, 2011b.

Fink, A. H., Brücher, T., Krüger, A., Leckebusch, G. C., Pinto, J. G., and Ulbrich, U.: The 2003 European summer heatwaves and drought–synoptic diagnosis and impacts, Weather, 59, 209–216, https://doi.org/10.1256/wea.73.04, 2004.

Fischer, E. M., Seneviratne, S. I., Vidale, P. L., Lüthi, D., and Schär, C.: Soil moisture – Atmosphere interactions during the 2003 European summer heat wave, J. Climate, 20, 5081–5099, https://doi.org/10.1175/jcli4288.1, 2007.

Galarneau, T. J., Hamill, T. M., Dole, R. M., and Perlwitz, J.: A Multiscale Analysis of the Extreme Weather Events over Western Russia and Northern Pakistan during July 2010, Mon. Weather Rev., 140, 1639–1664, https://doi.org/10.1175/mwr-d-11-00191.1, 2012.

García-Herrera, R., Díaz, J., Trigo, R. M., Luterbacher, J., and Fischer, E. M.: A review of the European summer heat wave of 2003, Crit. Rev. Environ. Sci. Technol., 40, 267–306, https://doi.org/10.1080/10643380802238137, 2010.

Giorgetta, M. A., Roeckner, E., Mauritsen, T., Bader, J., Crueger, T., Esch, M., Rast, S., Kornblueh, L., Schmidt, H., Kinne, S., Hohenegger, C., Möbis, B., Krismer, T., Wieners, K.-H., and Stevens, B.: ECHAM 6.1.00, available at: https://code.mpimet.mpg.de/projects/mpi-esm-users/files, last access: 15 January 2021.

Grumm, R. H.: The central European and Russian heat event of July–August 2010, B. Am. Meteorol. Soc., 92, 1285–1296, https://doi.org/10.1175/2011BAMS3174.1, 2011.

Hannart, A., Pearl, J., Otto, F. E. L., Naveau, P., and Ghil, M.: Causal Counterfactual Theory for the Attribution of Weather and Climate-Related Events, B. Am. Meteorol. Soc., 97, 99–110, https://doi.org/10.1175/bams-d-14-00034.1, 2016.

Hauser, M., Orth, R., and Seneviratne, S. I.: Role of soil moisture versus recent climate change for the 2010 heat wave in western Russia, Geophys. Res. Lett., 43, 2819–2826, https://doi.org/10.1002/2016gl068036, 2016.

Horton, D. E., Johnson, N. C., Singh, D., Swain, D. L., Rajaratnam, B., and Diffenbaugh, N. S.: Contribution of changes in atmospheric circulation patterns to extreme temperature trends, Nature, 522, 465–469, https://doi.org/10.1038/nature14550, 2015.

Hoskins, B. and Woollings, T.: Persistent extratropical regimes and climate extremes, Curr. Clim. Change Rep., 1, 115–124, https://doi.org/10.1007/s40641-015-0020-8, 2015.

Hurrell, J. W., Hack, J. J., Shea, D., Caron, J. M., and Rosinski, J.: A new sea surface temperature and sea ice boundary dataset for the Community Atmosphere Model, J. Climate, 21, 5145–5153, https://doi.org/10.1175/2008JCLI2292.1, 2008.

IPCC: Managing the Risks of Extreme Events and Disasters to Advance Climate Change Adaptation, in: A Special Report of Working Groups I and II of the Intergovernmental Panel on Climate Change, edited by: Field, C. B., Barros, V., Stocker, T. F., Qin, D., Dokken, D. J., Ebi, K. L., Mastrandrea, M. D., Mach, K. J., Plattner, G.-K., Allen, S. K., Tignor, M., and Midgley, P. M., Cambridge University Press, Cambridge, UK, and New York, NY, USA, 582 pp., 2012.

IPCC – Inter-governmental Panel on Climate Change: Summary for Policymakers, Global Warming of 1.5 °C: An IPCC Special Report on the Impacts of Global Warming of 1.5 °C Above Pre-industrial Levels and Related Global Greenhouse Gas Emission Pathways, in: the Context of Strengthening the Global Response to the Threat of Climate Change, Sustainable Development, and Efforts to Eradicate Poverty, edited by: Masson-Delmotte, V., Zhai, P., Pörtner, H.-O., Roberts, D., Skea, J., Shukla, P., Pirani, A., Moufouma-Okia, W., Péan, C., Pidcock, R., Connors, S., Matthews, J., Chen, Y., Zhou, X., Gomis, M., Lonnoy, E., Maycock, T., Tignor, M., and Watefield, T., World Meteorological Organization, Geneva, Switzerland, 32 pp., 2018.

Jeuken, A. B. M., Siegmund, P. C., Heijboer, L. C., Feichter, J., and Bengtsson, L.: On the potential of assimilating meteorological analyses in a global climate model for the purpose of model validation, J. Geophys. Res.-Atmos., 101, 16939–16950, https://doi.org/10.1029/96jd01218, 1996.

Kalnay, E., Kanamitsu, M., Kistler, R., Collins, W., Deaven, D., Gandin, L., Iredell, M., Saha, S., White, G., Woollen, J., Zhu, Y., Chelliah, M., Ebisuzaki, W., Higgins, W., Janowiak, J., Mo, K. C., Ropelewski, C., Wang, J., Leetmaa, A., Reynolds, R., Jenne, R., and Joseph, D.: The NCEP/NCAR 40-year reanalysis project, B. Am. Meteorol. Soc., 77, 437–471, https://doi.org/10.1175/1520-0477(1996)077<0437:Tnyrp>2.0.Co;2, 1996.

Kim, J. E. and Hong, S. Y.: A Global Atmospheric Analysis Dataset Downscaled from the NCEP-DOE Reanalysis, J. Climate, 25, 2527–2534, https://doi.org/10.1175/jcli-d-11-00534.1, 2012.

Lau, W. K. M. and Kim, K. M.: The 2010 Pakistan Flood and Russian Heat Wave: Teleconnection of Hydrometeorological Extremes, J. Hydrometeorol., 13, 392–403, https://doi.org/10.1175/jhm-d-11-016.1, 2012.

Lloyd, E. A. and Oreskes, N.: Climate Change Attribution: When Is It Appropriate to Accept New Methods?, Earths Future, 6, 311–325, https://doi.org/10.1002/2017ef000665, 2018.

Lloyd, E. A. and Shepherd, T. G.: Environmental catastrophes, climate change, and attribution, Ann. NY Acad. Sci., 1469, 105–124, https://doi.org/10.1111/nyas.14308, 2020.

Luterbacher, J., Dietrich, D., Xoplaki, E., Grosjean, M., and Wanner, H.: European seasonal and annual temperature variability, trends, and extremes since 1500, Science, 303, 1499–1503, https://doi.org/10.1126/science.1093877, 2004.

Matsueda, M.: Predictability of Euro-Russian blocking in summer of 2010, Geophys. Res. Lett., 38, L06801, https://doi.org/10.1029/2010gl046557, 2011.

Meinshausen, M., Smith, S. J., Calvin, K., Daniel, J. S., Kainuma, M. L. T., Lamarque, J. F., Matsumoto, K., Montzka, S. A., Raper, S. C. B., Riahi, K., Thomson, A., Velders, G. J. M., and van Vuuren, D. P. P.: The RCP greenhouse gas concentrations and their extensions from 1765 to 2300, Climatic Change, 109, 213–241, https://doi.org/10.1007/s10584-011-0156-z, 2011.

Meredith, E. P., Semenov, V. A., Maraun, D., Park, W., and Chernokulsky, A. V.: Crucial role of Black Sea warming in amplifying the 2012 Krymsk precipitation extreme, Nat. Geosci., 8, 615–619, https://doi.org/10.1038/ngeo2483, 2015.

Miguez-Macho, G., Stenchikov, G. L., and Robock, A.: Spectral nudging to eliminate the effects of domain position and geometry in regional climate model simulations, J. Geophys. Res.-Atmos., 109, D13104, https://doi.org/10.1029/2003jd004495, 2004.

Miralles, D. G., Teuling, A. J., van Heerwaarden, C. C., and Vilà-Guerau de Arellano, J.: Mega-heatwave temperatures due to combined soil desiccation and atmospheric heat accumulation, Nat. Geosci., 7, 345–349, https://doi.org/10.1038/ngeo2141, 2014.

Müller, W. A., Jungclaus, J. H., Mauritsen, T., Baehr, J., Bittner, M., Budich, R., Bunzel, F., Esch, M., Ghosh, R., Haak, H., Ilyina, T., Kleine, T., Kornblueh, L., Li, H., Modali, K., Notz, D., Pohlmann, H., Roeckner, E., Stemmler, I., Tian, F., and Marotzke, J.: A Higher-resolution Version of the Max Planck Institute Earth System Model (MPI-ESM1.2-HR), J. Adv. Model. Earth Syst., 10, 1383–1413, https://doi.org/10.1029/2017ms001217, 2018.

Muthers, S., Laschewski, G., and Matzarakis, A.: The Summers 2003 and 2015 in South-West Germany: Heat Waves and Heat-Related Mortality in the Context of Climate Change, Atmosphere, 8, 224, https://doi.org/10.3390/atmos8110224, 2017.

NAS – National Academies of Sciences Engineering and Medicine: Attribution of Extreme Weather Events in the Context of Climate Change, The National Academies Press, Washington, D.C., https://doi.org/10.17226/21852, 2016.

Otto, F. E. L.: Attribution of Weather and Climate Events, Annu. Rev. Environ. Resour., 42, https://doi.org/10.1146/annurev-environ-102016-060847, 627–646, 2017.

Otto, F. E. L., Massey, N., van Oldenborgh, G. J., Jones, R. G., and Allen, M. R.: Reconciling two approaches to attribution of the 2010 Russian heat wave, Geophys. Res. Lett., 39, L04702, https://doi.org/10.1029/2011gl050422, 2012.

Patricola, C. M. and Wehner, M. F.: Anthropogenic influences on major tropical cyclone events, Nature, 563, 339–346, https://doi.org/10.1038/s41586-018-0673-2, 2018.

Pearl, J. and Mackenzie, D.: The book of Why: The new science of cause and effect, Basic Books, New York, 2018.

Pfahl, S., O'Gorman, P. A., and Fischer, E. M.: Understanding the regional pattern of projected future changes in extreme precipitation, Nat. Clim. Change, 7, 423–427, https://doi.org/10.1038/nclimate3287, 2017.

Rahmstorf, S. and Coumou, D.: Increase of extreme events in a warming world, P. Natl. Acad. Sci. USA, 108, 17905–17909, https://doi.org/10.1073/pnas.1101766108, 2011.

Rasmijn, L. M., van der Schrier, G., Bintanja, R., Barkmeijer, J., Sterl, A., and Hazeleger, W.: Future equivalent of 2010 Russian heatwave intensified by weakening soil moisture constraints, Nat. Clim. Change, 8, 381–385, https://doi.org/10.1038/s41558-018-0114-0, 2018.

Rayner, N. A., Brohan, P., Parker, D. E., Folland, C. K., Kennedy, J. J., Vanicek, M., Ansell, T. J., and Tett, S. F. B.: Improved Analyses of Changes and Uncertainties in Sea Surface Temperature Measured In Situ since the Mid-Nineteenth Century: The HadSST2 Dataset, J. Climate, 19, 446–469, https://doi.org/10.1175/jcli3637.1, 2006.

Reick, C. H., Raddatz, T., Brovkin, V., and Gayler, V.: Representation of natural and anthropogenic land cover change in MPI-ESM, J. Adv. Model. Earth Syst., 5, 459–482, https://doi.org/10.1002/jame.20022, 2013.

Russo, S., Dosio, A., Graversen, R. G., Sillmann, J., Carrao, H., Dunbar, M. B., Singleton, A., Montagna, P., Barbola, P., and Vogt, J. V.: Magnitude of extreme heat waves in present climate and their projection in a warming world, J. Geophys. Res.-Atmos., 119, 12500–12512, https://doi.org/10.1002/2014jd022098, 2014.

Russo, S., Sillmann, J., and Fischer, E. M.: Top ten European heatwaves since 1950 and their occurrence in the coming decades, Environ. Res. Lett., 10, 124003, https://doi.org/10.1088/1748-9326/10/12/124003, 2015.

Schär, C., Frei, C., Lüthi, D., and Davies, H. C.: Surrogate climate-change scenarios for regional climate models, Geophys. Res. Lett., 23, 669–672, https://doi.org/10.1029/96GL00265, 1996.

Schär, C., Vidale, P. L., Lüthi, D., Frei, C., Häberli, C., Liniger, M. A., and Appenzeller, C.: The role of increasing temperature variability in European summer heatwaves, Nature, 427, 332–336, https://doi.org/10.1038/nature02300, 2004.

Schneider, D. P., Deser, C., and Okumura, Y.: An assessment and interpretation of the observed warming of West Antarctica in the austral spring, Clim. Dynam., 38, 323–347, https://doi.org/10.1007/s00382-010-0985-x, 2012.

Schneidereit, A., Schubert, S., Vargin, P., Lunkeit, F., Zhu, X. H., Peters, D. H. W., and Fraedrich, K.: Large-Scale Flow and the Long-Lasting Blocking High over Russia: Summer 2010, Mon. Weather Rev., 140, 2967–2981, https://doi.org/10.1175/mwr-d-11-00249.1, 2012.

Schubert-Frisius, M., Feser, F., von Storch, H., and Rast, S.: Optimal Spectral Nudging for Global Dynamic Downscaling, Mon. Weather Rev., 145, 909–927, https://doi.org/10.1175/mwr-d-16-0036.1, 2017.

Schupfner, M.: CMIP6 Scenario MIP DKRZ MPI-ESM1-2-HR historical – RCM-forcing data, available at: https://cera-www.dkrz.de/WDCC/ui/cerasearch/entry?acronym=RCM_CMIP6_Historical-HR, last access: 15 January 2021.

Scinocca, J. F., Kharin, V. V., Jiao, Y., Qian, M. W., Lazare, M., Solheim, L., Flato, G. M., Biner, S., Desgagne, M., and Dugas, B.: Coordinated Global and Regional Climate Modeling, J. Climate, 29, 17–35, https://doi.org/10.1175/jcli-d-15-0161.1, 2015.

Screen, J. A. and Simmonds, I.: Increasing fall-winter energy loss from the Arctic Ocean and its role in Arctic temperature amplification, Geophys. Res. Lett., 37, L16707, https://doi.org/10.1029/2010GL044136, 2010.

Shepherd, T. G.: Dynamics, stratospheric ozone, and climate change, Atmos.-Ocean, 46, 117–138, https://doi.org/10.3137/ao.460106, 2008.

Shepherd, T. G.: Atmospheric circulation as a source of uncertainty in climate change projections, Nat. Geosci., 7, 703–708, https://doi.org/10.1038/ngeo2253, 2014.

Shepherd, T. G.: A Common Framework for Approaches to Extreme Event Attribution, Curr. Clim. Change Rep., 2, 28–38, https://doi.org/10.1007/s40641-016-0033-y, 2016.

Stevens, B., Giorgetta, M., Esch, M., Mauritsen, T., Crueger, T., Rast, S., Salzmann, M., Schmidt, H., Bader, J., Block, K., Brokopf, R., Fast, I., Kinne, S., Kornblueh, L., Lohmann, U., Pincus, R., Reichler, T., and Roeckner, E.: Atmospheric component of the MPI-M Earth System Model: ECHAM6, J. Adv. Model. Earth Syst., 5, 146–172, https://doi.org/10.1002/jame.20015, 2013.

Stott, P. A., Stone, D. A., and Allen, M. R.: Human contribution to the European heatwave of 2003, Nature, 432, 610–614, https://doi.org/10.1038/nature03089, 2004.

Stott, P. A., Christidis, N., Otto, F. E. L., Sun, Y., Vanderlinden, J. P., van Oldenborgh, G. J., Vautard, R., von Storch, H., Walton, P., Yiou, P., and Zwiers, F. W.: Attribution of extreme weather and climate-related events, Wiley Interdisciplin. Rev. – Clim. Change, 7, 23–41, https://doi.org/10.1002/wcc.380, 2016.

Trenberth, K. E. and Fasullo, J. T.: Climate extremes and climate change: The Russian heat wave and other climate extremes of 2010, J. Geophys. Res.-Atmos., 117, D17103, https://doi.org/10.1029/2012jd018020, 2012.

Trenberth, K. E., Fasullo, J. T., and Shepherd, T. G.: Attribution of climate extreme events, Nat. Clim. Change, 5, 725–730, https://doi.org/10.1038/nclimate2657, 2015.

Trigo, R. M., García-Herrera, R., Díaz, J., Trigo, I. F., and Valente, M. A.: How exceptional was the early August 2003 heatwave in France?, Geophys. Res. Lett., 32, L10701, https://doi.org/10.1029/2005gl022410, 2005.

van der Wiel, K., Selten, F. M., Bintanja, R., Blackport, R., and Screen, J. A.: Ensemble climate-impact modelling: extreme impacts from moderate meteorological conditions, Environ. Res. Lett., 15, 034050, https://doi.org/10.1088/1748-9326/ab7668, 2020.

van Niekerk, A., Shepherd, T. G., Vosper, S. B., and Webster, S.: Sensitivity of resolved and parametrized surface drag to changes in resolution and parametrization, Q. J. Roy. Meteorol. Soc., 142, 2300–2313, https://doi.org/10.1002/qj.2821, 2016.

Vautard, R., Yiou, P., Otto, F., Stott, P., Christidis, N., Van Oldenborgh, G. J., and Schaller, N.: Attribution of human-induced dynamical and thermodynamical contributions in extreme weather events, Environ. Res. Lett., 11, 114009, https://doi.org/10.1088/1748-9326/11/11/114009, 2016.

von Storch, H., Langenberg, H., and Feser, F.: A spectral nudging technique for dynamical downscaling purposes, Mon. Weather Rev., 128, 3664–3673, https://doi.org/10.1175/1520-0493(2000)128<3664:Asntfd>2.0.Co;2, 2000.

von Storch, H., Cavicchia, L., Feser, F., and Li, D. L.: The Concept of Large-Scale Conditioning of Climate Model Simulations of Atmospheric Coastal Dynamics: Current State and Perspectives, Atmosphere, 9, 337, https://doi.org/10.3390/atmos9090337, 2018.

Waldron, K. M., Paegle, J., and Horel, J. D.: Sensitivity of a spectrally filtered and nudged limited-area model to outer model options, Mon. Weather Rev., 124, 529–547, https://doi.org/10.1175/1520-0493(1996)124<0529:Soasfa>2.0.Co;2, 1996.

Wallace, J. M., Fu, Q., Smoliak, B. V., Lin, P., and Johanson, C. M.: Simulated versus observed patterns of warming over the extratropical Northern Hemisphere continents during the cold season, P. Natl. Acad. Sci. USA, 109, 14337–14342, https://doi.org/10.1073/pnas.1204875109, 2012.

Wang, G., Hope, P., Lim, E. P., Hendon, H. H., and Arblaster, J. M.: An initialized attribution method of extreme

events on subseasonal to seasonal time-scales, J. Climate, https://doi.org/10.1175/JCLI-D-19-1021.1, in press, 2020.

Watanabe, M., Shiogama, H., Imada, Y., Mori, M., Ishii, M., and Kimoto, M.: Event attribution of the August 2010 Russian heat wave, Scient. Online Lett. Atmos., 9, 65–68, https://doi.org/10.2151/sola.2013-015, 2013.

Wehrli, K., Guillod, B. P., Hauser, M., Leclair, M., and Seneviratne, S. I.: Identifying Key Driving Processes of Major Recent Heat Waves, J. Geophys. Res.-Atmos., 124, 11746–11765, https://doi.org/10.1029/2019JD030635, 2019.

Wehrli, K., Hauser, M., and Seneviratne, S. I.: Storylines of the 2018 Northern Hemisphere heatwave at pre-industrial and higher global warming levels, Earth Syst. Dynam., 11, 855–873, https://doi.org/10.5194/esd-11-855-2020, 2020.

Yoshimura, K. and Kanamitsu, M.: Dynamical global downscaling of global reanalysis, Mon. Weather Rev., 136, 2983–2998, https://doi.org/10.1175/2008mwr2281.1, 2008.

B

Paper nr. 2: A storyline attribution of the 2011/2012 drought in Southeastern South America

A storyline attribution of the 2011/2012 drought in Southeastern South America

Linda van Garderen[1] **and Julia Mindlin**[2,3,4]

[1]*Institute of Coastal Systems - Analysis and Modelling, Helmholtz-Zentrum Hereon, Geesthacht, Germany*
[2]*Departamento de Ciencias de la Atmósfera y los Océanos, Facultad de Ciencias Exactas y Naturales, Universidad de Buenos Aires, Buenos Aires, Argentina*
[3]*Centro de Investigaciones del Mar y la Atmósfera, Consejo Nacional de Investigaciones Científicas y Técnicas, Universidad Nacional de Buenos Aires, Buenos Aires, Argentina*
[4]*Instituto Franco Argentino sobre estudios de Clima y sus impactos (IFAECI-UMI3351), Centre National de la Recherche Scientifque, Buenos Aires, Argentina*

Introduction

Often it is assumed that increased dryness will lead to increased droughts, the same for wetness and floods. Dryness refers to the climatological hydrological state of a region, whereas drought refers to an extreme event. However, in some regions, climate change is expected to increase both wetness *and* the intensity of droughts (Ault, 2020).

Southeastern South America (SESA) is a region of South America centred in the La Plata Basin, which includes Uruguay, the northeast of Argentina, the southern tip of Brazil and the southeastern tip of Paraguay. The climate in SESA experienced a pronounced wetting during the second half of the twentieth century. The regional precipitation trends are among the largest regional trends in the world (Vera and Díaz, 2015). This includes both an increase in mean annual rainfall (Doyle *et al*., 2011) and the frequency of extreme rainfall events (Penalba and Robledo, 2010). However, the SESA region also suffers from regular droughts, approximately every 5–10 years, which are part of the regional climate and are to a large extent associated with strong La Niña events (Grimm *et al*., 2000). Both short-term (3 months) and long-term (10–12 months) droughts impact SESA; the first affecting the agricultural sector and the second the water supplies.

Two examples of exceptionally severe droughts, in both extent and intensity, occurred during summer 1988/1989 and summer 2008/2009. In Uruguay, the 2008/2009 drought caused hydropower production (which normally accounts for roughly 80% of the national energy supply) to plummet to 20%. In Argentina, that same drought reduced grain production by 39%, and an estimated 1.5 million livestock were lost (Peterson and Baringer, 2009). The extent of agricultural impacts depends on the timing of each drought. Soybean and corn production will be hampered if a drought occurs in summer (December–February), whereas wheat is more sensitive to precipitation deficiency in spring (October–November). For this reason, shorter droughts may have equivalent impacts on crop loss as more persistent droughts if they occur during critical growth periods. The 2011/2012 summer drought is an example of such a short but devastating event, with damages to corn and soybean production running up to USD 2.5 billion (Sgroi *et al*., 2021). Since the strongest climate change signal in SESA is an increase in mean precipitation, drought impacts in this region have not received as much attention as might be needed for adaptation. However, one of the few studies available for SESA (Penalba and Rivera, 2013) showed that the frequency, duration and severity of these droughts are expected to increase under future climate scenarios. Thus, understanding the influence of a warmer climate on droughts in SESA is of clear societal relevance.

Drought attribution typically relies on statistical approaches that focus on changes in frequency, duration and severity. These aspects are essential and relevant, but the approaches struggle with large uncertainties. Such issues often are connected to our limited knowledge of climate change effects on dynamics and on the variability related to droughts in the present climate (Shepherd, 2014). Moreover, to allow for statistical significance, these methods depend on grouping similar events, resulting in the blurring-out of important details.

Conditional attribution–the attribution of the thermodynamic part of weather events–takes the uncertainties connected to the dynamics out of the equation. With spectrally nudged storylines (introduced in the next section), we can simulate historical events under different climatological backgrounds. Consequently, the method allows for specific event attribution of aspects we have physical understanding of, with limited loss of detail and without having to deal with uncertainties related to changes in frequency or duration (Shepherd *et al*., 2018; van Garderen *et al*., 2021).

In this study, we look at the effect of climate change on the thermodynamics of the 2011/2012 SESA drought. We focus on the differences between the storylines to conditionally attribute the event and subsequently place the results in climatological context.

Data

To produce our simulations, we use the ECHAM6 atmospheric model (Stevens *et al*., 2013) with T255 horizontal spectral resolution and 95 vertical levels (T255L95). This is the atmospheric component of the MPI-M coupled model (Tebaldi *et al*., 2021) used in the sixth coupled model intercomparison project (CMIP6). Boundary conditions such as sea surface temperature (SST) and sea ice concentration are prescribed using NCEP R1 reanalysis data (Kalnay *et al*., 1996). We spectrally nudge the large-scale free atmosphere of ECHAM6 with the divergence and vorticity from the NCEP R1 reanalysis data. Since we nudge in spectral space, we can use NCEP R1 reanalysis to nudge wavelengths in ECHAM6 that represent patterns of approximately 1000km and larger (Schubert-Frisius *et al*., 2017). Moreover, NCEP R1 captures the dynamical conditions of the drought well (see Figure 1). The 1948–2015 spectrally nudged simulation (ECHAM_SN) is used throughout this

Funding LvG received funding from Helmholtz-Zentrum Hereon and JM received funding from Universidad de Buenos Aires.

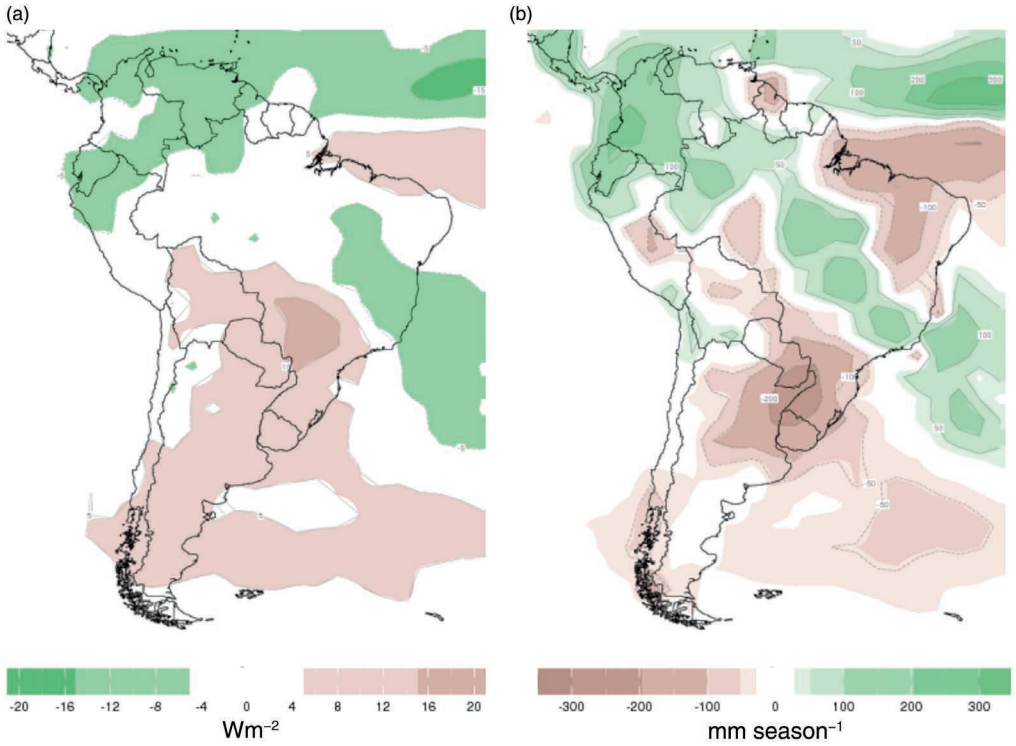

Figure 1. Drought characterisation. Seasonal anomalies with respect to the 1979–2020 climatological average over November–January of (a) outgoing longwave radiation (Wm^{-2}) (b) precipitation ($mm\,season^{-1}$). The data are from the NOAA NCEP Climate Prediction Center and were plotted using https://iridl.ldeo.columbia.edu/maproom/ (International Research Institute for Climate and Society, Columbia University, New York, USA).

study to compute climatology (Schubert-Frisius *et al*., 2017). We compare our precipitation results with Global Precipitation Climatology Centre (GPCC) observations (Schneider and Fuchs, 2008), and compare both the temperature and precipitation results with ERA5 reanalysis (Hersbach *et al*., 2020).

Spectrally nudged storylines

Spectral nudging has been applied in regional models for a wide range of extreme weather event research (Feser and von Storch, 2008; von Storch *et al*., 2018). We apply the spectral nudging technique to a global model and use this setup to create three storylines: (i) a world without climate change (counterfactual), (ii) the world as we know it (factual) and (iii) a world warmed by 2 degC above pre-industrial (plus2).

The factual and counterfactual simulations are according to van Garderen *et al*. (2021). The plus2 storyline is based on the same principle, but uses different SST and greenhouse gas (GHG) levels. The ssp585 scenario is based on the representative concentration pathways 8.5 global forcing in combination with the shared socioeconomic pathway (ssp) number five; both are simulating a future with high-end climate forcing (O'Neill *et al*., 2014). The 2m temperature (T2m) in CMIP6 MPI-ESM ssp585 scenario simulations exceed 2 degC of global warming (with respect to pre-industrial) between 2044 and 2053. That time period is then used to create an SST warming pattern and to set the GHG levels accordingly. Land use is kept equal between the storylines to ensure conditional attribution of global warming aspects only. For each of the three different storylines, we simulated three members each of 5 years (2010–2014). The average global T2m in the counterfactual storyline is 13.60°C; in the factual storylines, 14.28°C and in the plus2 storyline, 15.15°C.

2011/2012 SESA drought

Despite the 2011/2012 SESA drought having a short 3-month duration, neither as severe nor as persistent as, for example, the 2008/2009 drought, the timing of the event during crop-sensitive months caused large yield losses. The November 2011–February 2012 Standardized Precipitation Index in the Argentinian part of SESA indicates moderate to extreme drought conditions. The 3-month Palmer Drought Severity Index, for the same period and region, indicates a severe to extreme drought event (CREAN, 2017).

The dynamic situation, including La Niña and an intensified South Atlantic Convergence Zone (SACZ), favoured dry conditions. The event started in December 2011, during the second consecutive summer with a La Niña. The 2-year La Niña event of 2010–2012 was one of the strongest such events on record and caused extreme weather across the world (Blunden and Arndt, 2012). In South America, positive El Niño-Southern Oscillation (ENSO) phases (i.e. El Niño) are characterised by increased precipitation anomalies and negative ENSO phases by reduced precipitation anomalies (Grimm *et al*., 2000). The influence of La Niña on precipitation is strongest during the spring and summer following the event. Moreover, the SACZ intensified during the late spring–early summer season (NDJ) of 2011/2012, as shown using NCEP

R1 data in Figure 1(a) (negative outgoing longwave radiation anomalies indicating increased cloudiness). An intensified SACZ favours subsidence and clear sky conditions over SESA, hindering precipitation and increasing incoming shortwave radiation. Therefore, the state of the SACZ leads to anomalously high temperatures and dry conditions (Figure 1b). The atmospheric dynamical conditions for these types of droughts are well understood and explain a significant fraction of the summer variability (Cerne and Vera, 2011). It is reasonable to expect events of this kind in the near future as La Niña events combined with an active SACZ are part of the local climatology (Cerne and Vera, 2011).

In Figure 2(a), we show a domain average time series of T2m for each storyline, with ECHAM_SN climatology and ERA5 reanalysis (Hersbach *et al*., 2020) for comparison. The temperatures between the three storylines evolve comparably but are clearly separated in magnitude, revealing a strong climate change signal. The factual temperatures do not exceed the ECHAM_SN (1981–2010) climatological 95th percentile, except for two instances in February. The plus2 storyline, however, peaks beyond the 95th percentile nearly every 6–12 days, which is about three times more often than the factual storylines. The November to February average temperature difference between counterfactual and factual is 1.0 degC; between factual and plus2, 1.4 degC and between counterfactual and plus2, 2.4 degC, which is in line with the mean global warming over land. There is strong intra-seasonal variability in the daily temperature signal (10- to 90-day period oscillations) with particularly strong and significant 10- to 15-day variability. Such variability has been found in various summer seasons that were dominated by an active SACZ (Cerne *et al*., 2007; Cerne and Vera, 2011).

In Figure 2(b), we show the domain average of daily total precipitation for the three storylines, climatology and ERA5 reanalysis. For daily and cumulative precipitation, the results match well with both ERA5 and GPCC, up until 10 January. Following that period, the timing of precipitation events remains well-simulated; however, there is some mismatching of peak precipitation volume. For this reason, there is an overestimation in cumulative precipitation starting in the second half of January and throughout February. Just like temperature, the precipitation events can be explained by the intra-seasonal variability, where Rossby wave activity forces pulses of diagonally aligned precipitation events (van der Wiel *et al*., 2015) controlling the wet and dry conditions over the SACZ and SESA regions, respectively (Nogués-Paegle and Mo, 1997). However, there is no apparent climate change signal between storylines as there is considerable overlap in total precipitation. In Figure 2(c), the cumulative precipitation of the different storylines, the climatological background and ERA5 reanalysis, confirms the lack of climate change signal given the dynamic situation. It was a dry season in all storylines, with precipitation well below the climatological mean for December and January. In other words, the drought would have been there, with or without climate change.

The potential evapotranspiration (PET) according to Thornthwaite (1948), as shown in Figure 3, directly reflects the impact of increased temperatures between the storylines. Such increased temperatures cause a deficit in water vapour pressure, which in turn increases the PET. Higher PET values can be interpreted as a higher risk of drought, as the soil loses an increased amount of moisture to the atmosphere. In SESA, the PET peaks in January with values around 14cm for counterfactual, 15cm for factual and 17cm for plus2. Between factual and counterfactual, the largest difference of 1.2cm is in February. The largest difference between plus2 and factual, 2cm, and plus2 and counterfactual, 3cm, is in January. The highest difference in PET is thus found in the months with the largest PET values.

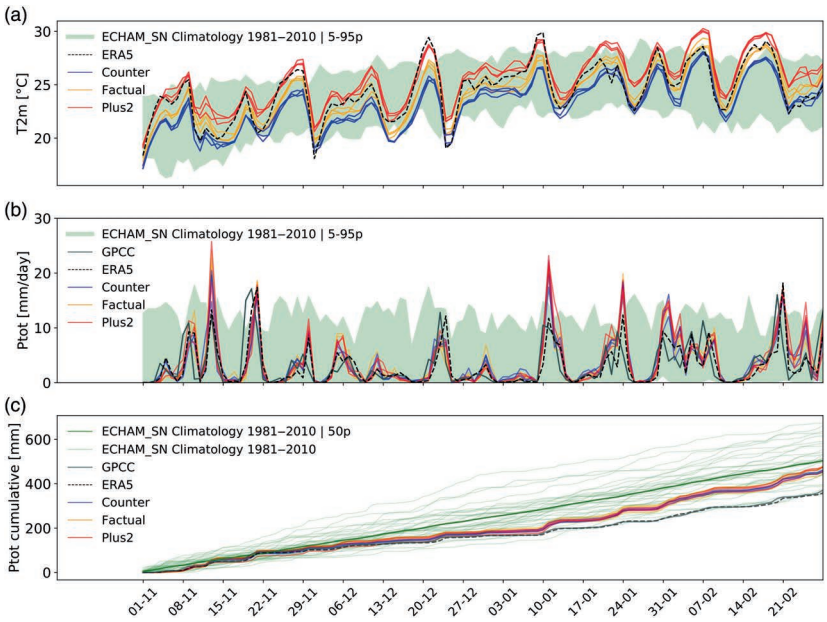

Figure 2. (a) Daily 2m temperature (T2m) averaged over SESA from November 2011 until February 2012 for counterfactual, factual and plus2 storylines, climatology 1981–2010 5th–95th percentile and ERA5 reanalysis (°C), (b) same as (a), but for daily total precipitation over SESA (mm day^{-1}), (c) daily cumulative total precipitation over SESA (mm) for counterfactual, factual and plus2 storylines, climatology is taken from yearly ECHAM_SN values from 1981 to 2010 (Schubert-Frisius et al., 2017). ERA5 reanalysis for comparison.

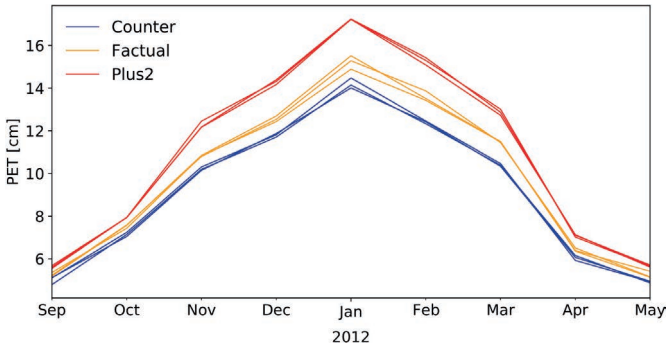

Figure 3. Monthly potential evapotranspiration (PET) (cm) over SESA according to Thornthwaite from September 2011 until April 2012.

In Figure 4, the half-monthly averaged water budget (WB) for the factual, factual minus counterfactual, plus2 minus factual and plus2 minus counterfactual, shows the difference of input (precipitation) minus output (evapotranspiration) between the storylines. Especially in January, there are pockets of robust signal (stippling), meaning a true split between the members of each world, for both reduced and increased WB. Nonetheless, in the WB, the effect of increased T2m and PET is not visible on a regional scale, as precipitation shows locally varying patterns. It is surprising that with increased temperatures and PET, in combination with an equal volume of precipitation, the WB is not showing a clearer drought severity change between the different storylines.

Dryness in SESA

To place the 2011/2012 SESA drought in a hydroclimatological context, we use the Budyko framework (Budyko, 1951). The Budyko framework provides physical insight on the climatological dryness or wetness of a specific region by evaluating both the atmospheric demand and water balance. The Budyko graph (Figure 5) could be interpreted as a hydrological supply-and-demand graph. The atmospheric water 'demand' on the *x*-axis is the Budyko aridity index ($\varphi = (R/\lambda)/P$, where R is net surface radiation, λ is latent heat of vaporisation ($2.45 \times 10^6 Jkg^{-1}$) and P is precipitation). The water 'supply' on the y-axis is the balance between precipitation and evapotranspiration (E/P). E/P is limited to 1 (marked with a horizontal black line), as income (P) limits outcome (E). Above the supply limit, other sources of water such as surface and groundwater are evaporated.

In Figure 5, we present a Budyko graph that shows the hydrological state of SESA's climate for the counterfactual, factual and plus2 storylines. In the period between 2010 and 2014, SESA becomes slightly more humid in warmer storylines (round markers, average of three members, each 5 years). The plus2 storyline has increased wetness due to a decrease of E/P, meaning a larger water availability. Coincidently, there is a decrease in the aridity index, meaning the precipitation increase (i.e. plus2-counter 2010–2014 is 66mm) is larger than the change in atmospheric water demand (i.e. plus2-counter 2010–2014 is 52mm). This places the plus2 storyline left and below the counter and factual storylines (labelled with a grey arrow), as was also found by Zaninelli *et al.* (2019). The 2011/2012 hydrological year (June 2011–May 2012, average of three members, each 1 year) (squared markers) is to the right and above the reference years, indicating a drier year than the reference. Nevertheless, the change in this specific year and drought is in line with the mean increase towards wetness.

Discussion and conclusion

By using spectrally nudged storylines, we have conditionally attributed the climate change effect specific to the 2011/2012 summer drought in SESA, which had a devastating effect on corn and soybean production. We approached this event from an event attribution perspective and additionally included a climatological background analysis to place the event in climatological context. Understanding drought impacts in a region that exhibits a climatological wetting trend, like SESA, is relevant for decision-making and adaptation.

Conditional attribution allows for new insights in understanding the effect of climate change on thermodynamic aspects of extreme events. We therefore took the dynamic field as a given and set the dynamics to be the same for all storylines by nudging the large-scale vorticity and divergence in the free atmosphere. Our analysis is complementary to extreme event attribution, as fully understanding the climate change effect on this event would also require dynamical attribution. To address changes in drought due to altered circulation patterns, which influence drought frequency and duration, dynamical storylines could be added to the attribution toolbox. Dynamical storylines represent uncertainties related to dynamics and involve a better understanding of the remote physical drivers of regional circulation anomalies and their response to a warming climate (Mindlin *et al.*, 2020).

The total precipitation compares well to GPCC and ERA5 (regridded to T255), although peak precipitation volume tends to be slightly overestimated. This precipitation bias can be associated to the resolution being too crude to resolve convective precipitation correctly. Our storylines are simulated using ECHAM6_SN in T225L95 resolution. The 2011/2012 drought is connected to a large-scale pattern, namely the South American Convection Zone (SACZ), which is well resolved by the model. Smaller scale precipitation events, either in space or in time, would require a higher resolution model. Our results are computed with one model only, a comparison with several other models would clarify the influence of model bias uncertainties on the results.

In our framework, we consider GHG and SST changes to create a storyline of a possible 2 degC warmer world and keep land use and aerosols unchanged. Note that there is an indirect aerosol influence alteration through the changed SSTs. Therefore, these results do not predict the future, and it should be taken into account that land use and landscape changes such as deforestation can have a significant effect on the hydroclimate. Our storylines could be expanded to consider these factors. Even so, our results do give an insight on how thermodynamic aspects of a past event may be influenced by a possible future world. In addition, applying our method to longer droughts, outside our present simulation time frame, is needed to fully understand the balance between drought extremes and the climatological wetting.

Throughout our study, we have considered temperature, evapotranspiration (PET) and precipitation as the main contributors to drought. For temperature, the counterfactual, factual and plus2 storylines show a climate change induced warming in line with the mean global warming over land. The temperature peaks, passing the 95th percentile, are more frequent in the plus2 storyline, compared to counter and factual. The impact and frequency of heatwaves can thus be expected to increase with a plus2 degree warming in seasons with similar dynamical conditions (e.g. active SACZ conditions). The Thornthwaite method

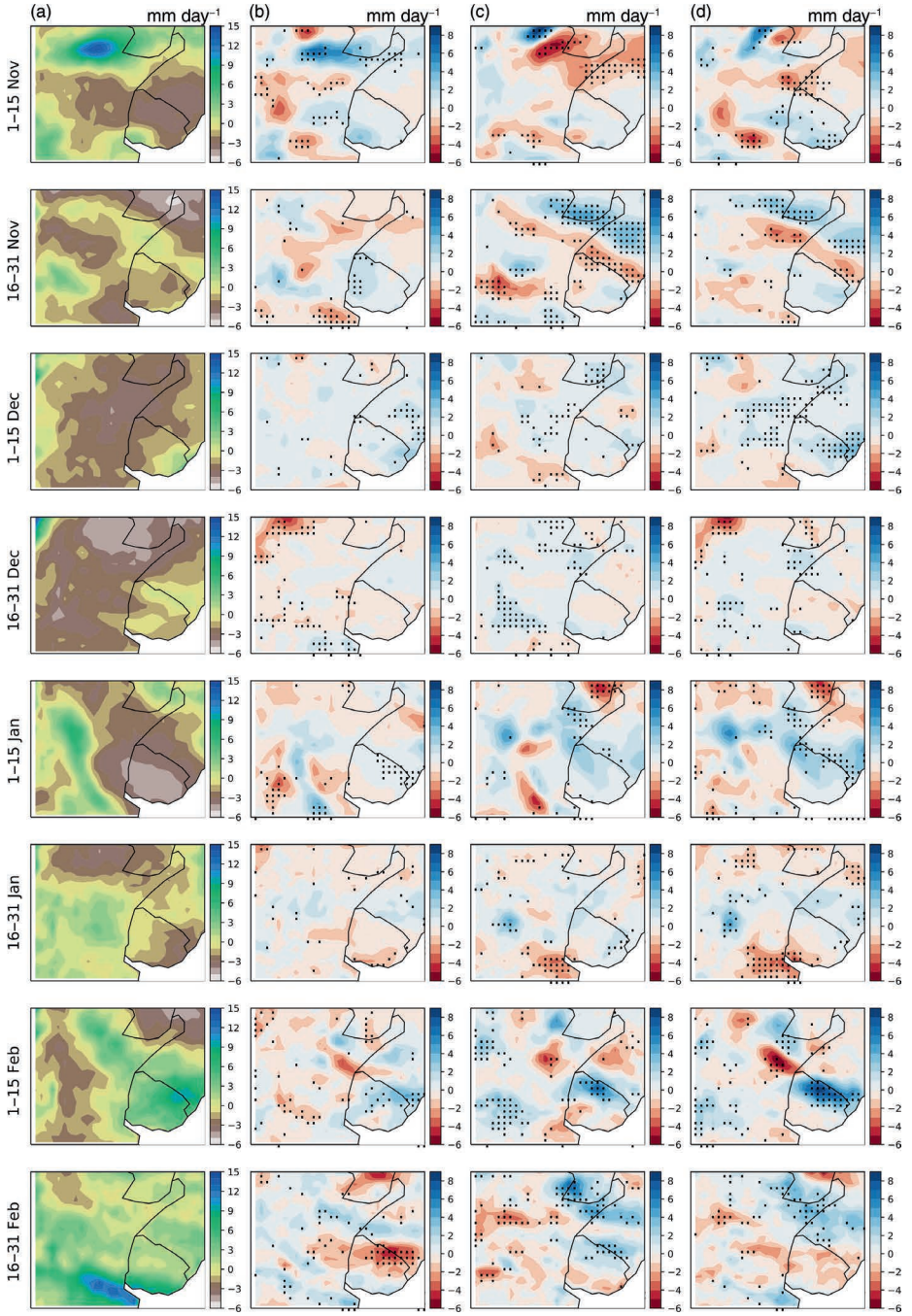

Figure 4. Half-month average WB (precipitation–evaporation) (mm day^{-1}) between November 2011 and February 2012 for ensemble member averages of (a) factual, (b) difference between factual and counterfactual, (c) difference between plus2 and factual and (d) difference between plus2 and counterfactual. Stippling shows robustness, meaning the three members of the first storylines are split by at least 0.1mm day^{-1} from the three members of the second storyline.

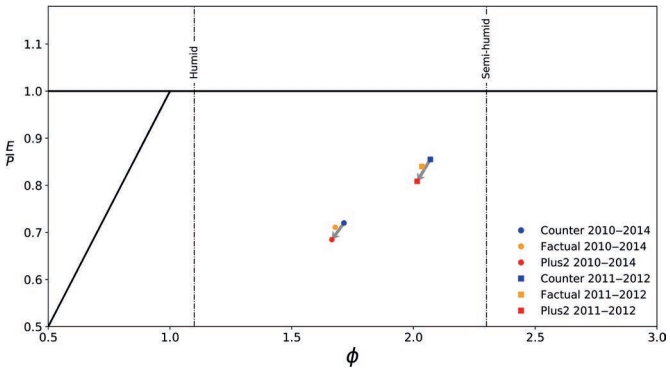

Figure 5. Budyko analysis over SESA for 2010–2014 (circles) averaged over the three members and the hydrological year of 2011/2012 (squares) averaged over the three members. Blue for counterfactual, yellow for factual and red for plus2. The Budyko aridity index (ϕ) is on the x-axis and evapotranspiration divided by total precipitation (E/P) on the y-axis. Grey arrows show the direction from the counterfactual towards the plus2 storyline.

for calculating PET is temperature-based and may have a non-linear temperature forcing bias when used in the light of climate change induced warming (Shaw and Riha, 2011). That said, PET is clearly higher in the factual and plus2 storylines, compared to counterfactual. However, we do not see differences in daily average nor cumulative precipitation between the storylines. Consequently, higher temperature and PET with equal amounts of precipitation place the region at a higher risk of drought. Be that as it may, we found no large-scale decrease or increase in the half-monthly WBs: the drought is not stronger in climate change impacted storylines.

These apparently contradictory results can be explained by taking into account the climatological hydrological background. We found that the general climate change induced trend in SESA is wetting. In the 2011/2012 hydrological year, storylines with increased climate change signal show increased precipitation volume before and after the drought. When considering both the atmospheric water demand and the water balance, we see that the precipitation increase is large enough to outweigh the increased evapotranspiration and PET during the drought. Hence, the wetting background counters the increased temperature and PET, reducing the potential impact on agriculture. If under a different level of warming, the effect of climate change on drought extremes would bypass the wetting background remains unclear.

Acknowledgements

We would like to thank our colleagues Carolina Vera, Frauke Feser and Ted Shepherd for their input. We are also grateful for the input given by Claudio Menéndez on the Budyko analysis. Many thanks to our reviewers Karin van der Wiel and one anonymous reviewer, whose input has strongly increased the quality of our paper. L.vG. received funding from Helmholtz–Zentrum Hereon and J.M. received funding from Universidad de Buenos Aires. Open Access funding enabled and organized by Projekt DEAL.

References

Ault TR. 2020. On the essentials of drought in a changing climate. *Science* **368**(6488): 256–260.

Blunden J, **Arndt DS**. 2012. State of the climate in 2011. *Bull. Am. Meteorol. Soc.* **93**(7): S1–S282.

Budyko MI. 1951. On climatic factors of runoff. *Probl. Fiz. Geogr.* **16**: 41–48.

Cerne SB, **Vera CS**. 2011. Influence of the intraseasonal variability on heat waves in subtropical South America. *Clim. Dyn.* **36**(11–12): 2265–2277.

Cerne SB, **Vera CS**, **Liebmann B**. 2007. The nature of a heat wave in Eastern Argentina occurring during SALLJEX. *Mon. Weather Rev.* **135**(3): 1165–1174.

CREAN. 2017. Monitoreo de extremos hídricos. Centro de Relevamiento y Evaluación de Recursos Agrícolas y Naturales. https://www.crean.unc.edu.ar/monitoreo-de-sequias (Accessed 7 March 2022)

Doyle ME, **Saurral RI**, **Barros VR**. 2011. Trends in the distributions of aggregated monthly precipitation over the La Plata Basin. *Int. J. Climatol.* **32**: 2149–2162.

Feser F, **von Storch H**. 2008. A dynamical downscaling case study for typhoons in Southeast Asia using a regional climate model. *Mon. Weather Rev.* **136**(5): 1806–1815.

van Garderen L, **Feser F**, **Shepherd TG**. 2021. A methodology for attributing the role of climate change in extreme events: a global spectrally nudged storyline. *Nat. Hazards Earth Syst. Sci.* **21**(1): 171–186.

Grimm AM, **Barros VR**, **Doyle ME**. 2000. Climate variability in Southern South America associated with El Niño and La Niña Events. *J. Clim.* **13**(1): 35–58.

Hersbach H, **Bell B**, **Berrisford P *et al***. 2020. The ERA5 global reanalysis. *Q. J. R. Meteorol. Soc.* **146**(730): 1999–2049.

Kalnay E, **Kanamitsu M**, **Kistler R *et al***. 1996. The NCEP/NCAR 40-Year Reanalysis Project. *Bull. Am. Meteorol. Soc.* **77**(3): 437–471.

Mindlin J, **Shepherd TG**, **Vera CS *et al***. 2020. Storyline description of Southern Hemisphere midlatitude circulation and precipitation response to greenhouse gas forcing. *Clim. Dyn.* **54**(9–10): 4399–4421.

Nogués-Paegle J, **Mo KC**. 1997. Alternating wet and dry conditions over South America during summer. *Mon. Weather Rev.* **125**(2): 279–291.

O'Neill BC, **Kriegler E**, **Riahi K *et al***. 2014. A new scenario framework for climate change research: The concept of shared socioeconomic pathways. *Clim. Chang.* **122**(3): 387–400.

Penalba OC, **Rivera JA**. 2013. Future changes in drought characteristics over Southern South America projected by a CMIP5 multi-model ensemble. *Am. J. Clim. Chang.* **02**(03): 173–182.

Penalba OC, **Robledo FA**. 2010. Spatial and temporal variability of the frequency of extreme daily rainfall regime in the La Plata Basin during the 20th century. *Clim. Chang.* **98**(3–4): 531–550.

Peterson TC, **Baringer MO**. 2009. State of the climate in 2008. *Bull. Am. Meteorol. Soc.* **90**(8): S1–S196.

Schneider U, **Fuchs T**. 2008. *Global Precipitation Analysis Products of the GPCC*. Global Precipitation Climatology Centre (GPCC), DWD: Offenbach a. M., Germany.

Schubert-Frisius M, **Feser F**, **von Storch H *et al***. 2017. Optimal spectral nudging for global dynamic downscaling. *Mon. Weather Rev.* **145**(3): 909–927.

Sgroi LC, **Lovino MA**, **Berbery EH *et al***. 2021. Characteristics of droughts in Argentina's core crop region. *Hydrol. Earth Syst. Sci.* **25**(5): 2475–2490.

Shaw SB, **Riha SJ**. 2011. Assessing temperature-based PET equations under a changing climate in temperate, deciduous forests. *Hydrol. Process.* **25**(9): 1466–1478.

Shepherd TG. 2014. Atmospheric circulation as a source of uncertainty in climate change projections. *Nat. Geosci.* **7**(10): 703–708.

Shepherd TG, **Boyd E**, **Calel RA *et al***. 2018. Storylines: an alternative approach to representing uncertainty in physical aspects of climate change. *Clim. Chang.* **151**(3–4): 555–571.

Stevens B, **Giorgetta M**, **Esch M *et al***. 2013. Atmospheric component of the MPI-M Earth System Model: ECHAM6. *J. Adv. Model. Earth Syst.* **5**(2): 146–172.

von Storch H, **Cavicchia L**, **Feser F *et al***. 2018. The concept of large-scale conditioning of climate model simulations of atmo-

spheric coastal dynamics: current state and perspectives. *Atmosphere* **9**(9): 337.

Tebaldi C, **Debeire K**, **Eyring V *et al***. 2021. Climate model projections from the Scenario Model Intercomparison Project (ScenarioMIP) of CMIP6. *Earth Syst. Dyn.* **12**(1): 253–293.

Thornthwaite CW. 1948. An approach toward a rational classification of climate. *Geogr. Rev.* **38**(1): 55.

Vera CS, **Díaz L**. 2015. Anthropogenic influence on summer precipitation trends over South America in CMIP5 models: preccipitation trends over South America in CMIP5 models. *Int. J. Climatol.* **35**(10): 3172–3177.

van der Wiel K, **Matthews AJ**, **Stevens DP *et al***. 2015. A dynamical framework for the origin of the diagonal South Pacific and South Atlantic Convergence Zones. *Q. J. R. Meteorol. Soc.* **141**(691): 1997–2010.

Zaninelli PG, **Menéndez CG**, **Falco M *et al***. 2019. Future hydroclimatological changes in South America based on an ensemble of regional climate models. *Clim. Dyn.* **52**(1–2): 819–830.

Correspondence to: L. van Garderen

linda.vangarderen@hereon.de

doi: 10.1002/wea.4185

Zusammenfassung

Hitzewellen, Dürreperioden, Überschwemmungen, Stürme und andere Arten von Extremwetterereignissen führen zu menschlichem Leiden sowie materiellen und wirtschaftlichen Schäden. Das Verständnis, wie Klimawandel verschiedenen Extremeereignisse beeinflusst, ist eine Voraussetzung um abzuschätzen, wie sich diese in der Zukunft entwickeln werden und wie sich mögliche Todesfälle und Schäden reduzieren lassen. Die gängige Methode, Extremereignisse dem Klimawandel zuzuschreiben ist ein wahrscheinlichkeitsbasierter Ansatz. Dieser beruht auf einer statistischen Analyse der dynamischen Gegebenheiten, die zu dem Extremereignis führen. Er berechnet die Wahrscheinlichkeit eines Extremereignisses in einer Welt mit und einer Welt ohne Klimawandel. Allerdings lassen sich die dynamischen Auswirkungen des Klimawandels auf Grund der großen natürlichen Variabilität der Atmosphärenzirkulation nur schwer quantifizieren. Ein Ansatz, der auf unbedingten Wahrscheinlichkeiten beruht, ist daher generell mit hohen Unsicherheiten verbunden. Die thermodynamischen Auswirkungen des Klimawandels hingegen basieren auf physikalischem Verständnis und lassen sich viel genauer quantifizieren. Ein neuer Ansatz für die bedingte Zuschreibung von Extremen, welcher nicht auf Wahrscheinlichkeiten beruht, ist der sog. storyline-Ansatz. Dieser quantifiziert den thermodynamischen Effekt des Klimawandels auf ein Extrem und nimmt dabei die auslösende dynamische Situation als gegeben an. In einer solchen storyline kann ein Extrem unter verschiedenen klimatischen Bedingungen - beispielsweise keine oder verstärkte globale Erwärmung - untersucht und der Effekt des Klimawandels auf die thermodynamischen Aspekte des Extrems quantifiziert werden. Das Hauptziel der vorgelegten Arbeit ist eine qualitativ hochwertige bedingte Klimawandelzuschreibung einzelner Extremereignisse. Hierfür wird eine geeignete Methode zur Erzeugung bedingter storylines entwickelt.

Hier werden spektral genudgte Ereignis-storylines vorgestellt, bei denen in einem Atmosphärenmodell die großskalige Wirbelstärke und Divergenz der oberen freien Atmosphäre spektral an ReanalyseDaten angepasst werden, während sich der untere Teil der Atmosphäre frei entwickeln kann. Tatsächlich aufgetretene Extremereinisse

werden hier in drei storylines simuliert: (1) die faktische storyline, die der tatsächlichen Welt mit Klimawandel entspricht, (2) eine vorindustrielle kontrafaktische Welt ohne Klimawandel und (3) eine 2 °C wärmere kontrafaktische Welt, die einer möglichen Welt mit einer globalen Erwärmung von 2 °C über dem vorindustriellen Temperaturniveau entspricht.

Die Ergebnisse zeigen einen konsistenten Anstieg sowohl in der globalen Mitteltemperatur wie auch im global gemittelten Niederschlag. Dies stimmt mit Ergebnissen der Klimawandelzuschreibung mit unbedingten Methoden überein. Daher geht bei der Anwendung eines bedingten Ansatzes nichts verloren. Regional können saisonale Niederschlagstrends hiervon abweichen, so wurde beispielsweise der mexikanische Monsun in den Jahren 2012 und 2014 trockener und der indische Monsun wurde in den Jahren 2011 und 2014 feuchter. Temperaturextreme sind auf kleinen räumlichen Skalen und kurzen Zeitskalen konsistent. Die europäische Hitzewelle im Jahr 2003 war durch den Klimawandel im Mittel 0.6 °C wärmer. Die russische Hitzewelle im Jahr 2010 wurde durch den Klimawandel im Mittel um 2 °C verstärkt. Bei letzterem handelt es sich um ein Signal, das über dem Niveau der mittleren globalen Erwärmung liegt. Die Dürreperiode im südöstlichen Südamerika in 2011/2012 wäre durch erhöhte Temperaturen und Verdunstung im Zuge des Klimawandels verstärkt worden. Dieser Effekt wurde allerdings durch eine – ebenfalls vom Klimawandel bedingte – langfristig reduzierte Aridität kompensiert.

Spektral genudgte Ereignis-storylines ermöglichen eine kontinuierliche und spezifische Klimawandelzuschreibung von Extremereignissen, indem sie Klimawandel-Signal und natürliche interne Variabilität auf kurzen Zeit- und kleinen räumlichen Skalen robust voneinander trennen. Das Beispiel der Dürreperiode zeigt, dass die Methode zwischen entgegengesetzten Klimawandeleffekten unterscheiden kann, die auf unterschiedlichen Zeitskalen agieren. Die Methode ist nicht auf das hier vorgestellte technische Setup beschränkt, sondern kann in vielen Kontexten angewendet werden. Sie kann beispielsweise mit einem hochaufgelösten Regionalmodell, welches Konvektion nicht parametrisieren muss, verbunden werden und so eine präzise Klimawandelzuschreibung von lokalen Niederschlagsextremen ermöglichen. Darüber hinaus wird nur eine geringe Anzahl von Simulationen in einem Ensemble benötigt, um robuste Ergebnisse zu erzielen, was den Rechenaufwand reduziert. In Verbindung mit einem sogenannten Impact Modell kann die Methode für realistische Stresstests von Resilienz-Strategien genutzt werden. Auch ließe sich mit den spektral genudgten Ereignis-storylines ein operationelles System zur Klimawandelzuschreibung von Extremereignissen erstellen, welches bis dato schwierig war. Zusammengefasst ist die Methode der globalen spektral genudgten Ereignis-storylines ein wichtiger Schritt

in Richtung ganzheitlicher Klimawandelzuschreibung einzelner Extremereignisse, da sich mit ihr die jeweilige Rolle der dynamischen Variabilität und der thermodynamischen Auswirkungen des Klimawandels, sowie deren Zusammenspiels, quantifizieren lässt.

List of Publications

Peer reviewed publications

van Garderen, L. and J. Mindlin (2022). "A storyline attribution of the 2011/2012 drought in Southeastern South America". In: Weather. doi: 10.1002/wea.4185.

Feser, F., O. Krueger, K. Woth, **L. van Garderen** (2021). "North Atlantic winter storm activity in modern reanalyses and pressure-based observations". In: Journal of Climate 34.7, pp. 2411-2428. doi: 10.1175/JCLI-D-20-0529.1

van Garderen, L., F. Feser, and T. G. Shepherd (2021). "A methodology for attributing the role of climate change in extreme events: a global spectrally nudged storyline". In: Natural Hazards and Earth System Sciences 21.1, pp. 171–186. doi: 10.5194/nhess-21-171-2021.

Publications in progress

van Garderen, L., T. G. Shepherd and F. Feser (in progress). "Continuous precipitation attribution for past, present and future using spectrally nudged event storylines".

Publications prior to PhD

van Garderen, L., E.C. van der Linden, G. van de Schrier, L. Ganzeveld, A.M.G. Klein Tank (2018). "Stormen van de Toekomst". In: Meteorologica 4, pp. 4-7 (Dutch).

van Garderen, L., F. Ludwig (2013). "Climate change adaptation options for the Congo basin countries". In: Climate change scenarios for the Congo Basin. [A. Haensler, D. Jacob, P. Kabat, F. Ludwig (eds)]. Climate Service Centre Report No. 11, Hamburg, Germany, ISSN: 2192-4058.

Presentations

Feser, F., **L. van Garderen** "SCENIC" (2022). SCENIC pre-kickoff meeting, Alfred Wegener Institute for Polar and Marine Research (AWI), Bermerhaven - Germany (online).

van Garderen, L., F. Feser, and T. G. Shepherd (2021) "Attributing the role of climate change in extreme weather events using global spectrally nudged storylines". Student conference, Royal Meteorology Society (RMetS), Reading - United Kingdom (online).
Best presentation prize

van Garderen, L., F. Feser, and T. G. Shepherd (2021) "Attributing the role of climate change in extreme weather events using global spectrally nudged storylines". Atmospheric Science Conference, Royal Meteorology Society (RMetS), Reading - United Kingdom (online).

van Garderen, L., F. Feser, and T. G. Shepherd (2021). "A methodology for attributing the role of climate change in extreme events: a global spectrally nudged storyline". Virtual General Assembly, European Geosciences Union (EGU), Vienna - Austria (online).

van Garderen, L., F. Feser, and T. G. Shepherd (2020). "A methodology for attributing the role of climate change in extreme events: a global spectrally nudged storyline". 12th REKLIM workshop, the Helmholtz Climate Initiative for Regional Climate Change and Humans (REKLIM), Bad-Bentheim - Germany (online)
Invited speaker

Posters

van Garderen, L., F. Feser, and T. G. Shepherd (2021). "A methodology for attributing the role of climate change in extreme events: a global spectrally nudged storyline". International workshop on Storylines approach on regional extreme weather and their future change for better adaptations to the climate change, University of Tokyo, Tokyo - Japan (online).

van Garderen, L., F. Feser, and T. G. Shepherd (2021). "A methodology for attributing the role of climate change in extreme events: a global spectrally nudged storyline". Compound weather and climate events, University of Bern, Bern - Switzerland (online).

van Garderen, L., F. Feser, and T. G. Shepherd (2019). "A Spectrally Nudged Global Storyline: Attributing the Effect of Climate Change in Historical Extreme Events". 8th European Windstorm Workshop, University of Birmingham, Birmingham - United Kingdom.

van Garderen, L., G. van der Schrier, F. Feser, T. G. Shepherd (2019), "Storms of the future: Untangling the known unknown in climate change attribution using high resolution modelling". REKLIM workshop 2019, Helmholtz Climate Initiative for Regional Climate Change and Humans (REKLIM), Herrsching am Ammersee - Germany.
Best poster award

van Garderen, L., G. van der Schrier, F. Feser, T. G. Shepherd (2019), "Storms of the future: Untangling the known unknown in climate change attribution using high resolution modelling". Earth System PhD Conference, Max Planck Institute for Biogeochemistry (MPG), Jena - Germany.

van Garderen, L., G. van der Schrier, F. Feser, T. G. Shepherd (2019), "Storms of the future: Untangling the known unknown in climate change attribution using high resolution modelling". General Assembly, European Geosciences Union (EGU), Vienna - Austria.

List of Figures

List of Tables

List of Acronyms

AMO Atlantic Multidecadal Oscillation. 30

CESM Community Earth System Model. 99

CGTI Circumglobal Teleconnection Index. 52, 59, 107

CMIP climate model intercomparison project. 23, 30

DJF December-January-February. 46

ECHAM6 sixth European Centre/Hamburg Model. 23

ECHAM_SN 1948-2014 ECHAM spectrally nudged. 33, 77

ECHAM_SNC 1948-2014 spectrally nudged counterfactual. 33

ECMWF European Centre for Medium-Range Weather Forecasts. 23

EF Enhanced Fujita Scale. 3

ENSO El Niño–Southern Oscillation. 30, 52, 59, 68, 76, 107

ERA-Interim ECMWF Reanalysis vInterim. 41

ERA5 ECMWF Reanalysis v5. 40

GCM general circulation model. 23

GHG greenhouse gases. 6, 13, 30, 32, 37, 39, 91, 171

GPCC Global Precipitation Climatology Centre. 41, 78

GPCP Global Precipitation Climatology Project. 41, 47, 49, 50, 52, 98

HadSST3 Hadley Centre SST data set. 31

HadUK-Grid Met Office Hadley Centre United Kingdom gridded climate observations. 41, 83

IPCC Intergovermental Panel on Climate Change. 50

JJA June-July-August. 26, 46

JSBACH Jena Scheme for Biosphere-Atmosphere Coupling in Hamburg. 23

MAM March-April-May. 46

MERRA-2 Modern-Era Retrospective Analysis version 2. 34, 35, 37, 169

MPI-ESM Max Planck Institute - Earth System Model. 23, 30, 31

NAM North American Monsoon. 52

NAMOC North Atlantic Meridional Overturning Circulation. 46

NCEP-R1 National Centers for Environmental Prediction. 23, 30, 37, 97

NOAA National Oceanic and Atmospheric Administration. 3

NPP Net Primary Productivity. 66

OLR outgoing long-wave radiation. 76

PDSI Palmer Drought Severity Index. 76

PET potential evapotranspiration. 79, 87, 107

PiCon pre-industrial control. 30, 34

RCP representative concentration pathways. 37

SACZ South Atlantic Convergence Zone. 76, 78, 87, 105

SAM Southern Annular Mode. 13

SASM South Asian summer monsoon. 59

SESA Southeastern South America. 75, 87

SIC sea ice concentration. 23, 29–32, 37, 96, 169

SON September-October-November. 46

SPI Standardized Precipitation Index. 76

ssp shared socioeconomic pathway. 37

SST sea surface temperature. 6, 23, 30–32, 37, 46, 91, 96, 169

T2m two-meter temperature. 26, 34, 45

WB water budget. 81

Eidesstattliche Versicherung | Declaration on Oath

Hiermit erkläre ich an Eides statt, dass ich die vorliegende Dissertationsschrift selbst verfasst und keine anderen als die angegebenen Quellen und Hilfsmittel benutzt habe.

|

I hereby declare upon oath that I have written the present dissertation independently and have not used further resources and aids than those stated.

Ort,den | City,date — Unterschrift | Signature

Hamburg, April 8th. 2022 — Linda van Garderen